University of New Mexico
UNM Digital Repository

7-1-2012

Exploring the use of synthetic delivery platforms and small molecule adjuvants to improve the efficacy of spinal interleukin-10 gene therapy for chronic neuropathic pain

Ellen Dengler

Recommended Citation

ELLEN DENGLER

CANDIDATE

BIOMEDICAL SCIENCES- DEPT. OF NEUROSCIENCES

DEPARTMENT

THIS DISSERTATION IS APPROVED, AND IT IS ACCEPTABLE IN QUALITY AND FORM FOR PUBLICATION :

APPROVED BY THE DISSERTATION COMMITTEE:

ERIN D. MILLIGAN, PHD , CHAIRPERSON

JAMES WALLACE, PHD

LEE ANNA CUNNINGHAM, PHD

C. JEFFREY BRINKER, PHD.

EXPLORING THE USE OF SYNTHETIC DELIVERY PLATFORMS AND SMALL MOLECULE ADJUVANTS TO IMPROVE THE EFFICACY OF SPINAL INTERLEUKIN-10 GENE THERAPY FOR CHRONIC NEUROPATHIC PAIN

by

Ellen C. Dengler

B. S. Physical Therapy, University of Pennsylvania, 1975
M. S. Biology, San Diego State University, 2007

DISSERTATION

Submitted in Partial Fulfillment of the
Requirements for the Degree of

**Doctor of Philosophy
Biomedical Sciences**

The University of New Mexico
Albuquerque, New Mexico

July, 2012

Dedication

I'd like to dedicate this dissertation to my family. First, to my father who passed away from complications from brain trauma. He was my inspiration. A dedicated polymer researcher and wonderful father, his ability for precision and detail, and warmth and intelligence were to be envied. My mother is a rock, and without her I would surely falter. My three sisters have motivated me, aspired me, annoyed me but always loved me, surrounding me with rejuvenation, and validation that I am on the right path. My bother-in-laws aspire me with their determination for success and energy. My husband, the organizer par excellence, has whole-heartedly supported me in this educational endeavor. His spirit is a delight and his intelligence astonishes me. My children now adult, are so dear to me. Their brightness and confidence are wonderful, and let me know my job as a single mom was a success. I want to thank them for understanding my need to pursue my dream and apologize for all the times I ignored them when I was buried in my books. I love you all.

Acknowledgements

First, I would like to thank all my scholastic mentors, for providing me with the tools, advice and experiences to expand my world. You have all given me a means to think critically and logically. You have given me the strength, to know that I can achieve my inspirations and goals. During my career as a physical therapist, I have seen so many folks suffer from health problems and the consequences of disease. I'd like to commend you for your research and for all you do to educate the next generation.

I want to thank my all my lab colleagues, office staff, animal facility staff and the folks in the microscopy, flow cytometry and DNA sequencing facilities for all their assistance in getting this research accomplished. I am forever grateful to all of you.

I'd like to thank, my mentor Erin D. Milligan, PhD for all the time and effort she has put into my training as a scientist. She has always been available to help and offer support for my work. I am in awe of her energy, organizational skills and professionalism.

EXPLORING THE USE OF SYNTHETIC DELIVERY PLATFORMS AND SMALL MOLECULE ADJUVANTS TO IMPROVE THE EFFICACY OF SPINAL INTERLEUKIN-10 GENE THERAPY FOR CHRONIC NEUROPATHIC PAIN

by

Ellen C. Dengler

B.S Physical Therapy, University of Pennsylvania, 1975

M.S. Biology, San Diego State University, 2007

PhD Biomedical Sciences, University of New Mexico, 2012

Abstract

The focus of the work in this dissertation is to improve the efficiency of a gene therapy for the treatment of chronic pain. The introduction, Chapter 1, is intended to orient the reader to the underlying physiological principles and anatomical structures involved in general sensory and pain transmission in the peripheral and central nervous systems. Pain modulatory systems are described in detail. Also included, is a discussion of how peripheral nerve injury can provoke immune changes at the spinal level, including the activation of spinal macrophages and glial cells (microglia, astrocytes and oligodendrocytes) with the release of immune modulators, such as pro- and anti-inflammatory cytokines, that can lead to the development of chronic pain. One of the most important of these is the anti-inflammatory cytokine, Interleukin-10 (IL-10). As a framework for the experiments described in the dissertation, earlier studies using spinal injections of IL-10 protein and DNA containing the gene for IL-10 for the treatment of neuropathic pain in a chronic constriction injury (CCI) rodent model are introduced. Also

presented in this dissertation, are some of the key problems of delivering DNA to cells (tranfection). The studies in Chapter 2, explore the use of one novel non-viral synthetic platform, a silica/lipid nanoparticle or "protocell," as a potential platform for IL-10 transgene delivery to the central nervous system (CNS). These particles had never before been examined *in vivo* in the CNS. The first objective was to determine if they simply would be tolerated by animals following peri-spinal injection. The second objective was to determine their biodistribution in the whole body following these injections and the cell type interacting with them near the spinal injection site. The final objective was to determine if the IL-10 transgene produced functional IL-10 protein following loading on protocells and if the gene loaded on protocells would produce a therapeutic pain reversal in neuropathic animals. The studies in Chapter 3 are based on previously published results[72] of a critical interval following spinal injection of a transgene, the "sensitization period", during which there is immune cell enrichment in the cerebral spinal fluid (CSF) in the subarachnoid matrix. This local enrichment of immune cells in the spinal CSF, is key to the development of the experimental approach used in Chapter 3, which is to prime improved cellular uptake of the IL-10 gene with small molecules as immune adjuvants. In Chapter 2 and Chapter 3, each experimental data set is presented in the form of the original manuscripts, submitted for external peer-review and publication. Chapter 4 includes a discussion of the gene therapy approaches used in this work and by other investigators. Also considered are some future directions, including the use of a different synthetic polymer, polylactic co-glycolic acid, PLGA, that is FDA approved and highly biodegradable in the body. A concluding statement completes the work of this dissertation.

Table of Contents

List of Figures

Abbreviations

AAV	adeno-associated virus
AMPA	α- amino-3-hydroxy-5-methyl-4-isooxazole-proionate
AP-1	activator protein-1
APCs	antigen presenting cells
BBB	blood brain barrier
CAMK	calcium calmodulin dependent protein kinase
CGRP	calcitonin gene related peptide
CHO	chinese hamster ovary cells
CNS	central nervous system
COX	cyclooxygenase
CpG	cytosine-phosphate-guanine
CR	cytosine rich
CREB	cyclic AMP response element binding protein
CRPS	complex regional pain syndrome
CSF	cerebral spinal fluid
CTAB	cetyltrimethylammoniumbromide
CTLD	c-type lectin domain
CTLs	cytotoxic T lymphocytes
DC-SIGN	dendritic cell-specific intercellular adhesion molecule-3-grabbing non-integrin
DCIR	dendritic cell inhibitory receptor
DCs	dendritic cells
Dex	dexamethasone
DH	dorsal horn
DNA	deoxyribonucleic acid
DOPC	1,2-dioleoyl-sn-glycero-3-phosphocholine
DOPE	dioleoylphosphatidylethanolamine
DOTAP	1-(2,3-Dioleoyloxy)propyl]-N,N,N-trimethylammonium methyl-sulfate
DRG	dorsal root ganglion
dsDNA	dsDNA
DsREd	*Discosoma* red fluorescent protein
EH-1	ethidium homodimer-1
EISA	evaporation induced self assembly

EPSP	excitatory post synaptic potential
ERK	extracellular signal related kinase
FDA	Food and Drug Administration
FITC	fluorescein isocyanate
GABA	gamma amino butyric acid
GC	glucocorticosteroid
GDNF	glial derived neurotrophic factor
GFP	green fluorescent protein
GR	glucocorticosteroid receptor
GRE	glucocorticosteroid response element
HEK	human embryonic kidney cells
HIV-1	human immunodeficiency virus-1
I.T.	intrathecal
IB4	α-D-galactosyl-binding lectin
IL-10	interleukin-10
IL-13	interleukin-13
IL-4	interleukin-4
IL-6	interleukin- 6
IL1-β	interleukin1-beta
IL1Ra	interleukin1 receptor antagonist
INF-γ	interferon gamma
IPSP	inhibitory post synaptic potential
IRAK	interleukin-1 receptor-associated kinase 4
IκB-2	inhibitor of nuclear factor kappa light chain enhancer of activated B cells
JAK	Janus kinase
LVs	lentivirus
M1	classical pro-inflammatory macrophage activation
M2	alternative anti-inflammatory macrophage activation
MAPK	mitogen activated protein kinase
MHC	major histocompatibily complex
MINCLE	macrophage-inducible C-type lectin
MR	mannose receptor
MSNs	mesoporous silica nanoparticles
MTT	3-(4,5-dimethylthiozal-2-yl)-2,5-dipheyl-tetrazolium bromide
NFκ-B	nuclear factor kappa-light-chain-enhancer of activated B cells
NGF	nerve growth factor
NK1	neurokinin receptor

NMDA	N-methyl-D-aspartate
NO	nitric oxide
NPCs	nuclear pore complexes
ODN2006	oligodeoxynucleotide
PAG	peri-aqueductal grey
PAMAM	polyamidoamine
PAMPS	pathogen associated molecular patterns
pDNA	plasmid DNA
PEG	polyethylene glycol
PEI	polyethylenimine
PKA	protein kinase A
PKC	phosphokinase C
PKC	protein kinase C
PLC	phospholipase C
PLGA	poly-lactic-co-glycolic acid
PMI	phosphomannose isomerase
PNS	peripheral nervous system
PRRs	patterned recognition receptors
RNA	ribonucleic acid
ROS	reactive oxygen species
RVM	rostral ventral medulla
siRNA	silencing RNA
ssDNA	single stranded DNA
ssRNA	single stranded RNA
STAT	signal transducer and activator of transcription
TEOS	tetraethylorthosilicate
TGF-β	transforming growth factor
Th1	T helper 1 cells
Th2	T helper 2 cells
TLR	toll like receptor
TNF-α	tumor necrosis factor alpha
WDR	wide dynamic range

1. Introduction

1.1 Normal Pain Processing

1.1.1 The neuron

The primary and basic unit of the nervous system is a specialized cell, the neuron, composed of a cell body or soma from which extend many processes known as dendrites that receive incoming signals, and axons, which are long extensions of cytoplasm ending in nerve terminals for signal transmission. Some neuronal axons are myelinated by a layer of insulating myelin protein, while others are unmyelinated and lack this covering. Neurons communicate with other neurons across the synapse or space between them by releasing chemicals known as neurotransmitters. The cell body or soma houses the nucleus containing chromosomal DNA and the transcriptional machinery for cellular replication and protein synthesis. The cell soma also contains the subcellular organelles responsible for metabolic and neuronal nutritional support and the formation of the neurotransmitters. [1]

There are three types of morphologically distinct neurons. The classically depicted neuron is multi-polar, with many branching dendrites emanating from the cell body. From this neuron projects only one long axon that ends in multiple branched terminals. Bipolar neurons have two long processes, one a dendrite and one an axon, with a cell soma in the middle. Both ends are composed of many branches. These are found in the visual, auditory and vestibular systems. One category of sensory neurons is composed of nociceptors, having specialized receptors on their peripheral terminal endings that to

respond to and transmit painful stimuli that can cause tissue damage (harsh chemicals, high or low temperatures or hard pressure). Nociceptors have one axon with two terminal endings, one in the periphery, in the skin or viscera, and the other end synapsing onto neurons in the spinal cord or brainstem. All sensory neurons entering the spinal cord, including nociceptive neurons, have cell bodies outside the CNS in a structure referred to as the dorsal root ganglia (DRG).[2]

The resting membrane potential in neurons is about -60 mV. During resting conditions, passive inward diffusion of extracellular positive ions (cations; Na^+, K+) is opposed by an outward diffusion of intracellular negative ions (anions; Cl^-, negatively charged amino acids and proteins). Transient membrane currents make the neuronal membrane either more negative (hyperpolarized) or less negative (depolarized). Depolarization of the axon hillock to about -45 mV results in the firing of an action potential, caused by the rapid influx of Na^+ through volt sensitive Na^+ channels. This is countered by an efflux of K^+, that eventually returns the membrane to its resting state. The action potential courses along the axon as the voltage reaches that necessary to open voltage-gated Na+ ion channels. The velocity is dependent on the diameter of the axon and the amount of myelination. Along the course of myelinated axons are periodic gaps, known as Nodes of Ranvier. The low capacitance and concentration of Na^+ channels in these nodes allows the action potential to jump between nodes (salutatory conduction), increasing the speed of conduction over long distances in myelinated neurons. It is important to note that larger diameter myelin-insulated axons conduct more quickly than smaller myelinated axons. Unmyelinated axons, conduct slowly. Pain is transmitted by lightly myelinated Aδ and unmyelinated C-fibers.[3]

Sensory neuronal communication from the periphery, results from the release of neurotransmitters in a Ca^{2+} dependent manner from the axon terminals of presynaptic neurons. Thsese neurotransmitters act upon receptors on dendrites or the cell soma of the post-synaptic neuron in the spinal cord. If neurotransmitter binding generates depolarizing ionic fluxes of the post-synaptic membrane, the net result is an excitatory post-synaptic potential (EPSP). However, if the post-synaptic membrane is hyperpolarized, an opposite response or inhibitory post-synaptic potential or (IPSP) occurs. The intensity of a stimuli is transduced into a frequency code. That is, the more intense the sensory stimuli, the more rapid is the firing of axonal action potentials. The major consequence of nociceptor firing is the release of excitatory neurotransmitters from central terminals onto post-synaptic neurons in the spinal cord. Inhibitory neurons within the spinal cord, also respond to increased firing frequency from peripheral sensory neurons but release inhibitory neurotransmitters that change the membrane potential in the direction of hyperpolarization. In addition to frequency based, temporal summation of post-synaptic potentials, there post-synaptic potentials can be summated in a spatial manner because one axon terminal can converge on more than one dendrite in the spinal cord. Via summation, a painful stimulus transmitted by one primary nociceptive neuron is capable of generating high frequency post-synaptic action potentials on many nearby central spinal cord neurons. Temporal or spatial summation can lead to an exacerbation of the intensity of pain perception despite the fact that the stimulus remains constant.[4, 5]

1.2 Peripheral versus central sensory relay systems

Grossly, the nervous system in animals is composed of the central nervous system (CNS) and the peripheral nervous system the (PNS). The PNS conveys incoming or afferent messages and outgoing or efferent messages from the tissues and organs of the body and outside environment to and from the CNS (spinal cord and brain). The CNS is composed of both myelinated (white matter) and unmyelinated (gray matter) tissue. The spinal cord, a relay system of neurons, is housed in the vertebral canal formed anteriorly by the vertebral body and posteriorly by boney laminae connecting the tranverse and spinous processes. The peripheral nerves enter and exit from openings, or foraminae, between two adjacent vertebrae. The spinal cord and brain are protected by the meninges, which is composed of three connective tissue membranes. Closest and adhering to the spinal cord is a thin layer known as the pia mater. The outside layer is a thicker protective layer, the dura mater, while sandwiched between is the arachnoid membrane. Between the pia and arachnoid membranes is the subarachnoid space, in which the CSF is contained and circulates. This space is also known as the intrathecal (i.t.) space. The spinal cord extends from an opening in the skull, known as the foreman magnum, and ends inferiorly at level of the L1-2 vertebra in humans, forming a cone-like structure known as the conus medullaris. In this area are many nerve rootlets, collectively known as the cauda equina or "horses-tail" floating in a pool of CSF, within the lumbar cistern in the dural sac.[6, 7]

1.2.1 Sensory relay in the PNS

There are two major classes of sensory neurons carrying information from the periphery to the spinal cord, each classified by letters of the Greek alphabet or Roman numerals. The first class are non-nociceptors, possessing Aα (I) and Aβ (II) fibers that transmit non-painful stimuli such as light touch, pressure, vibration or proprioception (body position). These fibers have large diameters 12-20 and 6-13 μm respectively, and are highly myelinated, allowing for rapid conduction of action potentials. Under normal conditions, Aα (I) fibers respond to motion and limb position, while Aβ (II) fibers respond to vibration and light touch pressure.[8] Sensory neurons express many different types of receptors. In the skin, mechanoreceptors discriminate tactile, vibratory and body position sense (proprioceptive) stimuli. These receptors include Meissner corpuscles (tactile, shapes and surfaces), Merkel discs (indentations), hair follicle receptors (tactile), Ruffini endings (stretch), Pacinian corpuscles (vibrations). In the muscle, specialized muscle spindles respond to proprioceptive stimuli.[9]

The second class are the nociceptive neurons previously discussed. To reiterate, nociceptors have receptors that are only activated when mechanical, thermal or chemical stimuli reach, noxious harmful (tissue damaging) levels. There are two sub-types of nociceptive fibers. Aδ (III) fibers, are small in diameter (1-6 μm) and thinly myelinated, and are slow conducting and have a higher activation threshold, perceived as "fast" pain, described as a sharp, pricking, well-localized pain. Aδ fibers can be further divided into two sub-types. Type I, respond to low mechanical or chemical stimuli, such as pinprick but have a high heat threshold (> 50°C). Conversely, Type II fibers have a much lower

heat threshold, but a higher mechanical threshold. C (IV) fibers are unmyelinated and smallest in diameter, <1.5 μm, thus are very slow conducting, with a very high mechanical and thermal activation threshold. Pain perceived via these nociceptors is described as "slow", burning, diffuse and poorly localized. The nociceptors, Aδ and C fibers, can be further divided into two broad categories, the peptidergic class, which release the neuropeptides, substance P and calcitonin-gene related peptide (CGRP) and classical excitatory neurotransmitters such as glutamate. The non-peptinergic fibers release only the classical excitatory neurotransmitters. In addition, many non-peptidergic neurons express the purinergic ATP-gated ion channel receptor, P2X$_3$. It is important to note that PX$_3$ is part of a much larger 2PX receptor family. ATP binding to this receptor plays a role in the development of chronic pain.[10-12] In summary, nociceptors respond, via thermo and mechanoreceptors, to extremes of heat, cold and pressure.

While mechano and thermo-receptors are critical in nociceptor activation, their terminal endings also express chemo- receptors that respond to a host of chemical stimuli. One classic example is the chemical in red hot peppers, capsaicin, which activates transient receptor potential cation channel (TRPV1). Other TRPV receptors respond to natural cooling agents such as menthol and eucalyptol (TRPM8), or acids (ASICs). TRPV1 also responds to inflammatory factors generated following tissue damage.[11, 15, 16]

The major classical excitatory transmitter released in the dorsal horn of the spinal cord by primary sensory afferents, both nociceptive and non-nociceptive, is glutamate. Glutamate binds to fast acting ionotropic α-amino-3-hydroxy-5-methyl-4-isooxazole proionate (AMPA) receptors, causing an influx of Ca+ that raises baseline membrane

potential sufficiently to activate ionotrophic N-methyl-D-aspartate (NMDA) receptors. This response will be explained in greater detail below. Metabotropic NMDA, and kainite receptors also respond to glutamate. With membrane depolarization, petidergic Aδ and C-fibers release the small peptides substance P, which binds neurokinin-1 receptors (NK1) receptors, and CGRP,[15] which binds its receptor CGRP1.[16-18]

In summary, when nociceptive receptors are activated, an action potential is propagated along the course of primary (1°) axons terminating in the dorsal spinal cord where they synapse on secondary (2°) projection neurons that carry the message from the spinal cord to the brainstem or brain. Others synapse on interneurons that communicate with other neurons at the spinal cord level. Whereas nociceptive 1° neurons terminate in the dorsal horn (DH), non-nociceptive neurons also synapse locally in the DH, yet have major collateral branches that ascend in the dorsal column to the dorsal column nuclei in the medulla. Moreover, both nociceptive and non-nociceptive axons send collateral branches to other areas of the spinal cord several segments above or below their entry into the dorsal spinal cord or to other areas on the same level.[19, 20]

1.3 Sensory relay in the CNS

The DH is the primary spinal cord area for pain modulation. The gray matter of spinal cord is divided into ten layers or laminae, analogous to the layers of an onion extending from the posterior, Lamina I, to the anterior, Lamina IX. Lamina X is located in the center of the spinal cord, surrounding the central canal. The DH includes Lamina I-VI. Nociceptive sensory afferent axons enter the spinal cord through the dorsal root entry zone, collect in the Tract of Lissauer (dorsal lateral fasciculus) and then send axons

collaterals into the DH where they synapse on 2° pain projection neurons and interneurons in laminae I-VI in the dorsal horn. Nociceptive 2° projection neurons cross or decussate to the opposite of the spinal cord (contralateral) where they course rostrally toward the brain via the lateral spinothalamic tract, such that painful stimuli received on the left side of the body is processed in the right side of the brain. Axons of non-nociceptors ascend to the medulla, where they synapse in the dorsal column nuclei on the same side (ipsilateral). In humans, those non-nociceptive neurons originating below the thoracic 6 (T6) vertebral level, ascend in the dorsal column fasiculus gracilis (medial dorsal column), while those above T6 ascend in the fasiculus cuneatus (lateral dorsal column). At the level of the caudal medulla in the brainstem, axonal fibers from the cuneate and gracilis nuclei cross to the contralateral side and ascend via the medial lemniscus to the somatosensory cortex. As a result, non-nociceptive stimuli received from the left side of the body are also processed by the contralateral somatosensory cortex.[2, 20]

Important to the development of chronic pain, both myelinated and non-myelinated, 1° nociceptive and non-nociceptive fibers project to the superficial Lamina I and II of the spinal cord. While some nociceptive Aδ project more deeply to Lamina V, most synapse in Lamina I, and Lamina II.[21] In these lamina, there are inhibitory interneurons that release gamma-aminobutyric acid (GABA) or glycine. These inhibitory neurotransmittors can act both pre and post-synaptically.[12] Type I Aδ fibers have been shown to bifurcate upon entry into the dorsal horn and ascend and descend several segments. Type II Aδ have main branches that ascend in the dorsal columns giving rise to many collaterals that penetrate ventrally to the dorsal horn lamina I, where they arborize,

thus communicating with many neurons at several segmental levels.[15] Wide dynamic range (WDR) neurons that have cell bodies in Lamina V and dendrites in Lamina II-V that receive input from Aδ, Aβ and C fibers. WDRs are critical to pain relay and the development of pathological pain.[21] Peptidergic C fibers mostly terminate in Lamina I and II, while non-peptidergic C fibers terminate mostly on Lamina II interneurons.[11] Aβ fibers enter the dorsal spinal cord with ascending branches and in addition send collaterals to Lamina II and V.[16] It is possible to propose an anatomical mechanism, whereby non-noxious sensory information, such as light touch, is miscoded to noxious painful stimuli, based on the contacts that non-noxious Aβ fibers make with Lamina V, WDR neurons and the dendrites of Lamina I neurons.

1.3.1 Ascending pain transmission

From the spinal cord, 2° nociceptive projection neurons ascend to the brainstem or brain. These fibers travel to the medulla, through the pons and further rostrally to the mid-brain and on to the thalamus, the major sensory relay system of the brain. There they synapse on tertiary 3° (thalamic) sensory neurons that send projections to the post central gyrus of the cortex and other cortical areas involved in sensory processing. The post central gyrus processes the type, amplitude, location, duration of the noxious stimuli, while the hippocampus processes the memory of pain. Other pain processing occurs in the limbic system, including the amygdala, anterior cingulate and insular cortex, which together process the emotional experience of pain. Noxious stimuli activate the hypothalamic-pituitary adrenal axis, which in turn activates the sympathetic nervous system and the cardiovascular stress responses associated with pain. While there are

9

several other ascending pathways, two are important for pain transmission. First is the spino-reticular tract, composed of ipsilateral axons from laminae VII and VIII, which terminate in the reticular formation of the pons and the thalamus. The second, is the spinomesencephalic tract composed of neurons from laminae I and V, projecting from the anterolateral spinal cord to the mid-brain mesencephalic reticular formation and periaqueductal gray matter and from there via the spinoparabrachial tract to the parabrachial nuclei in the thalamus. Pain and touch sensations from the head and face mostly travel to the brainstem by the cranial nerve V, the trigeminal nerve. Most of these 1° trigeminal axons enter the mid-pons and descend in the spinal trigeminal tract to synapse with the spinal nucleus V which extends from the lower pons along the entire length of the medulla. The 2° projections from the trigeminal nucleus then cross to the contralateral side before ascending to the thalamus where they synapse on 3° neurons. A small portion of trigeminal neurons synapse on 2° projection neurons that remain on the ipsilateral side, and ascend directly to the thalamus.[19]

1.3.2 Descending modulation of pain

One of the best characterized systems of descending modulation upon the dorsal horn neurons begins in the mid-brain, peri-aquetuctal gray (PAG) and the rostral ventromedulla (RVM), including the nucleus raphe magnus and the adjacent reticular formations. The system, known as the PAG-RVM, receives ascending information from the dorsal horn of the spinal cord and responds to descending information from the higher pain processing areas in the forebrain. Conversely, the PAG-RVM sends output fibers, mostly serotonergic, back to the dorsal horn of the spinal cord, modulating nociceptive

input from peripheral sensory neurons and enkephalin releasing interneurons. The neurons of the PAG–RVM have been shown to be the main site in the CNS for the action of a number of pain suppressing agents such as endogenous opioids (enkephalins, β-endorphins, dymorphins, endomorphins and nociceptins) that bind the μ, δ, κ opioid receptors. Opioid drugs and endogenous opioids work partially by increasing inward K+ conductance, which hyperpolarizes the post-synaptic membrane and indirectly decreases Ca+ entry into the presynaptic terminals altering their GABA release.[20, 22] Other important inhibitors with receptors in this area are cyclooxygenase (COX) inhibitors[23] and cannabinoids.[24, 25] In addition, noradrenergic neurons, originating in the locus ceruleus of the pons exert descending modulation of dorsal horn interneurons via α_2-adrenergic receptors on these cells, with concurrent release of enkephalins.[26]

One role of the neurons of the PAG-RVM is to provide descending inhibitory control to the spinal cord. One example of this inhibition of pain responses or hypoalgesia (decreased response to painful stimuli) is that which occurs under extreme stress and fear. Such is the case when a soldier or athelete continues functioning on the battlefield or playing field following injury. The opposite response, hyperalgesia (increased responsiveness to painful stimuli), such as that experienced in inflammation or nerve injury, can at least in part be attributed to a shift in the balance of descending pain modulation from inhibition to facilitation.

Once thought to be only inhibitory, descending control is now recognized to be facilitory as well.[24, 27] A seminal study by H.L. Fields et al., using electrical stimulation and pharmacological blockade, demonstrated three types of cells in the RVM, ON-cells

and OFF-cells and NEUTRAL-cells.[28] When ON-cells were active, OFF-cells were silent and visa versa. Subsequent experiments confirmed that OFF-cells function to inhibit nociceptive neurons in the dorsal horn and as such are anti-nociceptive, while ON-cells are facilitory or pro-nociceptive. The role of NEUTRAL-cells in pain modulation has not yet been clearly established.[28] ON-OFF cells have also been shown to exert similar influence from the PAG.[29] The equilibrium between these two cell populations in the RVM has been associated with the subtle shifts of spinal nociceptive responses leading to chronic pain.

1.4 Pathological Pain

In some cases, such as after a traumatic injury or wound infection, pain itself can become pathological. Some examples are post-surgical pain, phantom pain following an amputation, diabetic neuropathy, fibromyalgia and complex regional pain syndrome (CRPS).[30] Normally, pain serves to protect individuals from harmful stimuli that might cause severe tissue damage or injury. Typically, when the harmful stimulus is removed the pain goes away.[30] Chronic pain, clinically defined as lasting greater than 3 months, is no longer adaptive or serving any useful purpose.[31] Neuropathic pain is typically characterized by hyperalgesia and/or allodynia, a condition in which stimuli not normally considered painful, such as a light touch, is perceived as excruciatingly painful.[32] Primary hyperalgesia occurs at the actual site of the peripheral injury and is very intense, while secondary hyperalgesia is in the surrounding, uninjured tissue, and is usually of lesser intensity.[33] Chronic neuropathic pain is a serious clinical problem that effects millions of people annually costing billions of dollars while current treatments are sorely inadequate.

[31] In a survey conducted by the American Pain Foundation, of 303 pain sufferers currently on opioid medications, 50% felt that they had little or no control over their pain and 60% experienced break through pain that severely affected their quality of life.[34]

There are at least four proposed hypotheses as to how acute pain becomes chronic.[35] The first is synaptic "plasticity" involving modulation of synaptic efficacy. Primary sensory neurons can become sensitized or respond to equal or lesser stimuli with greater firing frequency and more release of neurotransmitter. This can happen between either two similar (homosynaptic) types of neuronal fibers, or between two different (heterosynaptic) fiber types. A second important mechanism involves NMDA receptors, producing Ca+ dependent long-term potentiation. The third is loss of inhibition from descending pain modulatory pathways and interneurons. Finally, glial cells, activated by inflammatory immune responses have been shown to contribute to the onset of pathological pain. These mechanisms are explained in detail in the sections that follow.[35]

1.4.1 Peripheral Sensitization

If a 1° nociceptive terminal ending is exposed to sustained stimuli, it fires a barrage of action potentials that can lead to temporal and spatial summation accompanied by short-term changes at the terminals, known as peripheral sensitization. In now classic studies Medall, in 1984,[36] showed that a repeated low frequency firing of nociceptive C fibers leads to a progressive increase in action potential frequency, with the co-release of glutamate, substance P and CGRP from both peripheral and central terminals. The result is increased membrane excitability and lowered threshold for receptor activation, occurring centrally as well as peripherally. Now while there change in their intensity,

subsequent stimuli, even those that are non-noxious, can be perceived as more painful,.

This form of short-term potentiation of synaptic signaling terminates when the sensory stimulus is removed.[37-39]

With prolonged firing, endogenous factors are also released from terminal endings of nociceptors, including serotonin, cytokines interleukin-1β (IL-1β), substance P, protons such as H+, reactive oxygen species (ROS) and other factors that facilitate leukocyte migration or extravasation in the tissue injured region. In turn extravasating innate immune cells such as mast cells, macrophage and dendritic cells release even more factors that compound the excitement of nerve terminals. Together, these molecules are known as the "inflammatory soup".[40, 41] As a consequence, peripheral nerve terminals are dramatically sensitized, leading to decreased nociceptor-activation thresholds, which if sustained, can lead to pathological pain.[37, 39]

1.4.2 Central Sensitization

In the CNS there are essentially four general mechanisms that contribute to "central sensitization", a form of long term enhancement or facilitation of output from the dorsal horn of the spinal cord following injury. These include: 1) increased trafficking of AMPA receptor subunits to the synapse, particularly those that are Ca^{2+} permeable, 2) activation of NMDA receptors with sufficient depolarization of the neuronal membrane to allow expulsion of a magnesium ion (Mg^{2+}) that under resting conditions normally blocks the central channel of the NMDA receptor, 3) activation of kinases, enzymes capable of phosphorylating membrane channels and receptors altering their activity, and 4) activation of downstream intracellular signaling pathways.[38, 39, 41]

14

To expand in more detail, with repetitive and prolonged nociceptor firing, there is sufficient binding of glutamate to fast acting AMPA receptors, and generation of enough post-synaptic depolarization, to activate NMDA receptors. The voltage change results in expulsion of a magnesium (Mg^{2+}) ion normally blocking its central channel. The opening of this channel allows for a rapid influx of Ca^{2+} into the neuron and activation of Ca^{2+}dependent kinases. Some of these are the Ca^{2+}-calmodulin dependent protein kinase (Cam-KII), protein kinase C (PKC) and protein kinase A (PKA). All are capable of phosphorylating of tyrosine and serine residues on subunits of the AMPA and NMDA receptors with the subsequent activation of intracellular signaling pathways. The Ca^{2+}dependent signaling occurring in the development of chronic pain has been suggested to be similar to the changes thought to be occurring in long term potentiation (LTP) of memory in the hippocampus.[42] Elevated Ca^{2+} levels drive the calmodulin-induced activation of adenylyl cyclases, increasing cAMP and turning on PKA. Other pathways sustaining central sensitization are the phosolipase C/phosphokinase C (PLC/PKC) pathways that facilitate release of Ca^{2+} from the endoplasmic reticulum. Another is the mitogen-activated protein kinase (MAPK) pathway activating the kinases (ERK 1 and ERK 2), serine threonine kinases that turn on genes under the control of the cAMP response element binding protein (CREB), a nuclear transcription factor. Such signaling ultimately results in long term changes in gene expression, with transcriptional up regulation of pain neurotransmitters, modulators and their receptors with increased trafficking of the receptors to the cell surface and expansion of receptor fields. Nociceptors are now firing with greater frequency to stimuli of lesser intensity.[32, 39]

15

1.4.3 Loss of inhibition

Critical to the enhancement of excitatory pain responses is loss of local DH spinal inhibitory influences. Activation of Aδ fibers causes long term NMDA and CA2+ depression of DH inhibitory interneuron firing and internalization of AMPA receptors.[43] Peripheral nerve injury can cause the death or apoptosis of GABAergic interneurons in the dorsal horn contributing to disinhibition of nociceptive inputs. This cell death may be the direct result of glutamate in the synapse. High levels of glutamate are known to be toxic in neurons .[42, 44, 45]

Loss of descending pain inhibition also exacerbates the chronicity of pain. It has been shown that in conditions of chronic inflammation, such as in chronic arthritis that ON-cell firing predominates, with elevation of c-fos, a transcription factor up-regulated following recent neuronal activity.[46] Studies using c-fos labeling to demonstrate dynamic neuronal activity, have shown that descending inhibition from the VLM failed to inhibit the powerful nociceptive pain signaling from the spinal cord in the early stages of inflammation. Thus, the control from the brain and brainstem during inflammation or nerve injury can contribute to the positive feedback loops leading to pathologic pain states.

1.4.4 Glial cells

Research in the last 15+ years has shown that neuropathic pain is at least in part the consequence of activated immune cells and immune-like glial cells in the CNS.[40, 47] This activation has been shown to alter and amplify normal nociceptive signaling, leading

to alteration of the perception of pain and its chronicity. Both innate and adaptive immune cells are also important for pain modulation, not only in acute peripheral inflammation and nerve trauma, but also in development of persistent pain. [40, 47] Spinal glial cells are widely characterized to be activated by excitatory factors (e.g. substance P, ATP) released from the central terminals of Aδ, Aβ and C fibers. In turn these activated glia release factors, discussed below, that further stimulate nearby neurons and glia creating a positive feed-forward excitatory loop.[48, 40]

While there are three glial cell types found in the CNS, the most widely characterized to play a role in the development of neuropathic pain signaling are microglia, considered the resident immune cell of the CNS and astroglia, known for their role in glutamate uptake and neuronal homeostasis (neuronal nutritional support and participation in the blood brain barrier). [47, 49, 50] Recently, the oligodendrocyte, the third glial cell, responsible for myelination of axons, has been suggested to respond to pro-inflammatory signaling by IL1-β, in a white matter injury in mouse brain resulting in increased secretion of metalloprotease-9 (MMP-9) with the promotion of small blood vessels and capillaries (angiogenesis) into the injured area. [51] Another study has shown IL-1-β to disturb oligodendrogenesis and increase the number of nonmyelinated neurons in neonatal mice.[52] Under normal conditions quiescent astrocytes and microglia are scattered around the spinal parenchyma.[38] Once glial cells become activated, they secrete pro-inflammatory cytokines (IL-1β, Il-6 TNF-α, INF-γ) as well as prostaglandins, diffusible nitric oxide (NO), ROS, complement proteins, histamine and other small molecules. Concurrent with this release and glial activation, are phenotypic changes in their normal resting morphology to a more spindly, branched appearance when active.

Glial activation contributes to the dysfunction of excitatory signaling from nociceptors. [40, 47, 48] The result is altered expression of cytokines, cytokine receptors, volt-gated sodium channels, increased release of glutamate and enhanced glutamate receptor functions in both peripheral and central axon terminals. All these changes subsequently provoke disinhibiton at the level of spinal cord and from higher pain regulatory pathways and activation and migration of peripheral and CNS resident immune cells. To resolve inflammation and restore homeostasis to the extracellular environment, the onset of a pro-inflammatory state is followed by a delayed release of anti-inflammatory cytokines interleukin-4 (IL-4), interleukin-13 (IL-13), IL-10, and transforming growth factor-beta (TGF-β). These restore the local environment to its basal state. [40, 47, 48]

1.5 Immunological interactions mediate pathological pain

1.5.1 Innate and adaptive immunity

There are essentially two types of immune responses, each with its own specialized cells. The cells in the "innate" or early immune response, have genetically evolved to recognize specific molecular patterns on invading pathogens or microbes, known as pathogen associated molecular patterns (PAMPS). Innate immune cells, such as the antigen presenting cells (APCs), macrophage, dendritic cells (DCs), have specialized receptors known as patterned recognition receptors (PRRs) which bind PAMPs, activating cell signaling pathways. Receptor activation and the release of certain cytokines can stimulate a dynamic process known as phagocytosis in which the pathogen/receptor complex is engulfed by cytoplasm and carried into the cell in specialized cell surface sub-cellular vesicles or phagosomes. There, the foreign matter is

18

broken down in to small molecular pieces known as antigens. Antigens are then presented to the cells of the adaptive immune system, namely B and T cells, by protein complexes on the cell surface. These complexes are known as major histocompatibility complex (MHC). All cells of the innate immune system are capable of the processes involved in antigen presentation.[53]

When presented with antigen and in the presence of critical co-stimulatory molecules, B cells produce and secrete antibodies that are specific to each antigen. The antibody/antigen complexes then bind specialized receptors on phagocytic macrophages and are destroyed by cellular enzymes. The second response is cell-mediated immunity and relies chiefly on T helper 1 (Th1) cells and T helper 2 (Th2) and other T cells. [40, 53]

In the periphery and CNS innate leukocytes, like macrophage and DCs, are continually surveying for foreign materials or pathogens and are rapid responders. Adaptive immune responses directed by B and T cells are much more delayed as they must be presented antigen by APCs before becoming activated.

1.5.2 Innate Immune Cells Display Two Distinct Activation Profiles

Macrophages and DCs, are capable of two polarized states. M1 or "classical" activation is created by expression of pro-inflammatory cytokines, such as IL-1β, TNF-α and others, important for pathogen clearance following viral or bacterial derived recognition of PAMPs. M1 macrophage assume a rounded morphology, express more receptors for the pro-inflammatory cytokines and can be characterized by

immunohistochemistry using antibody to human CD68 (rat ED1) a 110 kD protein primarily expressed on M1 macrophage cells.[54-56]

Conversely, the M2 activation profile is distinguished by the presence of anti-inflammatory cytokines IL-4, IL-13 and IL-10,[54-56] and mostly associated with phagocytic activity during wound healing and clearance of dying cells or cells undergoing apoptosis. M2 polarized cells can be characterized by the markers, human CD163 (rat ED2), a 130 kD macrophage associated antigen, which is a member of the scavenger receptor family, exclusively expressed by monocytes and macrophages and mannose receptor (MR; human CD206), a classic marker of alternative macrophage activation.[47, 49, 50, 54-56]

In the past, the CNS was considered "immune privileged" such that under normal conditions, the neurons of the brain and spinal cord parenchyma were protected from immune cell invasion by the endothelial blood brain barrier (BBB). It was thought that only in the event of an infection or inflammatory process, did these barriers open and allow the passage of immune cells. The more recent perspective is that immune traffic is normal and necessary for protection from infection and cancer.[57, 58] In actuality, the CNS contains many cells that when activated can release and express receptors capable of responding to cytokines, inflammatory and pain mediators and contribute to pathological pain signaling. Antigen presenting macrophage, DCs and other leukocytes capable of mounting immune responses and cytokine release, reside in the meninges and around small spinal capillaries and blood vessels and in peri-vascular spaces around the central spinal canal. [47, 59]

1.6 Interleukin-10 a powerful anti-inflammatory cytokine

One of the most powerful anti-inflammatory cytokine, is interleukin-10 (IL-10). IL-10 dramatically inhibits the exacerbation of the pro-inflammatory responses preventing potential cellular and organismal damage.[60-62] In the CNS, IL-10 is endogenously produced by innate immune cells, such as microglia,[63-65] macrophages,[66, 67] and DCs.[60-62] Astrocytes also express receptors for this cytokine.

The binding of IL-10 to its receptor initiates a number of phosphorylation events that activate the Janus kinase (JAK)/ signaling transducer and activator of transcription (STAT) signaling pathway and leads to long-term transcriptional alterations. The receptor is composed of two subunits, IL-10R1 and IL-10R2 subunits. Two IL-10 molecules form a homo-dimer that bind the receptor and constitutively activate two tyrosine kinases, Jak1 and Tyk2, associated with the IL-10R1 and IL-10R2 cytoplasmic tails respectively.[62] Activation of these residues is followed by the recruitment of STAT3 to the receptor and phosphorylation of its Tyr705 residue.[60] Phosphorylated STAT3, then translocates to the nucleus, and binds a STAT3 recognition sequence in the transcriptional promoter for the interleukin 1 receptor antagonist (IL-1Ra). Subsequent chromatin remodeling and histone acetylation at this promoter exposes other transcription sites to transcription factors such as the p65/p50NFκ-B and upregulates expression of IL-1Ra. IL-1Ra is a cytokine capable of profound reduction in proinflammatory signaling by the IL-1β cytokine and others. A delayed expression of more IL-10 and IL-10 receptor contributes to a robust anti-inflammatory response.[60, 62]

21

1.6.1 IL-10 as a Therapeutic for Chronic Neuropathic Pain

Capitalizing on it natural anti-inflammatory effect, prior work has shown that peri-spinal intrathecal injection of IL-10 protein can reverse neuropathic pain. However, the reversal was only transient, lasting less than 24 hours, an observation explained as being due to the short, ~ 2 hour, half-life of the protein. Next, a similar injection strategy was attempted using a naked plasmid, containing the gene for IL-10. The hypothesis was that over-expression of IL-10 protein near the area of the dorsal spinal cord, responsible for pain modulation would prolong pain relief. Indeed, the hypothesis proved correct. Pain relief was prolonged to 3 months, but required two injections and excessive doses of DNA, (125 μg), which is of limited clinical usefulness when translated to humans.[68]

1.6.2 Period of Sensitization and Cell Enrichment

An important discovery was observed during these initial studies. There was a discrete interval or "sensitization period" between the two i.t. injections, between 5 hours and 3 days, during which the first injection served to sensitize the sub-arachnoid compartment to the second injection.[69] If the second injection was given outside this time window, the length of pain reversal was dramatically shortened, from 3 months to 10 days.[69]

Examination of CSF during the sensitization period showed that it was enriched with cells that were found to be mostly macrophage expressing an activated phenotype (possible proinflammatory), identified by the a cell surface glycoprotein, ED1(CD68).[69] By six hours, the number of ED1 positive cells had dramatically declined. Six days later,

the majority of cells expressed the anti-inflammatory phenotype, identified by ED2 (CD163), another cell surface glycoprotein. More importantly, increased expression of ED2 positive cells paralleled the increase of endogenous IL-10 production in the sub-arachnoid space, following injection of pDNA.[69]

Cell enrichment and sensitization by immune cells can be stimulated by factors that act as PAMPs but without the presence of actual bacteria or virus. [70, 71] An example are cytosine-phosphate-guanine (CpG) DNA sequences that occur with high frequency in bacterial DNA. Naked DNA used in these studies, contains many of these stimulatory sequences which may have been responsible for activation of immune cells following the first injection of pDNA-IL10 in these early experiments.[72] By the time of the second injection, three days later, M2 polarized macrophage were poised and ready for phagocytosis and efficient uptake of the IL-10 transgene.[72, 73] Facilitating a switch from M1 activation to M2 activation of the subarachnoid immune and spinal glial cell milieu was hypothesized to be one approach to harness innate immune responses for optimal transgene uptake and expression.

In an effort to improve transgene uptake by inducing M2 polarization of peri-spinal macrophage, Sloane et al. explored the use of a discrete CpG containing oligodeoxynucleotide sequence, ODN2006, as candidate gene transfer adjuvant.[72] This ODN sequence is a natural ligand for toll-like receptor 9 (TLR9), an endosomal receptor in macrophages, and part of a large family of Toll-like receptors (TLRs).[71] CpG sequences are taken up by macrophages and transported by clathrin-coated vesicles to the endosome where they fuse and bind to TLR9. This can induce the expression of

endogenous IL-10, leading to a phenotypic switch from a pro-inflammatory to an anti-inflammatory profile shown to facilitate phagocytosis.[71,74] A priming injection of ODN2006 (2 μg), administered 3 days prior to a low dose of naked pDNA-IL-10 (25 μg), causes pain reversal to baseline levels but only for approximately one month. This data can be interpreted that ODNs may act as adjuvants.

In Chapter 3 of this dissertation, two alternative transgene adjuvants, Dexamethasone (Dex) and D-mannose, are used with pDNA-IL-10 to achieve enduring pain reversal. Both Dex and D-mannose are known to bind their cognate receptors, glucocorticosteroid receptor (GR) and mannose receptor (MR), respectively. This binding triggers anti-inflammatory signaling cascades in leukocytes (macrophage and dendritic cells) and results in the release of IL-4, IL-10 with a concurrent reduction in pro-inflammatory cytokine levels, such as IL1-β and TNF-α, leading to a switch from an M1 to an M2 phenotype. M2 polarization is accompanied by enhanced phagocytic ability.[75-77] We hypothesized that a priming injection of Dex or D-mannose as an adjuvant might facilitate a switch from M1 to M2 polarization of leukocytes near the injection site in the spinal cord. The consequence would be the enhancement of IL-10 transgene uptake with subsequent IL-10 expression, thereby achieving allodynic reversal with lower doses and number of injections. Such expression of the anti-inflammatory IL-10 protein by meningeal cells, microglia, dendritic cells and astroglia near the injection site would allow for diffusion of the IL-10 cytokine directly near the source of the pathologic pain response.[78, 79]

1.6.3 Strategies for intrathecal delivery of pDNA-IL-10 for long term expression of IL-10

1.6.3.1 Naked Plasmid

One of the key barriers for transgene delivery of a naked plasmid DNA (pDNA) is translocation across the cell membrane. Moreover, the exact mechanisms by which the non-viral pDNA reaches the cell nucleus are not well characterized. One potential route is by pinocytosis, a process that all cells are capable of performing. The cell membrane surrounds the DNA engulfing it in a small vesicle which then travels through the cytoplasm and fuses to a larger vesicle known as an endosome (pH 5.0-5.5). The DNA must escape the endosome or it can be carried to a lysosome (pH 4.0-4.5) where DNA degradation occurs. If the DNA successfully escapes the endosome, it must travel across the cytoplasm to the cell nucleus where it must cross the nuclear membrane by fusion or passage through nuclear pores to reach the cellular transcription machinery. Other than pinocytic endocytosis, potential mechanisms for pDNA entry are 1) phagocytosis or engulfment by specialized cells such as macrophage, 2) receptor mediated endocytosis, or 3) entry during mitotic breakdown of the outer cell and nuclear membranes during cell division.[80]

As noted previously, in order to be transcribed pDNA must cross the nuclear membrane or envelope. In replicating mitoic cells, the membrane breaks down and the DNA easily crosses, but in cells that are post-mitotic, this process is more difficult. The nuclear envelope is a double membrane crossed by many large protein complexes known as nuclear pore complexes (NPCS) which regulate transport. NPCs have a pore size of ~9 nm, which allow free diffusion of small and medium ions and molecules up to 40-60 kD

or nucleic acids up to 300 bp. Non-dividing transport of larger molecules such as pDNA, requires a sequence specific nuclear localization signal (NSL), which is recognized by specialized proteins called importins. Protein-NLS/importin complexes dock at the NPC allowing DNA entry.[81] The nuclear entry of transfected DNA is accomplished indirectly by its association with NLS on transcription factors.[82]

1.6.3.2   Synthetic carriers for gene delivery

It is thought that synthetic delivery platforms can assist in enhancing transgene expression by protecting DNA from acidic degradation and promoting endosomal escape.[83] Certain synthetic formulations lower energy barriers and promote membrane fusion or attract protons (H+) creating an osmotic sponge attracting water molecules, which burst the endosomal membrane.[84, 85]

The studies presented in Chapter 1 of this dissertation investigate the potential of using a novel silica particle supporting a lipid bilayer known as a "protocell" as a possible platform to deliver the 5.9 kilobase pair (kb) pDNA-IL-10 to the CNS by intrathecal injection. At the time these studies began, protocells had never been taken *in vivo* in the CNS, so the initial goal was to simply see if they would be tolerated by the animals and to determine their anatomical biodistribution following intrathecal injection. In addition we wanted to know what spinal cells were interacting with them. Another question was whether the IL-10 transgene loaded on protocells could successfully transfect cells, and if the transgene generate functional IL-10 protein following transfection. Finally, as proof of concept, we wanted to know if IL-10 loaded on protocells could be utilized as therapeutic IL-10 gene vector that would reverse allodynic behavior in neuropathic rats. We set out to

determine these goals *in vivo* using 62 Sprague-Dawley rats and *in vitro* with cell culture studies. The protocells used in these experiments were "first generation" protocells similar to those used by Liu, et al.[100,101,215] The mesoporous silica core had a diameter from ~150-200 nm and a range of pore diameters of ~1-10 nm. The majority of pores were ~3 nm in diameter. The core supported either a positively charged, DOTAP:CHOL 1:1 lipid or a zwiterionic, neutrally charged DOPC lipid. Silica at pH7 is negatively charged[95] and would repel the negatively charged pDNA-IL10, so 10% aminoproyltriethoxysilane APTES was included to reverse the charge of the silica to positive. (Please refer to Chapter 1 (Methods) for more detail.) It is important to note that at the time of these experiments, these were the only protocells documented.[100,101,215] By the time the "next" generation of protocells was developed,[94] animals and materials had been utilized and the goals outlined above had been completed. It was imperative in these initial studies that we establish a fundamental understanding of protocell distribution in the CNS and any potential for toxicity in our animal model of neuropathic pain, before further modifying the delivery vector, protocells.

In total, 3 different protocell cargos were used in the experiments in Chapter 1. The first, was a red fluorphore Dextran tetramethyl rhodamine (DexRHO). The second was a FAM-tagged 18 base pair single stranded DNA oligomer. FAM is a green fluorophore used as a reporter in our microscopic examination of protocell distribution in the CNS and body following intrathecal injection of the particles. The third cargo was a 5.9 kilo base (kb) plasmid, encoding the gene for IL-10. While determining exactly how these cargos load on the protocell was not a goal of the studies in Chapter 1, we have speculated how these molecules would load on the protocell in the schematic below (Scheme 1 A-C).
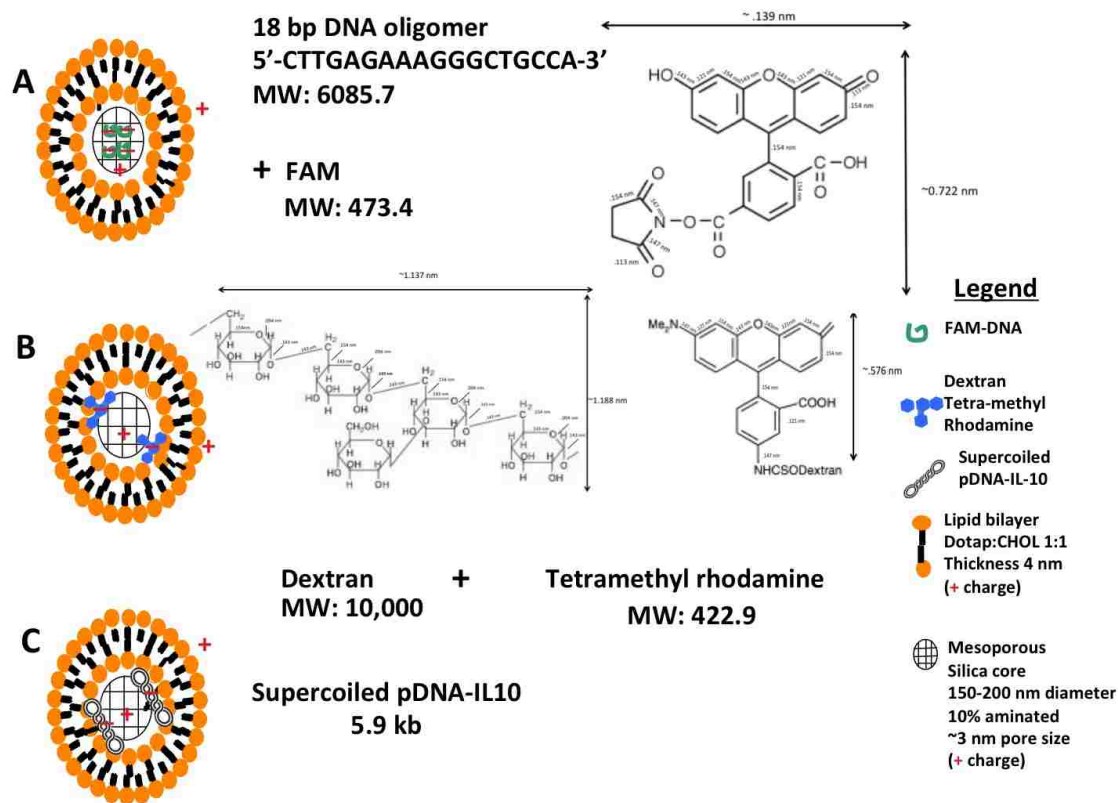
Scheme 1- Schematic showing theoretical loading of 3 protocell cargos- A) This cargo is a negatively charged, 18 bp DNA oligomer with an approximate length of 6.12 nm and a diameter of ~2. It is tagged with a negatively charged fluorophore, FAM, which has a MW of 473.4 and an approximate planar length of .139 nm and height of .722 nm, as calculated by bond lengths. FAM-tagged DNA may load directly into the silica pores (~3 nm diameter). B) Negatively charged dextran tetramethyl-rhodamine (DEXRHO) is composed of a dextran polymer with a MW of 10,000 conjugated tetra-methyl rhodamine groups. The tetramethyl-rhodamine group has an approximate planar length of .983 nm and height of .576 nm as calculated by bond lengths. This very large molecule is thought to load onto the protocell by adsorption with the positively charged DOTAP:CHOL 1:1 lipid bilayer and positively charged 10% aminated mesoporous silica core. C) Negatively charged plasmid encoding the gene for IL-10 most likely assumes a supercoiled structure and is thought to load by adsorption in a manner similar to DEXRHO. During the synthesis process each cargo was mixed with the silica and rinsed 3xs with PBS before the liposomes were added.

A more in depth discussion regarding the loading of these cargos and the advantages and disadvantages of using protocells and other synthetic platforms for gene delivery will presented in Chapter 4, the discussion section of this dissertation.

1.7 Global Hypothesis **Synthetic delivery platforms and small molecule adjuvants will improve the efficacy of spinal interleukin-10 gene therapy for chronic neuropathic pain.**

1.8 Research objectives and aims: original and revised

As experiments progressed, the sequence and content of the original research aims was revised to better correlate with the data being observed. The original aims and revised aims are outlined below for the reader's convenience.

Specific Aim I: Encapsulating pDNA-IL-10 in PLGA microparticles (pDNA-IL10-PLGA) will safely reduce the dose and number of injections required to provide pain relief of 3 months or greater

   Specific Aim IA: In vitro characterization of PLGA:

   1) To determine if cultured mammalian cells will remain viable following application of pDNA IL-10-PLGA.

   2) To determine if cultured mammalian cells transfected with pDNA-IL-10-PLGA will express higher levels of IL-10 protein than when transfected with naked pDNA-IL-10.

   Specific Aim IB: In vivo characterization of PLGA :

   1) To determine if pDNA-IL10-PLGA will produce pain relief for 3 months with only one i.t. injection

   2) To determine if pDNA-IL-10 must be encapsulated to produce pain relief for 3 months or greater

   3) To determine if there is an optimal dose of pDNA-IL-10-PLGA that will provide enduring pain relief lower both the doses of pDNA-IL-10 and PLGA while a ratio of 1:100 is maintained (1 ug pDNA-IL-10/100 ug PLGA; ratio = 1/100)

      a) Lower the dose of pDNA-IL-10 while the PLGA dose is constant (1 ug pDNA-IL-10/ 1 mg PLGA; ratio = 1/1000)

Specific Aim II: Protocells can be safely used to deliver small molecules or pDNA-IL10 (pDNA-IL-10-PCs) to the CNS for enduring pain relief of 3 months or greater

   Specific Aim IIA: In vitro studies: to determine the dissolution and biocompatibility characteristics of protocells

   1) To determine the dissolution rate of protocells over time at different physiological pH (temperature held at 37ºC)

   2) To determine if cultured mammalian cells will remain viable following application of pDNA-IL-10GFP-PCs

   3) To determine if cultured mammalian cells can be transfected with pDNA-IL-10GFP-PCs to produce measurable levels of IL-10 protein

Specific Aim IIB: In vivo studies: characterization of protocells and assessment of functional transgene delivery

    1) Biocompatibility following spinal delivery in rats

    2) Biodistribution in the CNS and body

    3) Characterization of cellular interactions

Specific Aim IIB1: Protocell delivery of pDNA-IL-10 will cause pain reversal in neuropathic rats

Specific Aim III: Protocells loaded with known adjuvants and co-administered with pDNA-IL10-PLGA will lower the transgene dose required to reverse pain for 3 months or greater

Specific Aim IIIA: In vitro studies-characterization of the cellular influence of adjuvants (Dex and ODNs)

    1) To determine if mammalian cell cultures are viable in the presence of adjuvant loaded protocells

    2) To determine if IL-10 protein levels are improved if adjuvant molecules are co-administered with pDNA-IL-10-PLGA

    3) Characterization of the pro or anti-inflammatory cellular profile of macrophage cells interacting with adjuvant loaded protocells

Specific Aim IIIB: In vivo studies- behavioral characterization

    1) To determine if protocells loaded with adjuvants co-injected with pDNA-IL-10-PLGA extend pain reversal

    2) To determine if IL-10 gene expression and pain relief will be blocked or altered by an anti-IL-10 neutralizing antibody

1.8.2 Revised Aims

Specific Aim I: Protocells can be safely used for spinal delivery of pDNA encoding the IL-10 gene.

Specific Aim IA: In vitro characterization: to determine the release and biocompatibility characteristics of protocells

    1) To determine the release rate of protocell cargo over time at different physiological pH (temperature held at 37ºC)

2) To determine if cultured mammalian cells will remain viable following application of pDNA-IL-10GFP-PCs

3) To determine if cultured mammalian cells can be transfected with pDNA-IL-10GFP-PCs to produce measurable levels of IL-10 protein

Specific Aim IB: In vivo characterization and assessment of functional transgene delivery

1) Biocompatibility following spinal delivery in rats

2) Biodistribution in the CNS and body

3) Characterization of cellular interactions

4) Protocell delivery of pDNA-IL-10 will cause pain reversal in neuropathic rats

Specific Aim II: Immune adjuvants will lower the transgene dose required to reverse chronic neuropathic pain

Specific Aim IIA: Characterization of immune adjuvants to initiate the sensitization period for improved pain reversal with low dose IL-10 gene

1) To determine if a priming injection of DEX will lower the required IL-10 gene dose for prolonged pain reversal

Specific Aim IIB: Characterization of D-mannose as an M2 polarizing agent

1) In vitro: To determine if D-mannose induces an M2 polarized profile in macrophage

2) In vivo: To determine if D-mannose alone leads to pain reversal

Specific Aim IIC: To identify an M2 polarized profile following the sensitization period in pain-reversed rats

1) In vivo: To determine if IL-10 or IL-1β protein levels are altered in the spinal cord if the best candidate adjuvant is delivered prior to naked pDNA-IL-10

Specific Aim IID: To determine if a single co-injection of D-mannose with low dose pDNA-IL-10 will generate enduring pain reversal

1.9 Brief Summary of Each Chapter

Chapter 2 describes experiments that characterize the release rates of protocell cargo, formulated with either DOPC or DOTAP:Cholesterol lipids. Different pH and time values were examined in an effort to understand cargo release under specific conditions. These two protocell formulations were tested *in vivo* by injecting them into the peri-spinal, i.t., space in Sprague-Dawley rats and found to be biocompatible and non-toxic over an 8 week time course. Interestingly, protocells supporting the two different lipids revealed not only slightly different release kinetics *in vitro*, but a clear difference in distribution patterns *in vivo* and transfection efficiency. These studies are the first demonstration that protocell vectors can be used as a non-viral platform for spinal delivery of a therapeutic gene to reverse allodynia in neuropathic rats, albeit for a short duration.

Chapter 3 explores the use of the two small molecules, Dex and D-Mannose, referred to as gene therapy M2 polarizing adjuvants. I observed that compared to Dex, D-Mannose was superior in priming prolonged and dose dependent suppression of pain in neuropathic rats at low transgene IL-10 doses. Macrophage cell culture studies demonstrated that D-Mannose was capable of reducing levels of proinflammatory modulators, the cytokines IL-1β and tumor necrosis factor TNFα and nitric oxide (NO) while increasing endogenous and transgene derived IL-10 protein levels of IL-10, supporting notion that the adjuvant, D-mannose altering spinal immune cells in the direction of an M2 phenotype and improved efficiency of transgene uptake.

2. Mesoporous silica-supported lipid bilayers (protocells) for DNA cargo delivery to the spinal cord

Ellen C. Dengler[a], Audra Kerwin[b], Juewen Liu[c], Clara M. Olcott[d], Brandi N. Bowman[e], Leisha Armijo[f], Katherine Gentry[g], Jenny Wilkerson[h], James Wallace[i], C. Jeffrey Brinker[j], Erin D. Milligan*[k]

[a] edengler@salud.unm.edu; Department of Neurosciences, Health Sciences Center, University of New Mexico, Albuquerque, New Mexico

[b] akerwin@salud.unm.edu; Department of Neurosciences, Health Sciences Center, University of New Mexico, Albuquerque, New Mexico

[c] liujuewen@gmail.com; Department of Chemical and Nuclear Engineering, University of New Mexico, Albuquerque, New Mexico

[d] colcott@salud.unm.edu; School of Medicine, University of New Mexico, Albuquerque, New Mexico

[e] bbowman@salud.unm.edu; Department of Neurosciences, Health Sciences Center, University of New Mexico, Albuquerque, New Mexico

[f] leisha.armijo@gmail.com; Department of Neurosciences, Health Sciences Center, University of New Mexico, Albuquerque, New Mexico

[g] k8gentry@gmail.com; Department of Anesthesiology and Critical Care Medicine, Health Sciences Center, University of New Mexico, Albuquerque, New Mexico

[h] jlwilkerson@salud.unm.edu; Department of Neurosciences, Health Sciences Center, University of New Mexico, Albuquerque, New Mexico

[i] jwallace@salud.unm.edu; Department of Neurosciences, Health Sciences Center, University of New Mexico, Albuquerque, New Mexico

[j] cjbrink@sandia.gov; Department of Chemical and Nuclear Engineering, University of New Mexico, Albuquerque, New Mexico

*[k] To whom correspondence should be addressed:

Erin D. Milligan
Department of Neurosciences, Health Sciences Center, School of Medicine
University of New Mexico,
Albuquerque, N.M., USA 87131-5223
PH: 505-272-8103
FAX: 505-272-8082
E-mail: EMilligan@salud.unm.edu

Abstract

Amorphous mesoporous silica nanoparticles ('protocells') that support surface lipid bilayers recently characterized *in vitro* as carrier constructs for small drug and DNA delivery are reported here as highly biocompatible both *in vitro* and *in vivo, involving* the brain and spinal cord following spinal delivery into the lumbosacral subarachnoid space (intrathecal; i.t.). Specifically, positively charged, 1, 2-Dioleoyl-3-Trimethylammonium-Propane (DOTAP)-cholesterol (DOTAP:Chol) liposome-formulated protocells revealed stable *in vitro* cargo release kinetics and cellular interleukin-10 (IL-10) transgene transfection. Recent approaches using synthetic non-viral vector platforms to deliver the pain-suppressive therapeutic transgene, IL-10, to the spinal subarachnoid space has yielded promising results in animal models of peripheral neuropathy, a condition involving aberrant neuronal communication within sensory pathways in the nervous system. However, these non-viral platforms are limited in terms of tuning cargo release-rates and surface chemistries, thereby minimizing flexibility in lowering dosage formulations. We report here that i.t. delivery of protocells, with modified chemistry supporting a surface coating of DOTAP:Chol liposomes and containing the IL-10 transgene, results in functional suppression of pain-related behavior in rats for extended periods. This study is the first demonstration that protocell vectors offer amenable and enduring *in vivo* biological characteristics that can be applied to spinal gene delivery.

2.1 Introduction

The development of synthetic non-viral vectors for gene therapeutic purposes has steadily increased during the past 10 years, an effort that is reflected by increased non-

viral gene therapeutic clinical trials worldwide.[86, 87] While viral vectors are superior in gene transfection efficiency, non-viral gene transfer systems are associated with less safety concerns. The application of central nervous system (CNS) non-viral gene transfer to express therapeutic proteins is significantly underexplored in light of the broad-ranging therapeutic potential in controlling a host of neurological diseases. The arsenal of potential clinical gene delivery platforms includes cationic lipids and peptides, co-polymers, polymeric micelles, and modified silica nanoparticles.[88-90] Indeed, a significant amount of progress toward our understanding and utilizing mesoporous silica nanoparticles (MSN) for controlled drug and gene release, while optimizing biocompatibility, has occurred in recent years.[91] Silicas are present in crystalline and non-crystalline (amorphous) forms, with amorphous silica occurring either naturally or are synthesized. While crystalline silica is widely associated with adverse health effects including silicosis that involves proinflammatory cytokine-mediated pathogenesis, virtually no toxicity has been identified with synthetic amorphous silicas at moderate doses.[92, 93] Therefore, synthetic amorphous silicas have been explored in biomedical applications including targeted drug delivery for cancer chemotherapeutics and DNA delivery for gene therapy.[94, 95] The major advantage of using synthesized MSNs is that their surface can be chemically modified, resulting in improvements in their drug cargo capacity, as well as facilitation of tunable release rates which further enhances their biocompatibility and functional capabilities.[96]

Mesoporous silicas contain a porous structure with hundreds of channels referred to as mesopores, which are able to adsorb bioactive molecules.[96] The properties of MSNs include a large surface area (> 900m2/g), large pore volumes (> 0.9 cm3/g), a tunable

36

pore size (~1-30 nm), and good chemical and thermal stability; all of which contribute to their suitability for controlled drug release applications. Additionally important, efficient cellular uptake of mesoporous silica particles is size-dependent, with optimal uptake occurring at the sub-micron scale with potential for controlled DNA release.[90]

Non-viral spinal gene therapy to suppress neuropathic pain is a relatively new approach that has resulted in successful therapeutic outcomes in a variety of animal models of pathological pain produced by peripheral nerve inflammation and/or trauma from systemic cancer chemotherapeutic administration, peri-sciatic immune activators, or chronic constriction injury.[73, 79, 97-99] However, high transgene doses and limited cargo loading efficiency of polymer platforms were observed, which may minimize the clinical utility of this delivery method. One approach to circumvent these limitations is to deliver therapeutic genes utilizing MSNs for transgene delivery due to their flexibility in cargo loading and release.

In the present work, *in vitro* and *in vivo* long-duration biocompatibility, biodistribution, and functional gene expression following delivery to the spinal cord was conducted using cationic amine-chemically-modified (functionalized) mesoporous silica cores with ~2 nm diameter pores prepared by aerosol-assisted self-assembly, with phospholipid bilayers fused to the core surface. The term 'protocell' will be used to reference MSN-supported lipid bilayers to maintain consistency of nomenclature with the initial published description of their manufacture and characterization.[94, 100,101] The principle attractiveness of utilizing these protocells as drug and gene delivery platforms is

37

in their potential for increased drug containment properties, and the tenability of surface chemistry modifications tailored to specific cargos.

2.2 Materials And Methods

Animals. A total of 62 adult, male Sprague-Dawley rats (Harlan Labs, Houston, TX); 300 +/- 5 g were double housed at 21 +/- 4°C in light controlled rooms (12:12 light: dark) and fed standard rodent chow and water available ad libitum. All procedures were approved by the Institutional Care and Use Committee (IACUC) of the University of New Mexico, and conducted in accordance to the guidelines recommended by the International Association for the Study of Pain for the handling and use of laboratory animals.

Behavioral assessment for sensory changes. Baseline spinal cord activity is evaluated using the well-characterized protocol for assessing threshold responses to light touch applied to the hindpaws with a series of calibrated monofilaments (0.4-15 g). The monofilaments generate a touch stimulus when applied to the hindpaw that induces a paw withdrawal response within 8 seconds.[102,103] Paw withdrawal sensory thresholds are highly sensitive to subtle inflammatory perturbations in the spinal cord, as normal hindpaw response thresholds (5-10 g) are present during healthy, non-pathological conditions, [103, 104] while response thresholds dramatically decrease (< 1 g) in the presence of inflammatory signaling.[103,104] This behavioral response phenotype is used as an indicator of spinal cord health. Prior to behavioral thresholds, rats were habituated to the testing conditions for 4 consecutive days, 1 hr/day, in a quiet dimly lit and temperature controlled room (26.0-27.0° C), where rats were placed on top of an open grid of bars

with 2 mm thickness, spaced 8 mm apart to allow access to the entire plantar surface of the hindpaw for tactile stimulation. Response thresholds were determined by a logarithmic series of calibrated Semmes-Weinstein monofilaments (von Frey hairs; Stoeling, Wood Dale, IL). Testing of behavioral thresholds were conducted identically to that described previously.[103,104] Briefly, baseline (BL) responses to light mechanical touch stimuli were assessed using 10 monofilaments, each with a log-stiffness value, defined as log10 (milligrams X 10), values in grams follow in parentheses: 3.61(.407), 3.84(.692), 4.08(1.202), 4.17(1.48), 4.31(2.04), 4.56(3.63), 4.74(5.49), 4.93(8.51), 5.07(11.75) and 5.18(15.14). BL values derived from three threshold assessments, at 20 min intervals, were averaged for the right and left hindpaws separately. After injection of protocells, threshold responses were re-assessed at .5, 1, 2, 3, 24 and 72 hrs. In those rats that underwent unilateral sciatic nerve injury, thresholds were reassessed at 3 and 10 days post surgery and every 2 days, up to 32 days post peri-spinal (intrathecal; i.t.) protocell injection. To assess normal food consumption as an indication of general health, body weights were measured following 2, 4, 8, 12, 14, 21, 28, and 56 days following i.t. administration of protocells.

Chronic constriction injury (CCI). The surgical procedure for chronic constriction injury (CCI) was performed identically as previously described [105, 106]. Briefly, under isofluorane anesthesia (1.5-2.0% vol. in oxygen), the mid to lower back and dorsal thigh were shaved and cleaned with diluted Bactri-Stat AE (EcoLab HealthCare Division, Mississauga, Ontario, Canada). Using aseptic procedures, the sciatic nerve was carefully isolated and four chromic gut sutures (Ethicon, Somerville, NJ) were loosely tied around one sciatic nerve. The overlying muscle was sutured closed

with two, sterile, silk sutures (Ethicon, Somerville, NJ), and the overlying skin was closed with wound clips. The sciatic nerve of sham-operated rats were identically exposed but not ligated. Animal body weight was recorded and recovery from anesthesia was observed within 10 minutes.

Intrathecal (i.t.) injections. Injections were acutely administered and conducted as described previously.[99,107] Briefly, rats were anesthetized with isofluorane (5.0% volume in oxygen) and an 18-gauge cannula constructed from an 18-gauge sterile hypodermic needle (Beckton Dickinson & Co., Franklin Lakes, NJ), removed from its hub, was inserted percutaneously between lumbar vertebra 5 and 6 (L5-6). During this time, a small amount of cerebral spinal fluid (CSF) efflux from the 18-gauge cannula and a tail flick were observed, indicating subarachnoid catheter placement. A 1 ml Hamilton syringe connected to a 30-gauge, 0.5 inch needle inserted into a catheter composed of a 30 cm-length polyethylene tubing (PE-10; cat# 427401; Becton Dickinson, Sparks, MD) was then used to draw up DOTAP:Chol or DOPC protocells (1.0, 0.1 or 0.01 mg) in a total volume of 20 µl sterile, isotonic saline. The drug-filled PE-10 catheter was then inserted into the open end of the 18-gauge guide cannula, and advanced 7.7 mm rostrally, placing the internal portion of the PE-10 catheter at the lumbosacral enlargement of the spinal cord where axon terminals of sciatic afferent nerve fibers synapse onto pain-relevant spinal cord neurons. Injections were given over a 0.5-1 minute interval. Following drug injection, the PE-10 catheter was removed followed by removal of the 18-gauge cannula, and both were discarded. The total time required for these i.t. injections was 2-3 minutes. All animals displayed full motor activity following recovery from anesthesia.

Preparation of plasmid DNA. The plasmid vector used in these studies was identical to that previously described.[107] This plasmid's transcriptional cassette consists of a cytomegalovirus enhancer/chicken beta-actin (CB) promoter driving expression of the rat IL-10 gene containing a point mutation (F129S) and the SV40 polyadenylation signal. The identical plasmid lacking the IL-10 gene was used as a control. Both plasmids were amplified in SURE II competent E. coli (Stratagene, Cedar Creek, TX.) and isolated using an endotoxin free Giga plasmid purification kit (Qiagen, Valencia, CA).

Preparation of mesoporous cationic silica "core" protocells. The mesoporous silica particles were prepared by the surfactant self-assembly method described previously.[100, 108] Briefly, a homogeneous solution of the soluble silica precursor, tetraethylorthosilicate (TEOS; Sigma-Aldrich Corp., St. Louis, MO), and hydrochloric acid was mixed in ethanol and water. A surfactant, cetyl trimethylammonium bromide (CTAB; Sigma-Aldrich Corp., St. Louis, MO), with an initial concentration much less than the critical micelle concentration was added to lower the surface tension of the liquid mixture and act as the mesoporous structure-directing template. Aerosol solutions of soluble silica plus surfactant were then generated with nitrogen as a carrier atomizing gas using a commercially available atomizer (Model 9392A, TSI, Inc., St. Paul, MN). The aerosol droplets were solidified in a tube furnace at 400 °C until dry. Once dried, a durapore membrane filter, kept at 80 °C, was used to collect the particles. As a final step, the surfactant was removed at 400 °C for 5 hrs via calcination. The surface of the mesoporous silica core in these studies was chemically modified with 10% by wt. aminopropyltriethoxysilane (APTES; Sigma-Aldrich Corp., St. Louis, MO) to create a positive surface charge to increase loading efficiency of negatively charged cargo.

Preparation of liposomes for protocells. The lipids used in this study were either positively charged, 1, 2-Dioleoyl-3-Trimethylammonium-Propane (DOTAP; cat. # 890890C; Avanti Polar Lipids Inc. Alabaster, AL) or zwitterionic and neutrally charged, 1, 2- dioleoyl-sn-glycero-3-phosphocholine (DOPC; cat. # 850375; Avanti Polar Lipids Inc., Alabaster, AL). Cholesterol was added to DOTAP in a 1:1 ratio, as it has been reported to improve transfection efficiency when included in cationic liposomes.[109] Phospholipids were dissolved in chloroform at concentrations of 10-25 mg/ml. Lipid aliquots of 2.5 mg were placed in scintillation vials. Alexa Fluor 647, a red fluorescent dye (absorption 650 nm and emission 658 nm; Invitrogen, Carlsbad, CA), was added at 2% for labeling studies. Chloroform was then evaporated under nitrogen flow. The vials were then stored overnight in a vacuum oven to remove remaining chloroform. Samples were stored at -20°C until used.

To prepare liposomes, vials were brought to room temperature and samples rehydrated with 1 ml buffer (10 mM MOPS, pH 7.0, 60 mM NaCl) and shaken for 1 hr, which resulted in a cloudy suspension. The suspension was extruded through a 100 μm pore diameter membrane with in a mini-extruder (Avanti Polar Lipids), and repeated for a minimum of 21 times. The resulting liquid was placed in a fresh vial and stored at 4 °C until used in the preparation of DNA loaded protocells.

Preparation of DNA loaded "protocells". An 18 bp-DNA oligomer (5′-CTTGAGAAAGGGCTGCCA-3′) tagged with 6-carboxylfluorocein (FAM; absorption 492 nm emission 520 nm; Invitrogen, Carlsbad, CA) was used to identify the safety profile and anatomical location of protocell cargo following i.t. injection. To load the

silica core with DNA, 35 µl of 200 µM DNA was added to 3.5 mg of cationic silica nanoparticles, gently mixed in sterile 0.5X PBS (25 mg/ml; 140 µl per 3.5 mg particles) and allowed to incubate for 5 min. In a sterile microcentrifuge tube, 300 µl of 2.5 mg/ml of liposome mixture was added and mixed with the nanoparticle/ DNA mixture by pipetting until homogeneous. The resulting mixture was allowed to sit at room temperature for 1 hr with occasional agitation by pipetting and then centrifuged for 2 min. at 6000 RPM to remove excess lipids. The supernatant was discarded, and the pellet was washed in sterile PBS followed by centrifugation at 6000 RPM. Pellets (protocell/18mer-DNA-FAM/ lipid mixture) were washed 3X and resuspended in sterile PBS at 50, 5 or 0.5 mg/ml. Identical steps were followed when loading pDNA-IL-10 and resuspended in 50 mg/ml.

Characterization of silica. Transmission electron microscopy (TEM) images were acquired with a JEOL 2010 200kV high-resolution transmission electron microscope. The pore diameter was calculated by the Barrett-Joyner-Halenda (BJH) method.[110] The total surface area was calculated by the Brunauer, Emmett & Teller (BET) method,[111] from the N2 sorption isotherm shown in Supplemental Figure 1.

Characterization of cargo release-rate from protocells. Mesoporous silica nanoparticles (25 mg) modified with 10% APTES were dispersed in 1 ml PBS to give a concentration of 25 mg/ml, 12.5 µl of 20 mM dextran-tetramethylrhodamine (DexRho;Molecular Probes, Invitrogen, Carlsbad, CA) was added to yield ~250 µM. The solution was agitated at room temperature for 45 min, and 50 µl aliquots of each protocell formulation for each time point were centrifuged for 2 min, washed 3X with 200 µl of

0.25X PBS to remove unincorporated dye. The dye-loaded cores were then mixed with DOTAP:Chol 1:1 (DOTAP:Chol) or DOPC liposomes as outlined above. A total of 200 µl of pH appropriate buffer was added to each sample to give a final concentration of 6.25 µg/µl. The particles and buffers were kept at 37°C. At designated time points, 1, 3, 6, 24, 48, 72, 96 and 168 hours (1 week), samples were removed, centrifuged at 14000 RPM for 2 minutes to precipitate the silica. A 100 µl sample of supernatant was then transferred into a borosilicate microcuvette to measure absorbance at 555 nm on a Beckman DU 530 UV/vis spectrophotometer (Beckman-Coulter, Inc., Fulterton, CA). In order to determine the quantity of dye released, absorbance readings from the supernatant samples were compared against a serial dilution curve based on known concentrations of dextran-tetramethylrhodamine. (100% loading was determined as 200 ng/ul). The following buffers were brought to a 1L volume in dH20 to generate the corresponding pH values: 0.1 M Acetic acid (pH 2), 0.1 M Citrate with 0.03% H_2O_2 (pH 4), 10.0 mM PBS (pH 7.4), 10.0 mM PBS with 0.1% BSA (pH 8.0), and 0.1 M Amino-Methyl-Propanediol (pH 10).

Microscopy. For tissue collection, rats were euthanized by overdosing with sodium pentobarbital (Abbott Laboratories, North Chicago IL) at 72 hr, and 2, 4 and 8 wks (N=3 rats for each time point and each protocell formulation (DOTAP:Chol or DOPC). Blood samples were taken and mixed with 0.1 ml heparin (APP Parmaceuticals, LLC., Schaumour, IL) to prevent clotting. Transcardial PBS (warmed to ~45°C; 3-5 min) perfusion, followed by room temperature .01M PBS; (3-5 min), and then ice cold 4% paraformaldehyde (pH 7.24; 6-8 min) perfusion. Spinal cord, brain, cervical nodes, thymus, spleen, kidney and liver were harvested and post fixed in 4% paraformaldehyde

overnight and transferred to PBS and stored at 4°C. Bone encased spinal cords were placed in 10% ethylenediaminetetraacetic acid (EDTA) solution (~3-4 weeks) to chelate calcium and soften bone for sectioning spinal cord encased in the spinal column to maintain anatomical integrity of the perispinal meninges. The entire spinal cord was cut and cross-sectioned into five, 5 mm, segments starting at the i.t. injection site (pt 0) and proceeding both rostrally and caudally. Brain and organ tissues were cryoprotected in 30% sucrose in (0.1M PBS + 50 μl 10% sodium azide) for 24 hrs, embedded in O.C.T. compound in cryomolds (cat# 4565-Sakura Finetek, Torrence, CA), flash frozen in 45°C isopentane on dry ice and finally stored at -80°C until the time of sectioning. For cryosectioning, 10 μm tissue slices were cut on a cryotome, Microm HM505E (Zeiss, Thornwood, NY), and placed on Vectabond (Vector Laboratories, Burlingame, CA) coated slides.

Quantitative spectral imaging. For FAM-tagged DNA, multi-spectral tissue imaging and quantification was conducted as previously described.[106] Briefly, images were obtained using an Axioscope microscope connected to a Nuance Camera 2.8 (FX) Multispectral Imaging System, (Cambridge Research and Instrumentation Inc., (CRI) Wolburn, MA).[112] This camera contains a liquid crystal tunable filter (LCTF) capable of filtering light from 400-720 nm, and can capture a series of images of a particular tissue region at 10 nm wavelength increments. Every pixel of every image (series collected at specific 10 nm wavelength increment) was then analyzed by CRI software to determine its peak spectral intensities from 400-720 nm. For each tissue type examined, the software subtracts background fluorescence, defined as any spectral emission falling below that of specific fluorescence. True FAM signal (excitation 494 nm; emission 522

nm) was determined from a control cover-slipped slide on which a small drop of 100X diluted FAM-tagged DNA 18-oligomer was placed. The autofluorescence was determined by imaging naïve tissue. The intensity of FAM fluorescence across the full wavelength range (400-720 nm) was calculated using the computer software. A minimum threshold intensity was set automatically by the software and FAM spectral emissions below this point were not included in the calculation. The FAM intensity signal "counts" were then averaged per exposure time (sec) per mm^2 area for each image collected (signal counts/sec/ mm^2). An image was acquired for each of 4 slices (n=4) per tissue region (e.g. spinal cord) per rat, and then averaged to generate a mean value for a tissue region per rat (N=3 rats/treatment group). An overall mean value is calculated for each treatment group, and the data are reported as signal counts/sec / mm^2. Detailed information regarding the computer software can be found on the Caliper Life Science website, a subsidiary of Perkin-Elmer(URL:http://www.caliperls.com/products/microscopy-imaging-analysis/microscopy-imaging/nuance-fx.htm).

Immunohistochemistry. Tissues were collected and sliced identically as described above (n=3 rats with 12 slices per anatomical area). Next they were permeabilized and blocked against non-specific antibody binding in PBS + 5% BSA + 0.5%Triton-X for 1 hr at RT. Primary antibodies were diluted in a solution of PBS with 0.1% BSA, 0.3% Triton-X with 0.1% sodium azide and incubated overnight at RT in a humidity chamber with slight rotation. Primary antibodies were diluted as follows: ED1 (a.k.a CD68, a classic marker of pro-inflammatory macrophage activation) 1:300; ED2 (a.k.a. CD162, a marker of alternative activation, anti-inflammatory) 1:300 (ED1- Cat# SC-7084 and ED2- Cat # SC-18796; Santa Cruz Biotechnology, Santa Cruz, CA); GFAP

(astroglia) (Cat#AB5804,Millipore,Temecula, CA) 1:300; OX42 (microglia/macrophage) monoclonal (Cat# MCA 275EL, AbD Serotec, Raleigh, NC) 1:300; and Cleaved-Caspase 3 (Asp175) (apoptotic cells) (Cat#9664 Cell Signaling Technology, Beverly, MA) 1:200. Slices were washed 3Xs with 0.1M PBS and then incubated for 2 hrs at room temperature in a dimly lit room at a 1:200 dilution of a Rhodamine Red-labeled secondary antibody (Jackson Immunoresearch Laboratories, West Grove, PA) in the same solution as that used for primary antibodies. Unbound secondary antibody was removed with three, 5 min washes in 0.1M PBS. Slices were then covered with a fluoro-protectant, Vectashield, containing the nuclear stain DAPI (4, 6-diamidino-2-phenylindole) (Vector Laboratories, Burlingame, CA), cover slipped, and stored at 4°C. Three slides, with 3 tissue sections on each slide (n=9), were examined for each primary antibody. As a negative control, no primary antibody was added to an additional slide. A positive control for the Caspase-3 antibody was also included in this experiment. Cultures of Raw 264.7 mouse macrophage cells, representative of CNS meningeal macrophage, were treated with bacterial lippopolysaccharide (LPS; 1 μg/ml) for 2 hours to initiate apoptosis, and then were subjected to the activated Caspase-3 antibody. Red Apoptotic cells stained positively and confirmed the integrity of the Caspase-3 antibody (data not shown). Tissues or cells were examined using an Olympus BX- 60 fluorescent microscope, Olympus D71 camera and software (Olympus America, Inc., Center Valley, PA).

Confocal imaging. To determine subcellular location of FAM-tagged protocells, 40X confocal image z-stacks of ED-1 + Raw 264.7 macrophage were obtained with a Zeiss Axiovert 100 inverted microsope (Carl Zeiss Laser Optics, Oberkochen, Germany) using LSM510 Image Acquisition software. The microscope excited the fluorophore of

interest DAPI, FAM, and rhodamine with one of three lasers: argon-405 nm; NeHe1-543 nm; HeNe2-633nm respectively.

Cellular transfection. For HEK 293 cell culture procedures, human embryonic kidney cells (HEK 293) cells were purchased from American Type Culture Collection (ATCC; Manassas, VA-cat# CRL-1573) and maintained in Minimum Essential Medium, containing Earle's Salts and L-glutamine (Invitrogen- cat# 11095) to which was added 10% heat inactivated fetal calf serum (FCS) (Gibco-Cat#10438) and 100 U/ml penicillin and 100 μg/ml Streptomycin (Gibco-Cat#15140). Cells were allowed to grow to 80% confluence and were then trypsinized with 0.05% Trypsin-EDTA (Gibco-Cat# 15400) to loosen cells. The cell suspension was centrifuged in a sterile 50 ml conical tube at 1500 RPM for 5 mins at 4° C. After adding 20 ml of fresh media, the cells were counted by standard technique on a hemocytometer and passed to a new sterile T-75 flask, plated at 10.0–15 X 106 at each pass. Cells were incubated at 37°C with an atmosphere of air, 95% and CO2, 5%.

For transfection with protocells, HEK 293 cells were plated at 1.0 X106 cells/mL on 24 well, sterile, poly-D lysine coated, culture plates (Becton Dickinson, Twin Oak Park, Bedford, MA) in 1 ml sterile MEM or DMEM respectively, both supplemented with 10% heat inactivated FCS and 100 U/mL penicillin and 100 μg/ml streptomycin and allowed to grow 24 hrs to 80% confluency. Media was exchanged with 1 ml fresh media containing 500, 50, 25, 10, and .5 μg/ml DOTAP or DOPC protocells loaded with pDNA-IL-10-GFP or pDNA-IL-10. Blank protocells without pDNA served as a control. The protocell containing media was removed after 5 hrs and replaced with fresh media.

48

Media was collected 24 hrs later and analyzed for GFP transfection (green fluorescence) and/or IL-10 using IL-10 ELISA (R&D Systems, Minneapolis, MN) according to manufacturer's instructions or immunostaining with IL-10 primary antibody (R&D Systems, Minneapolis, MN) with rhodamine 2° antibody in a procedure identical to that used for the immunohistochemical staining outlined above.

Cell viability assay. HEK 293 cells were plated at 5-6 X106 cells/mL on 24-well sterile poly-D lysine coated culture plates (Becton Dickinson, Twin Oak Park, Bedford, MA) in 1 ml sterile MEM supplemented with 10% heat inactivated FCS, 100 U/ml penicillin and 100 µg/ml streptomycin, and allowed to grow to 80% confluency. Media was removed and 1 ml of fresh media was added containing 500, 50, 25, 10, and .5 µg/ml DOTAP or DOPC protocells loaded with pDNA-IL-10-GFP, or blank protocells. The media was removed after 5 hrs and replaced with fresh media and the cells allowed to incubate for an additional 21 hrs. Cells were removed with a standard sterile cell scraper and 500 µl of cell suspensions placed in a flow cytometry tube on ice (Falcon Cat# 352008- Becton Dickinson Labware, Franklin Lakes, NJ). Three minutes before examination by flow cytometry (Facscan4, Becton Dickinson), 50 µl of 10 µM ethidium-homodimer D-1 was added to label dead cells.

Mouse macrophage (RAW 264.7) cells. RAW264.7 cells were obtained from American Type Culture Collection (ATCC, Manassas VA, USA-cat # TIB-71) and cultured as adherent cells in Dulbecco's Modified Eagle's Medium (Sigma-Aldrich, cat# D6429) supplemented with 10% heat-inactivated fetal bovine serum (Gibco, cat # 10082-147) and 100 U/ml penicillin and 100 µg/ml streptomycin (Gibco- cat#-15140122) and

maintained at 37°C under humidified 5% CO2 atmosphere. Cells were grown to 85% confluency, collected by scraping, and sub-cultured for 3 passages. For these experiments, dead cells were counted by hemocytometer using trypan blue exclusion.

Measurement of nitric oxide production

RAW 264.7 cells were seeded at a density of 2.75 x 105 cells/ml in 24 well plates 24 hours prior to experimentation and maintained at 37°C under humidified 5% CO2 atmosphere. At 85% confluency, the supernatant was exchanged with DMEM containing different formulations of DMEM and protocells or protocell constituents and followed by a 2 hour incubation then washed twice in PBS (pH 7.4, Gibco-cat # 10010). Wells treated with 10 ng/ml lipopolysaccharides from Escherichia coli (LPS, Sigma-Aldrich, cat #L6529) were exposed to DMEM containing LPS for 10 minutes followed by removal and washed twice in PBS. Nitric oxide production was measured using the commercially available Griess Reagent System (Promega, USA, cat #-G2930) according to the manufacturer's instructions. Absorbance was measured at 550 nm using a Tecan Infinite® plate reader (Tecan Systems, Inc., San Jose, CA). All experiments were run in triplicate.

Data analysis. Psychometric behavioral analysis was performed as previously described[103] to compute the absolute threshold that resulted in the 50% hindpaw withdrawal response. As described previously[103, 104, 113] withdrawal thresholds were determined by using the software program, PsychoFit. The software for PsychoFit may be downloaded from L.O. Harvey's website (http://psych.colorado.edu/~lharvey). This program fits the pattern of hindpaw responses for each timepoint to a Gaussian integral

psychometric function and generates a 50% threshold value for that time point. As such, parametric statistical analyses (repeated measures ANOVA) are applied to determine the statistical significance between treatment groups at multiple timepoints using the computer software, GraphPad Prism, version 4.03 (GraphPad Software Inc., San Diego, CA). All other statistical analyses were performed using the computer software, GraphPad Prism, version 4.03 (GraphPad Software Inc., San Diego, CA). All data is expressed as mean +/- SEM. Post hoc analysis was completed using Bonferroni's test.

2.3 Results

2.3.1 Characterization of protocells

Mesoporous silica particle cores were prepared by the surfactant templated aerosol-assisted self-assembly method previously developed and communicated.[114] The resulting hydrophilic nanoparticles were further modified with APTES and characterized by a uniform, ordered and connected mesoporosity (**Figure 2.1, A**), with a specific surface area or 935 m2/g and pore diameter of 2-5 nm **(Figure 2.1, B, C)**. Each 50 μl aliquot containing 1.25 mg protocells was examined for loading capacity using the negatively charged molecule, dextran tetramethylrhodamine (DexRho) (**Figure A.13 B**). Protocells formulated with DOPC lipids resulted in a cargo loading capacity of ~ 13.49 μg Dex Rho, and protocells formulated with DOTAP:Chol lipids exhibited a cargo loading capacity of ~ 16.12 μg DexRho.

Protocells with either DOPC or DOTAP:Chol formulations were characterized separately for their release of DexRho cargo. Separate aliquots were individually

incubated in pH solutions ranging from 2-10, for durations of 1 to 168 hours. While both DOTAP:Chol and DOPC formulated protocells revealed pH-dependent increases in cargo release with increased duration **(Figure 2.1, D, E)**, a statistically insignificant trend toward greater cargo release at pH 4 compared to pH 7.4 was observed with DOTAP:Chol protocells. These cargo release profiles are relevant to physiological conditions of cellular organelles, such as lysosomes, that have acidic compartments typically near pH 4. Additionally, physiologically relevant pH 7.4 occurs in extracellular regions, suggesting that protocell cargo may remain associated with protocells until cellular uptake and trafficking into the more acidic late endosomes and lysosomes where the cargo is released.
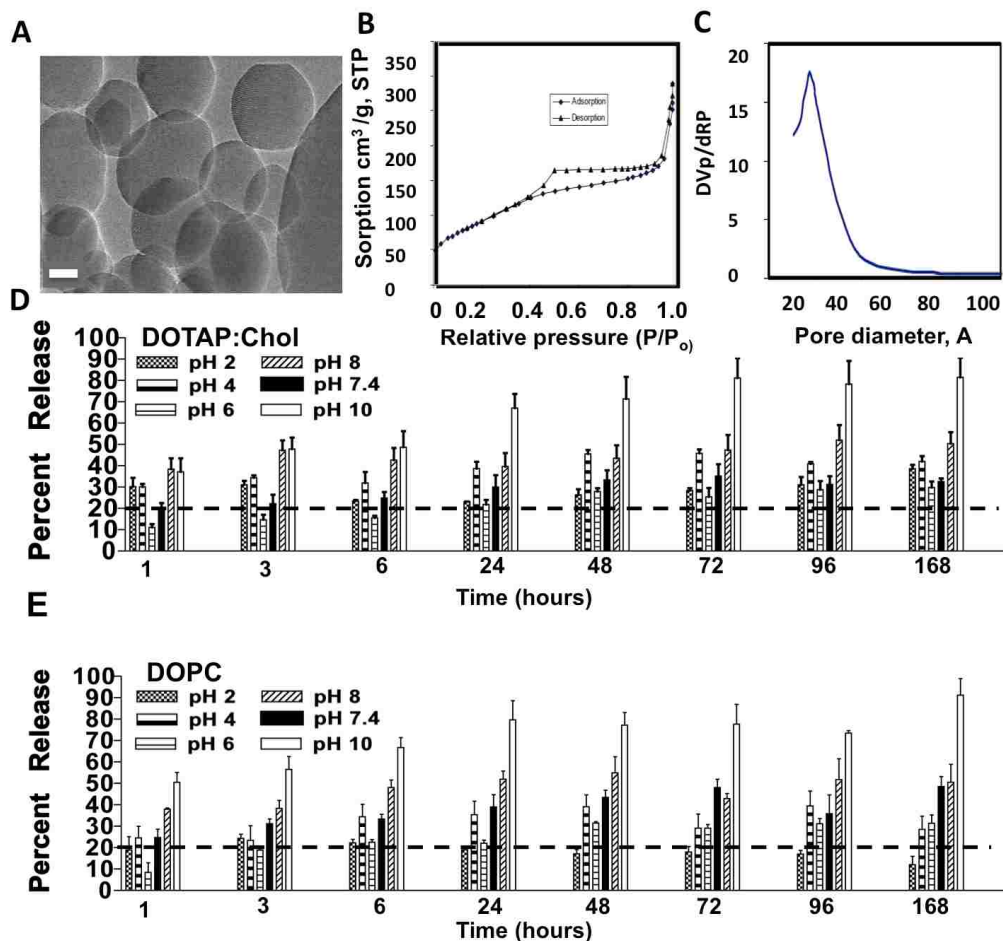
Figure 2.1 Characterizations of protocells.

(A) TEM image of mesoporous silica nanoparticles; scale bar = 50 nm. (B) Nitrogen sorption isotherm of 10% aminated silica nanoparticles. (C) Determination of pore size of 10% aminated silica nanoparticles by the Barrett-Joyner–Halenda (BJH) method.[110] (D) DOTAP:Chol protocells and (E) DOPC protocells examined from 1 – 168 hours in specific pH solutions. The negatively charged fluorophore, dextran tetramethylrhodamine (DexRho) loaded into the protocells served as cargo. Dashed line indicates 20% release for ease of comparison between groups and conditions. For both DOTAP:Chol and DOPC protocells cargo release increased as time and pH increased. A significant interaction between time and pH was revealed (DOTAP:Chol: $F_{(35, 84)}$ = 2.16, p = 0021; DOPC: $F_{(35, 84)}$ = 2.35; p = 0.0008). A trend for increased cargo release at pH 4 compared to pH 7.4 from DOTAP:Chol protocells was observed. DOTAP:Chol protocells at pH 6 revealed the greatest degree of cargo retention at 3 and 72 hours (p < 0.05). The pattern of greater cargo retention (~15%) at pH 7.4 and 6.0 in DOTAP:Chol protocells suggests that cargo will remain associated with protocells until taken up within the cell and released within the late

lysosome for optimal cargo delivery. (A, B, C – Data provided by the Brinker Group; D, E- Experiment performed by Audra Kerwin; statistical analysis and graphic by Ellen Dengler)

2.3.2 In vitro cellular viability

Cells remain viable following application of protocells formulated with DOTAP:Chol or DOPC. HEK cells were incubated with 10-500 μg/ml protocells formulated with DOTAP:Chol or DOPC containing plasmid DNA encoding the anti-inflammatory cytokine, interleukin-10, and the reporter gene, green fluorescent protein (pDNA-IL-10/GFP; 10 μg/mg protocells) for 24 hrs. Protocells without cargo served as controls. To examine the effects of DOTAP:Chol or DOPC protocells containing pDNA-IL-10/GFP cargo on cellular viability, flow cytometry was used by applying Ethidium-Homodimer-1 (EH-1) to stain the cells. EH-1 enters the cell nucleus and intercolates with DNA only in dead or dying cells in which the membrane is breaking down. Thus, EH-1 does not interact with DNA of live cells with intact membranes. Excitation of EH-1 at 528 nm leads to 617 nm emission (red fluorescence), which is detected by the flow cytometer, and each dead cell is counted. The percentage of dead cells is quantified per 10,000 cells. The percent of live cells was determined (**Figure 2.2**). Cells left untreated served as an index of basal cell viability, which was observed to be > 98%. To ensure dead cell quantification, a separate group of cells were treated with 0.1% saponin, and only ~3% remained viable. Protocells formulated with either DOTAP:Chol or DOPC resulted in < 5% dose-related decrease in cell viability compared to live controls and remained stable even at the highest dose of 500 μg/ml. Thus, cells exposed to DOTAP:Chol or DOPC protocells remained healthy, suggesting that DOTAP:Chol or DOPC protocells lack overt toxicity *in vivo*.

54
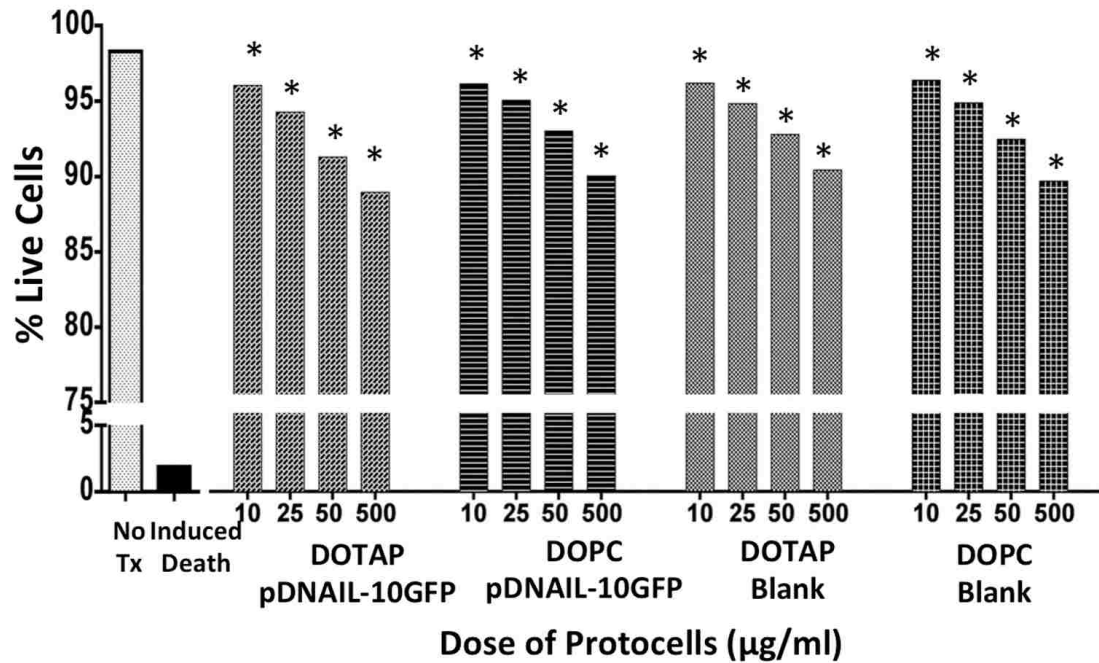
Figure 2.2 Cells remain highly viable following application of DOTAP:Chol and DOPC protocells containing pDNA-IL-10-GFP.

Cells were incubated for 24 hours with DOTAP:Chol or DOPC protocells loaded with pDNA-IL-10-GFP or blank control protocells (no pDNA) at varying concentrations across a 50-fold dose range, 500, 50, 25 and 10 ug/ml. Dead cells were identified by flow cytometry after staining with ethidium-homodimer-1. Results are representative of the percentage of gated cells (average of 4 experiments) compared to untreated control cells, **$p < 0.01$; ***$p < 0.0001$. (Experiment, statistical analysis and graphics by Ellen Dengler)

2.3.3 Protocells are well tolerated in an animal model.

Light touch sensory threshold assessment is highly sensitive to subtle perturbations in spinal cord homeostasis. Increases in local spinal immune signaling molecules lead to spinal sensitization of pain-related projection neurons resulting in a hypersensitivity to light touch stimuli applied to the body area innervated by axons whose central terminals also project to the affected spinal segment.[102, 103] Thus, assessing alterations in light touch thresholds from basal values following central nervous system

protocell application can be a timely, robust and reliable *in vivo* examination of protocell early-phase toxicity within the local spinal cord compartment. Baseline (BL) sensory threshold values for both hindpaws were recorded prior to an i.t. injection of DOTAP:Chol or DOPC formulated protocells loaded with a FAM-18 bp single stranded DNA oligomer. Thresholds close to 10 grams of stimulus intensity were observed in all rats prior to treatment (**Figure 2.3**). Following an i.t. injection of 0.01 or 1 mg DOTAP:Chol formulated protocells, a small increase in light touch sensitivity of the left paw was observed at 30 min and rapidly recovered to basal levels and remained stable during a 72 hr observation period (**Figure 2.3, A, B**). Normal insignificant basal variations in paw thresholds were observed in 0.01 mg protocell and control, vehicle injected rats. Conversely, both 0.01 and 1 mg DOPC formulated protocells induced a small increase in light touch sensitivity (values dropped to <1.0 g stimulus intensity) in both the left and right hindpaws at 2 hrs, that mostly recovered to BL values during the remaining 72 hr observation period (**Figure 2.3, C, D**). The transient 2-hr increase in light touch sensitivity following DOPC formulated protocells was unexpected given reports show that *in vitro,* DOPC toxicity is virtually absent. However, *in vivo* subtle changes in the local spinal milieu may occur to a greater extent that alters early-phase toxicity and corresponding neuronal processing of normal sensory stimuli. Nevertheless, normal body weight gain was observed in all rats throughout an 8 week observation period during which time, animals remained active and well-groomed (**Figure 2.3, E**). Taken together, these data support that i.t. administration of DOTAP:Chol, lack alterations from normal sensory processing and both DOTAP:Chol and DOPC formulated protocells are well-tolerated in the peri-spinal region of rats.
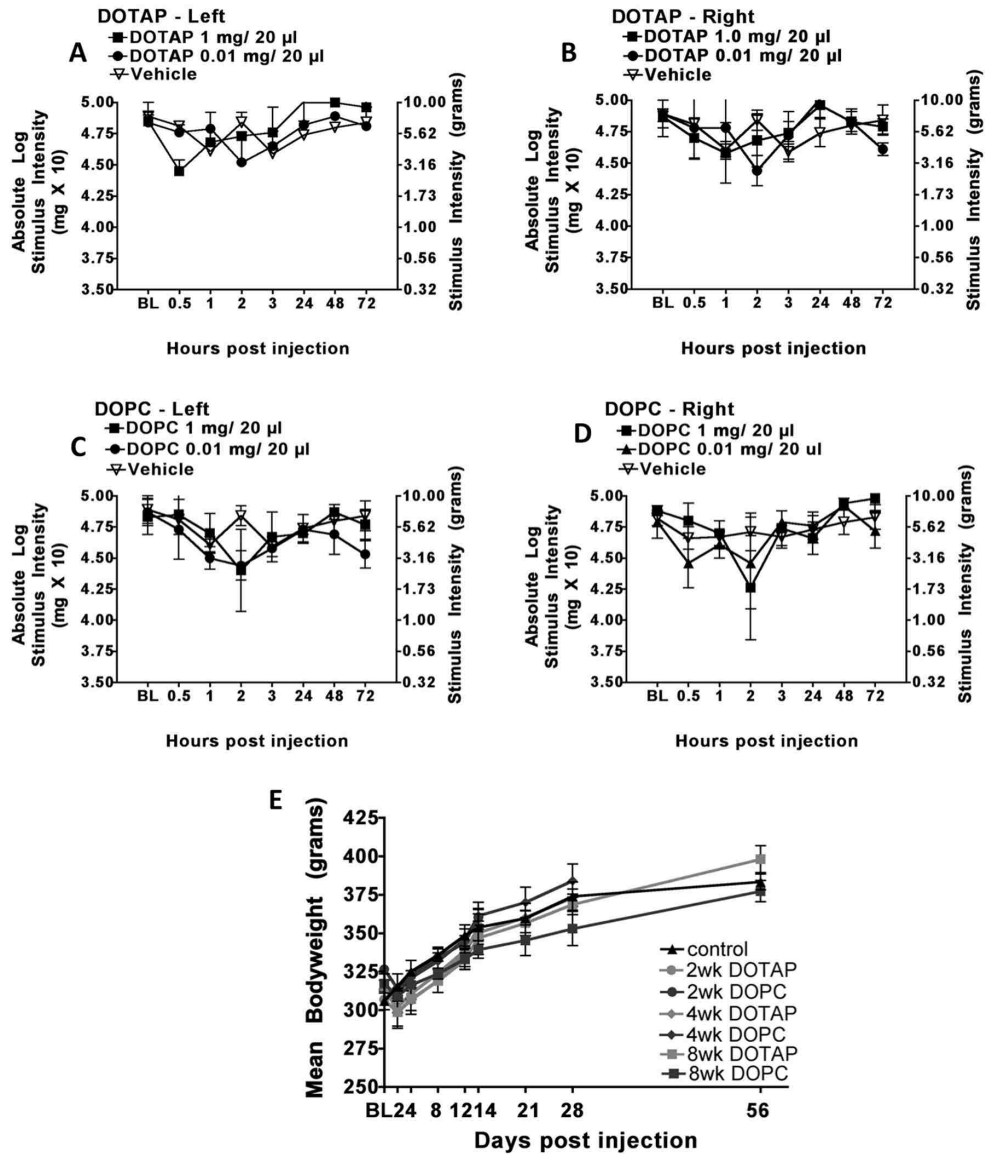
Figure 2.3 In vivo subtle differences in biocompatibility are revealed between DOTAP:Chol and DOPC protocells.

Baseline threshold responses of both hindpaws (left and right) between animal groups were similar; at 10 g (right y-axis) ($F_{(4, 14)}$= 0.3721; $p > 0.05$). (A, B) Following i.t. injection with either 1 or 0.01 mg of DOTAP:Chol or (C, D) DOPC protocells, threshold responses remained unchanged throughout the timecourse (0.5, 1, 2, 3, 24, 48 and 72 hrs) suggesting no spinal inflammation. (C, D) For DOPC - treated animals, while a decrease in thresholds was not observed across the majority of the timecourse left- $F_{(24, 60)}$= 1.88, $p > 0.05$; right- $F_{(24, 60)}$= 1.01 $p > 0.05$), there was a small but significant decrease at 2 hours in both hindpaws ($p < 0.05$ left and right), indicating a subtle and transient spinal cord inflammation resulting in decreased sensory thresholds . All animals exhibited normal feeding, grooming and exploratory behavior

57

throughout the 8-week observation. (E) Body weight gain remains normal following i.t. injection with DOTAP:Chol or DOPC protocells. At BL, there was no significant difference in body weight between untreated (open triangles) and treated animals that received i.t. DOTAP:Chol (2 wks, solid circles; 4 wks, solid diamonds; 8 wks, solid squares) or DOPC protocells (2 wks, open circles; 4 wks, open diamonds; 8 wks, open squares)($F_{(6, 14)}$= 2.837, p = 0.0506), followed by a normal gain in body weight. This normal gain in body weight between control animals and those receiving protocells by i.t. injection remained consistent over time in all groups of animals (n = 3 per group). (Behavioral testing, statistical analysis and graphics by Ellen Dengler)

2.3.4 Intrathecal (.i.t) DNA delivered by DOTAP:Chol or DOPC protocells remains closely associated with meninges.

Non-coding 18 bp oligonucleotide DNA labeled with the fluorophore, FAM (Ex/Em 492/517 nm; green) delivered by either DOTAP:Chol (**Figure A.13 A**) or DOPC formulated protocells remained closely associated with the cells of the meningeal layer in the spinal cord, but did not penetrate tissue parenchyma. A representative spinal tissue section near the i.t. injection site, revealed DOTAP:Chol protocells containing FAM-tagged DNA (green) in/adjacent to the meningeal layer (**Figure 2.4, A, B, D**), with cellular nuclei counter-stained with the nuclear specific flurophore, DAPI. Glial cell astrocyte processes and endfeet (astocytes stained for glial fibrillary acidic protein, GFAP; red) are typically present at the neural-pial meningeal interface, which are capable of taking up extracellular material. Yet, no co-localization of FAM-tagged DNA protocell cargo within astrocytes was observed (**Figure 2.4, A, white arrow**). However, immune-relevant macrophage and microglia that normally reside in meninges and at the neural-pial interface are highly efficient phagocytic cells. Indeed, FAM-tagged DNA containing protocells robustly co-localized with macrophages/microglia (stained for CD11b marker; red) in the meningeal peri-spinal region. Co-localization appears yellow **(Figure 2.4, B,**

white arrow). While microglia are present (red) in the deeper spinal parenchyma, FAM-tagged DNA is absent **(Figure 2.4, B)**.

Caspase-3 is a well-characterized enzyme that plays a critical role in the late stages of programmed cell death (apoptosis). Immunohistochemical detection of Caspase-3 (red) was entirely absent in the spinal cords and brains of rats where DOTAP:Chol formulated protocells were present. A representative image of protocells containing FAM-tagged DNA (green) in the meninges reveals no positive Caspase-3 immunoreactivity at 8 wks following i.t. injection **(Figure 2.4, C)**. Confocal examination of meningeal macrophage/microglial cells immunostained for expression of ED1, a marker for activated immune cells with a proinflammatory phenotype, revealed DOTAP:Chol protocells containing FAM-tagged DNA were closely associated with the DAPI-stained peri-nuclear area of ED1 expressing cells **(Figure 2.4, D, white arrow)**.
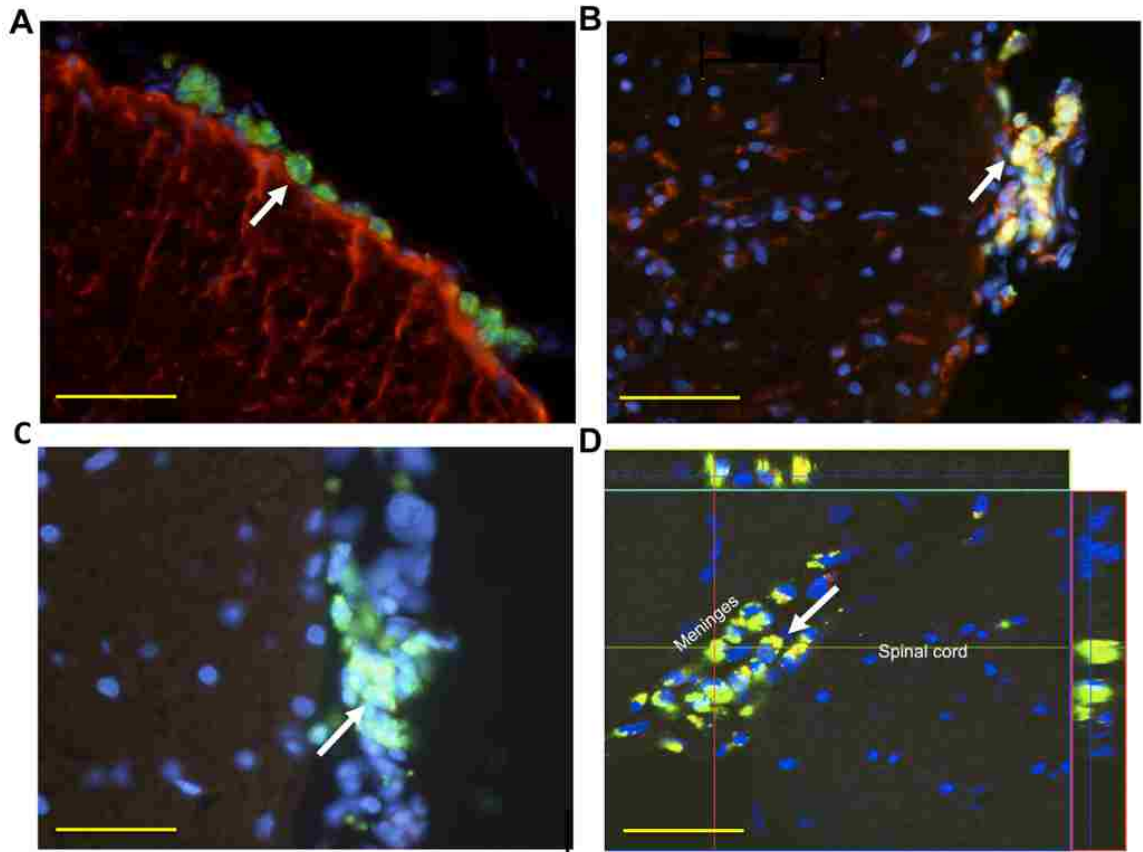
Figure 2.4 Histological examination of DOTAP:Chol protocells with DNA cargo.

Fluorescent histological examination of spinal cord sections near the lumbar spinal cord injection site (segments L3-4) 8 weeks after i.t. injection of DOTAP:Chol protocells loaded with FAM-tagged 18 base pair (18bp) DNA oligomer. (A) Protocells containing DNA cargo (green; white arrow) are not colocalized with astroglia stained for glial fibrillary acidic protein, GFAP (red). (B) However, protocells are colocalized in the pial meninges with activated microglia/macrophage stained for OX2 (red). Colocalization of microglia with DNA cargo (green) results is indicated (white arrow). (C) There is no evidence of cellular death in the meninges or spinal cord, as indicated by the absence of positive staining for the apoptotic marker, activated Caspase 3 (red) while protocell-containing DNA cargo (green; white arrow) is clearly present. (D) Confocal image identifying DOTAP:Chol protocell cargo of FAM-tagged 18 bp DNA (green) in the peri-nuclear area (cell nuclei stained with DAPI; blue) of meningeal macrophage cells stained for the classic activation marker, EDI (red; white arrow) in the dorsal spinal cord. Overlap reveals yellow cytoplasmic and peri-nuclear staining. All images are at 20X; scale bar = 40 μm. (A-D- IHC and fluorescent imaging by Ellen Dengler; D- confocal imaging by Tamara Roitbach)

2.3.5 In vivo biodistribution of protocells.

Eight weeks following i.t. injection, protocells remain in the CNS and are not found in peripheral tissue. As the animals appeared to experience no adverse effects from DOTAP:Chol or DOPC formulated protocells, even at the highest dose, the biodistribution of protocells within and outside of the central nervous system (CNS) was quantified. In these experiments, rats received an i.t. injection of DOTAP:Chol or DOPC protocells loaded with FAM (1 µg FAM 18bp DNA oligomer/1 mg protocells), and tissues were harvested 2, 4, and 8 weeks later. Blood, the immune organs (cervical lymph nodes, thymus and spleen), the filtering organs (kidney and liver), as well as sections from the brain, cervical, thoracic and lumbar spinal cord were examined to quantify protocells by spectral microscopy analysis that allows computerized de-convolution and quantification of the true FAM-signal from background autofluorescence (**Figure 2.5, and Table 1**).

The blood was negative for FAM detection (data not shown). The highest amount of FAM levels at 72 hr post DOPTAP:Chol or DOPC protocell injection were observed at the i.t. injection site in the lumbar spinal cord, which significantly decreased by 8 wks (**Figure 2.5, B**). Only DOPC formulated protocells containing FAM-tagged DNA accumulated in the brain by 8 weeks (**Figure 2.5, A**). Thus, differences in the biodistribution between the two protocell lipid formulations were observed. Also at 8 weeks, the DOTAP:Chol protocell FAM signal had diminished and was only significant locally, near the injection site, suggesting that DOTAP:Chol formulated protocells may

61

be optimal to maintain localized drug effects, while leaving the brain and the body primarily undisturbed.

Outside the central nervous system, FAM signal was negligible including in the liver and kidney. At 72 hours, a minor but significant amount of FAM was detected in the thymus following treatment of both DOTAP:Chol and DOPC formulated protocells. The data represented in **Figure 2.5, A and B** are included in **Table 1** to provide relative comparisons in FAM detection levels with respect to FAM levels observed in other tissue regions that in most cases, appear negligible.

Table 1 — Biodistribution of Fluorescent Tagged 18mer Signal: Quantification by Spectral Analysis (All numbers 1 X E-04)

| | Auto fluorescence Naïve tissue | | 72 hours | | | | 8 weeks | | | |
| | | | DOTAP | | DOPC | | DOTAP | | DOPC | |
	Mean	SEM	Mean	SEM	Mean	SEM	Mean	SEM	Mean	SEM
Inside CNS										
Brain [1]	1.53	0.136	65.3	14.6	104	72.3	7.2	7.2	**491	0.248
Cervical spine	2.62	0.158	15.6	11.4	119	110	2.68	1.5	**580	359
10 mm rostral	22	16.2	624	232	682	262	26.7	5.7	286	16.4
Lumbar protocell delivery site [2]	6.6	5.9	*689	359	*434	222	*134.8	0.013	*320.2	121.9
5 mm caudal	17.7	10.5	325	147	230	175	17.1	9.69	***2419	259.9
1.5 mm caudal	10.5	5.8	194	76.7	158	169	24.5	1.23	***2111	274.1
2.5 mm caudal	7.14	3.45	*203	68.7	*250	55	3.16	0.625	2737	519
Outside CNS										
nodes	0.11	1.5	19.2	11.7	12.3	1.34	8.01	4.61	4.2	2.6
Thymus	13.3	6.8	*1044	471	648	97.4	9.4	0.657	16.4	4.66
Spleen	10.5	0.422	*45.2	10.07	10.4	12.69	12.2	12.7	6.2	1.8
Liver	25.2	3.7	24.1	4.87	36.6	6.45	14.6	0.395	18.7	2.65
Kidney	96.2	2.93	1.13	1.5	10.5	0.244	8.92	0.587	11.7	1.21

*** $p < 0.001$ **$p < 0.01$ *$p < 0.05$ [1] See figure 5A   [2] See figure 5B

Figure 2.5 The spread to brain following i.t. protocell injection is determined by the lipid bilayer formulation.

Graphs are representative of the key data in the corresponding Table I. Fluorescent spectral signal from FAM-tagged 18bp DNA cargo in cryo-sliced tissue sections (n = 4) of DOTAP:Chol or DOPC protocell i.t. treated animals is compared to the spectra of background autofluorescence from naïve animals. (A) In the brain, after 72 hours, there was no significant signal from FAM-tagged DNA delivered by either DOTAP:Chol or DOPC protocells. By 8 weeks, background signal in DOTAP:Chol protocell treated tissue

was comparable to that of auto-fluorescence (p > 0.05), while the signal from FAM-tagged DNA delivered by DOPC protocells had significantly increased compared to autofluorescence ($F_{(2, 6)}$ = 8.60; p = 0.0173. (B) At the lumbar spinal cord protocell delivery site, FAM-tagged DNA delivered by both DOPC and DOTAP:Chol prototocells was clearly present at both 72 hours and 8 weeks when levels of FAM signal analysis was compared to levels from autofluorescence ($F_{(2, 6)}$ = 6.18; p = 0.0348), with the signal at 72 hours significantly higher than that at 8 weeks ($F_{(1, 6)}$= 10.71; p = 0.0170). (Table 1) Values (1 X E-04) of each anatomical region are an average of computer-generated spectral analyses taken from 4 separate images of four 10 μm sliced tissue sections. Yellow boxes indicate those areas in which the signal from FAM-tagged DNA cargo reached levels that were significantly higher than control autofluorescence for that tissue. Asterisks indicate the amount of significance. Very low levels of DOTAP:Chol protocells were detected in the lymph organs, such as thymus and spleen, while DOPC remained in the CNS. *p < 0.05; **p < 0.01; ***p < 0.0001. (Tissue slicing by Ellen Dengler with assistance from Leisha Armijo; Spectral microscopy and computerized analysis by Ellen Dengler with assistance from Kate Gentry)

2.3.6 Protocell IL-10 gene delivery leads to robust transgene expression.

Following a 24 hr incubation with DOTAP:Chol formulated protocells containing pDNA-IL-10/GFP, robust GFP protein was observed in ~40% of HEK cells **(Figure 2.6, A)**. Transfection of HEK cells with a bicistronic plasmid containing the gene for IL-10 and GFP successfully resulted in expression of both proteins, GFP and IL-10, indicating functional IL-10 transgene expression in GFP expressing HEK cells (**Figure 2.6, A; insert**). Protocells formulated with either DOTAP:Chol or DOPC and loaded with plasmid DNA encoding the IL-10 gene alone (pDNA-IL-10) or in combination with the reporter gene, pDNA-IL-10/GFP, were incubated with HEK cells to examine transgene IL-10 protein expression. It is important to note that HEK cells do not produce IL-10 protein thus providing a reliable assay to quantify transgene-specific IL-10 gene activation. The cell culture supernatants were examined for IL-10 protein using ELISA assay procedures **(Figure 2.6, B,C)**. Surprisingly, only those protocells formulated with DOTAP:Chol containing pDNA-IL-10 or pDNA-IL-10/GFP resulted in a robust dose-

dependent increase in protein IL-10 levels compared to untreated controls, with the greatest amount of protein (~900 pg/ml) produced following incubation with 500 μg/ml DOTAP:Chol formulated protocells. In contrast, IL-10 protein from transgene IL-10 delivered by DOPC protocells containing either pDNA-IL-10 or pDNA-IL-10-GFP was significantly lower and reached maximal values of no greater than 100 pg/ml.
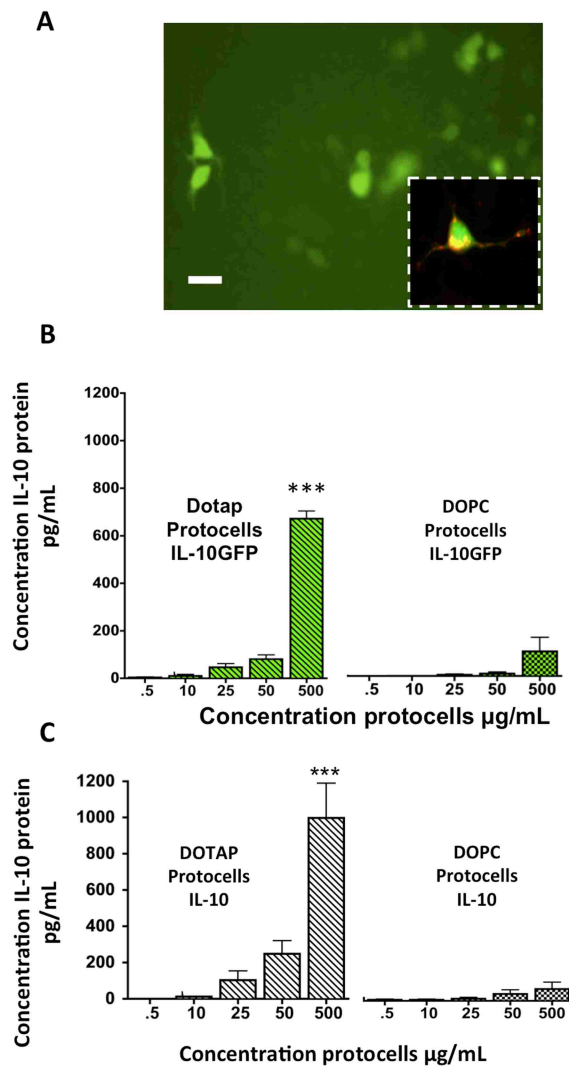
Figure 2.6 DOTAP:Chol protocells improve cellular transfection of pDNA-IL10 transgene.

In vitro transfection of HEK cells with a bicistronic plasmid containing the genes for both IL-10 and GFP employing an internal ribosomal entry site results in expression of GFP (A; green). Staining with antibody

for IL-10 (red) shows colocalization (yellow) in a GFP-positive HEK cell (green), indicating functional bicistronic transgene expression (A; insert). pDNA IL-10-GFP (B) or pDNA-IL-10 (C) delivered by DOTAP:Chol protocells results in functional transgene expression as measured by IL-10 protein release in culture supernatants following a 24 hour incubation. Results are the average of 4 representative experiments ($F_{(1, 4)}$ = 24.85; ***p < 0.0001, **p < 0.01). Scale bar = 10 μm in both Figure 6A and insert. (A- Transfection experiment and IHC by Ellen Dengler; B-ELISA by Ellen Dengler with assistance from Brandi Bowman)

2.3.7 Protocells are functionally effective as gene delivery platforms.

Given that IL-10 transgene delivered by DOTAP:Chol formulated protocells yielded robust transgene-derived IL-10 protein levels in cell culture (**Figure 2.6**) and DOTAP:Chol protocells appeared to show minimal toxicity in vivo (**Figure 2.3**), we next asked whether DOTAP:Chol formulated protocells containing pDNA-IL-10 (**Figure A.13 C**) could act therapeutically by delivering sufficient amounts of the IL-10 transgene to suppress light touch hypersensitivity (allodynia), a neuropathic condition mediated by sensitization of spinal neurons that communicate to brain areas about pain-related stimuli. Allodynia occurs when non-painful stimuli are coded as painful. Following BL assessment of withdrawal behavior to light touch tactile stimuli, rats underwent either sham surgery or CCI of the sciatic nerve. Clear development of allodynia was observed 3 and 10 days later **(Figure 2.7, A, B)**. On Day 10, rats received an i.t. injection of DOTAP:Chol formulated protocells containing pDNA-IL-10, pDNA-control (non-coding DNA), or equivolume vehicle (20 μl). While sham rats remained stably non-allodynic, a rapid and complete reversal from neuropathic allodynia was observed in IL-10 treated rats. Neuropathic rats injected with i.t. control pDNA or vehicle remained stably allodynic throughout a 26-day timecourse. It is important to note that a prior report demonstrated an equivalent dose of i.t. naked pDNA-IL-10 lacks efficacy to reverse

66

allodynia.[14] Taken together, these data show that pDNA-IL-10 delivered to the peri-spinal regions by DOTAP:Chol protocells was able to reverse allodynia to BL levels for almost 2 wks. These data support that the production of IL-10 protein from pDNA-IL-10 transgene loaded on protocells is functionally and physiologically effective.in reversing pain thresholds.

Materials composing protocells do not lead to nitric oxide (NO) production. In order to assess subtle and transient cell-stress responses to the identical DOTAP:Chol protocell formulation examined for in vivo spinal gene therapy, cultured macrophage cells (Raw 264.7) were examined, given the observed in vivo spinal co-localization of DOTAP:Chol protocells with macrophages/microglial cells, as described above in figure 4. Macrophages were assayed for NO following a 2-hour incubation with whole protocells or the component silica core and lipid (DOTAP:Chol) (**Figure 2.7**). Lipspolysaccharide (LPS) was included, as it is known to produce robust enhancement of NO in this cell line.[115-118] As expected, cells incubated with LPS for 10 minutes produced increased levels of NO compared to untreated controls. However, similar basal NO levels were observed between untreated controls, whole protocells, silica cores and DOTAP:Chol lipid, suggesting that these materials do not generate transient or even subtle cell stress events.
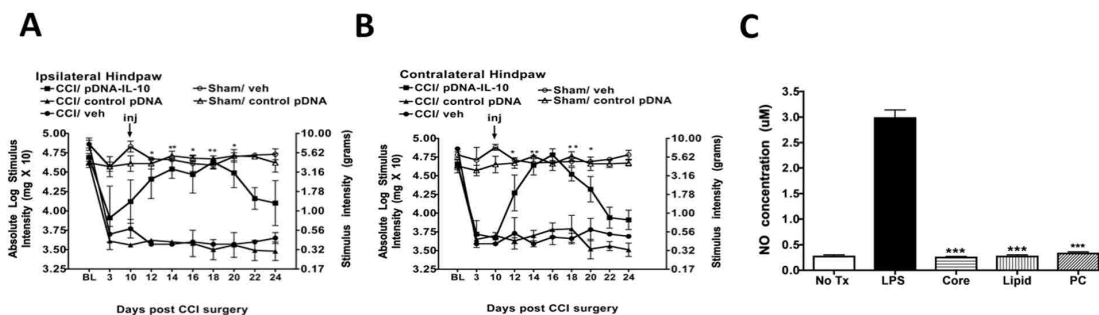
Figure 2.7 Intrathecal delivery of protocells loaded with pDNA-IL-10 causes therapeutic reversal of allodynia.

(A and B) At pre-treatment baseline (BL) values, no significant differences were observed (ipsilateral and contralateral; $p > 0.05$). Following BL assessment, animals underwent CCI of the left sciatic nerve, and threshold values were reassessed 3 and 10 days later. Robust allodynia was observed compared to sham-treated controls (ipsilateral- $F_{(8, 36)} = 4.94$; $p < 0.0004$; contralateral- $F_{(8, 36)} = 19.89$; $p < 0.0001$). On day 10 after CCI, rats then received an i.t. injection with DOTAP:Chol/ pDNA-IL-10 protocells or control DOTAP:Chol protocells without DNA. A significant bilateral reversal of allodynia beginning on day 12 after CCI (day 2 after i.t. injection), and continuing through day 22 was observed (overall treatment effect, ipsilateral- $F_{(4, 108)} = 44.91$; $p < 0.0001$; contralateral- $F_{(4, 108)} = 85.09$; $p < 0.0001$). Each CCI operated group (closed symbols) received an i.t injection of DOTAP:Chol protocells loaded with pDNA-IL-10 (squares; n = 7) or a non-coding DNA (triangles; n = 5) (10 µg pDNA in 1mg protocells in 20 µl PBS) or PBS vehicle (circles; n = 3) (20 µl). Each sham-operated group (open symbols) received an i.t. injection of non- coding DNA (triangles; n = 5) (10 µg pDNA in 1 mg protocells in 20 µl PBS) or PBS vehicle (circles; n = 3) (20ul). Black arrow indicates i.t. injection; *$p < 0.05$; **$p < 0.01$; ***$p < 0.0001$. Nitric oxide concentration was measured in cultured Raw 264.7 cells (C) in LPS (black bar) and non LPS-stimulated cells (white bar) and those treated with whole protocells or constituents of protocells; silica core (500 µg) or Dotap:Chol lipid (20 µl)(hatched bars); All three treatments resulted in significantly less NO production than the LPS stimulated positive control ($F4,14 = 321.8$; $p < 0.0001$). (A, B – Behavioral testing by Ellen statistical analysis by and graphics by Ellen Dengler; C- Experiment run by Audra Kerwin; statistical analysis and graphics by Ellen Dengler)

2.4 Discussion

Our results demonstrate that mesoporous silica nanoparticle (MSN) cores with their surface fused to either DOTAP:Chol or DOPC formulated liposomes (protocells)

differentially release cargo (Dextran Rhodamine; a negatively charged fluorophore) when exposed to a wide range of pH values, with both formulations resulting in high cellular-viability values (>90%) following a 50-fold dose range exposure (**Figure 2.1, Figure 2.2**). Additionally, peri-spinal application (subarachnoid, intrathecal; i.t.) of either DOTAP:Chol protocells or DOPC protocells in separate groups of rats resulted in different toxicity and biodistribution profiles. Subtle but significant differences in hindpaw sensory threshold values were generally lower in DOPC protocell-treated rats at 3 hrs compared to thresholds of DOTAP:Chol protocell treated rats (**Figure 2.3, A-D**). Importantly, assessment for threshold changes in light mechanical touch from baseline is a surrogate indicator for physiological perturbations involving early-phase toxicity or spinal cord inflammation[104] that can go undetected by overt observations for general health measures such as ambulatory function and body weight gain. Indeed, an 8-wk observation period for body weight gain revealed no differences between i.t. DOTAP:Chol protocell and DOPC protocell-treated animals (**Figure 2.3, E**). Spinal immunohistochemical examination of DOTAP:Chol protocells containing DNA revealed clear co-localization with macrophage/microglial cells at the spinal-meningeal interface (**Figure 2.4, A, B, D**), with a complete lack of cell death, as indicated by the absence of immunoreactivity for the late phase necessary apoptotic enzyme, caspase-3 (**Figure 2.4, C**). These finding support that DOTAP:Chol protocells offer a significant degree of biocompatibility. However, clear differences were observed between the in vivo biodistribution of DOTAP:Chol protocells and DOPC protocells. While both DOTAP:Chol and DOPC formulated protocells surrounding the spinal cord injection site were identified for as long as 8 wks following administration, only DOPC protocells

revealed an increased spread to brain observed at 8 wks (**Figure 2.5, A and Table 1**). Furthermore, IL-10 transgene expression *in vitro* was significantly greater following cellular incubation with DOTAP:Chol-protocells containing plasmid DNA encoding IL-10 (pDNA-IL-10) than cells incubated with DOPC-protocells-pDNA-IL-10 (**Figure 2.6**). Based on the overall profile of DOTAP:Chol protocells in their biocompatibility, localized biodistribution and greater transgene expression, DOTAP:Chol protocells were loaded with pDNA-IL-10 to examine their therapeutic potential as a novel non-viral gene transfer vector delivered to the spinal cord to treat peripheral neuropathic pain. Compared to various control-treated rats, i.t. injections of DOTAP:Chol pDNA-IL-10 protocells resulted in robust bilateral reversal of allodynia for as long as 12 days (**Figure 2.7, A, B**). Importantly, inflammatory nitric oxide, used as a sensitive and specific factor indicative of cell stress, was virtually absent in macrophages exposed to the composite DOTAP:Chol protocell formulation or its constitutive components (**Figure 2.7, C**).

Our data show that protocells are capable of prolonged drug delivery, as DOTAP:Chol-protocells bilayers retain ~60% of negatively charged cargo at pH 7.4, which mimics CSF as well as extracellular pH, during a 1 week timeframe. Importantly, protocells at lower pH values release 25-50% of cargo within a 72 hr window. Importantly, a substantial amount of protocell cargo content remains by 1 week (**Figure 2.1, D, E**), supporting the possibility that enduring cargo release for many weeks can be achieved resulting in long-duration therapeutic transgene efficacy. Future studies will determine whether trafficking to late lysosomes containing ~3-4 pH values results in a significant amount of cargo release as well as enduring efficacy. While the mechanism of protocell escape from lysosomes remains unknown, the general pattern of pH-dependent

70

cargo release may support an approach that optimizes cargo delivery to the intracellular compartment. Of further note is the stability of cargo-associated protocells formulated with either DOTAP:Chol or DOPC at pH 6, suggesting that early endosomal organelles (typically near pH 6) stabilize protocell cargo until subsequent trafficking to lysosomes. Confocal microscopy shown in the current report demonstrates that protocell cargo is indeed present within and adjacent to cellular nuclei of macrophages in the spinal meninges surrounding the injection site. These observations suggest that while protocells do not necessarily need to enter the nucleus for transgene host cell gene activation, nuclear localization is possible.

While MSNs have been widely studied and are known for in vitro biocompatibility, high cargo capacity, tunable pore diameters and surface chemistries [114, 119-124], this report is the first *in vivo* demonstration of protocell constructs as being non-toxic and functionally capable as non-viral spinal gene therapy vectors. The therapeutic application of protocells is highly beneficial for several critical reasons. First, a low *in vitro* toxicological effect by the components of protocells is observed (**Figure 2.7, C),** as our data show unaltered levels of inducible nitric oxide, a factor that is rapidly produced following cell stress and inflammation known to mediate the induction of reactive oxygen species further contributing to cell stress.[125, 126] The current data also reveal a lack of *in vivo* toxicological effects following spinal protocell application (**Figure 2.3, A-D**), as spinally-mediated sensory hindpaw response-thresholds remained unchanged from baseline, a physiological 'read-out' of healthy conditions. Further, we demonstrate that spinal tissue immunohistochemical examination indicated the complete absence of activated Caspase-3 (**Figure 2.4 C**), a critical enzyme that mediates programmed cell

71

death.[127] Second, these protocells offer simpler manufacturing methods aimed at controlling cargo displacement compared to more sophisticated methods that employ additional organic molecules used for 'gating' silica pores.[128] Third, a high degree of flexibility to modify silica surface chemistry and pore size to tailor adsorption of specific cargo[129] is available. Collectively, these properties of protocells make them attractive platforms for non-viral drug or gene delivery using a wide range of formulations. In the current study, this first-generation protocell supporting a DOTAP:Chol lipid bilayer appears to be functionally effective as spinal gene delivery vehicles for pain-related therapeutic purposes.

The majority of worldwide clinical trials using non-viral gene delivery techniques currently represents ~27% of the total gene therapy clinical trials,[130] with these trials mostly applying naked plasmid DNA, and none aimed at neuropathic pain control. However, the examination of gene therapy applications for neuropathic pain in animal models has significantly increased during the past dozen years, with candidate gene products intended to disrupt pain-associated biochemical changes, or themselves, act as analgesics.[131] These trends point to the extraordinary need for new approaches toward developing novel pain therapeutics, as currently available drugs are minimally effective for pathological pain. Thus, the emerging area of CNS gene therapeutics for pain control is rapidly growing.

Neuropathic pain results from pathology in the nervous system and arises from aberrant signals in sensitized injured axons in the peripheral and/or central nervous system.[132] The anti-inflammatory cytokine, IL-10, leads to exceptionally robust

suppression of several pain-related conditions including allodynia in various animal models.[133] Allodynia, as assessed in this study, is a pathological sensory condition whereby non-noxious stimuli such as mechanical light touch to the skin are processed as painful.[134] and spinal IL-10 gene therapy results in prolonged suppression of chronic allodynia.[97] Indeed, non-viral naked plasmid DNA or polymer-encapsulated gene therapy to control neuropathic pain has been successfully demonstrated in animal models of neuropathic pain.[73,79,135] Interestingly, these non-viral approaches are thought to harness phagocytic innate immune cells that are present at low levels in the peri-spinal meninges and subarachnoid space,[97] as an increase in phagocytic macrophages accumulate surrounding the intrathecal lumbar spinal injection site. However, the transgene dose, release rate and cellular targets are constrained by the method of gene delivery used in these prior studies. Conversely, increased transgene dose (cargo retention) and greater flexibility in DNA release rate and cellular targeting can be achieved via protocells as delivery platforms.

The prior established efficacy of IL-10 for pain control allows comparisons with novel gene delivery approaches, like protocells, that result in therapeutic pain-suppression, and enables one to identify new and improved gene and drug carrier platforms with promising clinical applications. Our data demonstrate that this first-generation DOTAP:Chol protocell formulation is a highly feasible carrier platform for spinal gene therapy. It is important to note that developing next-generation protocell platforms are aimed at delivering cargo that act to stimulate transgene uptake; a multi-therapy approach, and may be superior to existing approaches.

2.5 Conclusions

This work characterizes the *in vitro* and *in vivo* toxicological profile of liposomes fused on MSNs, and examines their use as gene therapeutic vectors delivered to the spinal cord. These liposome-supported MSN constructs are referred to as protocells, which act to retain and protect DNA cargo used in these studies. The advantage of applying protocells as cargo delivery systems (drug and genes) lies not only in their potential for exceptional cargo capacity, cell-specific targeting and tunable release rates, but also, as demonstrated in this report, in their high and enduring biocompatibility within the CNS. As non-viral vectors, protocells allow transgenes of interest to remain physiologically functional. Most intriguing is the potential application of this approach to other CNS diseases.[136, 137] The data in this report demonstrate that protocells loaded with the IL-10 transgene and delivered peri-spinally produce robust pain suppression supporting prior reports that spinal IL-10 gene therapy leads to a reduction of pain.[68,72,73, 98,138] Thus, protocells offer a potentially new drug delivery vessel to the CNS with intrinsic flexibility to tailor drug therapy.

Acknowledgments

3. Improvement of spinal non-viral IL-10 gene delivery using D-Mannose as a transgene adjuvant to control chronic neuropathic pain

Ellen C. Dengler[1], Jenny L. Wilkerson[1], Lauren A. Alberti[1], Brandi N. Bowman[1], Audra A. Kerwin[1], Pamela S. Platero[1], Daniel R. Moezzi[1], Vanessa E.D. Garcia[1], Eugene Limanovich[2], James A. Wallace[1], Erin D. Milligan[*1]

1 Department of Neurosciences, Health Sciences Center, University of New Mexico, Albuquerque, New Mexico

2 Department of Anesthesiology and Critical Care Medicine, Health Sciences Center, University of New Mexico, Albuquerque, New Mexico

Ellen C. Dengler, PT, MS; email: EDengler@salud.unm.edu

Jenny L. Wilkerson, BS; email: JLWilkerson@salud.unm.edu

Audra A. Kerwin, BS; email: AKerwin@salud.unm.edu

Lauren A. Alberti; email: LAlberti@unm.edu

Brandi N. Bowman, BS; email: Bbowman@salud.unm.edu

Pamela S. Platero, email: PamSue@unm.edu

Daniel R. Moezzi; email: DMoezzi@unm.edu

Vanessa E.D. Garcia; email: VGarcia9@unm.edu

James A. Wallace, PhD; email: JWallace@salud.unm.edu

ELimanovich@salud.unm.edu

*To whom correspondence should be addressed:

Erin D. Milligan
Department of Neurosciences, Health Sciences Center, School of Medicine
University of New Mexico,
Albuquerque, N.M., USA 87131-5223
PH: 505-272-8103
FAX: 505-272-8082
E-mail: EMilligan@salud.unm.edu

Abstract

Non-viral naked plasmid DNA gene therapy encoding the anti-inflammatory cytokine, interleukin-10 (pDNA-IL-10), results in therapeutic efficacy when delivered to the peri-spinal subarachnoid region (intrathecal; i.t.) to suppress chronic neuropathic pain in animal models. However, two sequential i.t. naked pDNA injections must occur within a discrete 5-72 hr period, defining a time of local immune cell sensitization for improved transgene uptake and prolonged pain suppression assessed by decreases in light touch sensitivity known as allodynia. Utilizing the anti-inflammatory M2-polarizing properties of the synthetic glucocorticoid, dexamethasone, or the hexose sugar, D-mannose, to prime local peri-spinal immune cells, we examined improvement of transgene efficacy with reduced naked pDNA-IL-10 doses previously determined ineffective when delivered without a priming pre-treatment. Compared to dexamethasone, i.t. mannose priming significantly and dose-dependently prolonged pDNA-IL-10 pain suppressive effects, reduced spinal IL-1β and enhanced spinal and dorsal root ganglia IL-10 immunoreactivity. Macrophages exposed to D-mannose revealed reduced proinflammatory tumor necrosis factor-α, IL-1β, and nitric oxide, and increased endogenous and transgene-derived IL-10 protein production. A single co-injection of mannose with a 25-fold lower pDNA-IL-10 dose produced prolonged pain suppression in neuropathic rats, supporting this novel approach of tuning spinal immune cells toward an activated M2 phenotype for improved non-viral gene therapy.

Key Words: M2 polarized, cytokine, sciatic nerve, gene therapy, intrathecal injection, spinal, allodynia, rat

3.1 Introduction

Existing drugs, which primarily target neurons, partially reduce pain (~25-40%) in less than half of the 7-8% of patients suffering from chronic neuropathic pain in the US,[139, 140] which underscores the need to develop new therapeutic approaches to treat pathological pain. Modern views of pain processing are emerging which include critical roles of factors released from non-neuronal cells in the central nervous system (CNS), like glial cells,[141, 142] and glia in the dorsal root ganglia (DRG) that house pain-related neurons.[143, 144] Glial proinflammatory cytokines like interleukin-1β (IL-1β) and tumor necrosis factor-alpha (TNF-α), and inducible factors such as calcium-independent nitric oxide (NO) are characterized to mediate the initiation and maintenance of experimental neuropathic pain. Leukocytes (e.g. macrophages, dendritic cells, T cells), responding to glial cytokines and NO, accumulate in DRG sites as well as peri-spinal subarachnoid regions immediately adjacent to spinal pain transmission neurons during pain neuropathies produced by remote, localized peripheral nerve lesions,[145, 48, 146-150] suggesting that leukocytes may further contribute to neuropathic pain. Leukocyte-derived IL-1β, TNF-α and other immune-related signaling factors in peri-spinal subarachnoid regions can create continuous feed-forward cytokine production and activity. Notably, accumulation of leukocytes into these sites concomitant with neuropathic pain is generated in the absence of infection. Together, the actions of spinal and DRG glia, as well as local leukocytes, enhance signaling processes that mediate neuropathic pain in animal models.

Because IL-1β, TNF-α and NO are so powerful, leukocytes and glial cells have evolved the means to create negative feedback suppression of their activity. This is achieved by mechanisms that include the production of anti-inflammatory cytokines, of which interleukin-10 (IL-10*)* is one of the most potent. IL-10 can inhibit a variety of cytokines including IL-1β and TNF-α by preventing intracellular kinase activation pathways, and preventing IL-1β and TNF-α transcription, translation, post-translational processing and protein release.[151, 152] Additionally, IL-10 is both a natural product of glia (astrocytes and microglia)[153] and leukocytes, such as macrophages and dendritic cells, which express IL-10 receptors.[62] Importantly, adult spinal cord neurons do not produce IL-10 and do not express IL-10 receptors, even under neuropathic conditions.[154, 155] Prior reports demonstrate that IL-10 administration is an effective strategy to produce pain relief by blunting glial mediators of neuropathic pain signaling.[156, 97, 98,157,158] Thus, the application of IL-10 is a therapeutic intervention of pathological cytokine and NO-mediated pain signaling, without exerting direct actions on neurons.

Gene therapy has received some recognition as a tool to target glia for pain control.[131, 159, 160] While gene transfer using non-viral naked plasmid DNA (pDNA) is the least effective method to transform host cells with therapeutic genes of interest,[161] our prior work demonstrates that utilizing pDNA encoding the IL-10 transgene (pDNA-IL-10) delivered to the peri-spinal subarachnoid (intrathecal; i.t.) region produces robust and enduring pain reversal in animal models.[68, 97] While a clearly defined mechanism by which spinal cord non-viral pDNA gains access to host cell machinery for transgene expression is poorly understood, one strong possibility is that gene transfection can result from non-specific phagocytosis by macrophages/dendritic cells.[80] Although virtually

every cell type is capable of phagocytosis, macrophages and dendritic cells are specialized immune phagocytic cells that reside within healthy and intact peri-spinal meninges.[78] Additionally, spinal cord microglia and astrocytes are ascribed as highly efficient phagocytic cells of the CNS.[162, 163] Indeed, microglia are "the macrophages of the CNS", and astrocytes maintain a healthy microenvironment by routinely clearing/digesting dying cells. Naked pDNA can stimulate macrophages, dendritic, and glial cells,[71, 164, 165] leading to the rapid production of cytokines that trigger leukocyte extravasation from circulation into peri-spinal meninges and the i.t. space.[72] The cell-enriched peri-spinal subarachnoid region may be a key component for augmented transgene uptake and expression.

Different phenotypic profiles of immune and glial cell activation in the meninges may be particularly permissive for non-viral, DNA-based gene transfer, which can be a unique target for therapeutic long-duration pain control. Activation of phagocytic leukocytes (particularly macrophages and dendritic cells) leads to the production and release of a family of proinflammatory cytokines including IL-1β and TNF-α that are characterized as possessing an M1 polarized/classical activation phenotype (pro-inflammatory state). More recently, these same cell types have been described with an M2 polarized/alternative activation phenotype that is characterized by a distinct set of anti-inflammatory cytokines[55] including IL-4 and IL-10.[54,166-169] One hallmark of alternative activation is increased expression the mannose receptor (MR)[167] in the presence of increased IL-4 and IL-10 protein production with decreased IL-1β, TNF-α and NO production.[54, 166-169] Moreover, the synthetic glucocorticoid, dexamethasone, is characterized to induce MR expression and induces an M2 polarized/alternative

activation phenotype.[167] M2 polarized/alternatively activated leukocytes (e.g. macrophage/dendritic cells) and glial cells express low levels of pro-inflammatory IL-1β, TNF-α, cytokines, and higher levels of IL-10, and reveal enhanced IL-10-mediated phagocytic capacity.[170] Thus, spinal transgene uptake may be substantially improved by targeting M2 polarized/alternatively activated leukocytes, including macrophages present in the peri-spinal subarachnoid region, to phagocytose naked pDNA encoding IL-10.

We recently reported the discovery of a sensitization period between two sequential peri-spinal i.t. injections of naked pDNA that exploits immune phagocytes (e.g., macrophages) for improved IL-10 transgene uptake (**Scheme 1**).[72,107] The components of the naked pDNA used in the first injection does not require the presence of the IL-10 transgene. However, the IL-10 transgene must be present in the pDNA used for the second injection to result in long-duration pain relief. Thus, the pDNA used for the first injection may simply act to stimulate the surrounding local leukocytes and is thought to initiate a local cellular response that leads to enhanced uptake of the IL-10 transgene used for the second injection.[72] The sensitization period is discrete within the spinal subarachnoid microenvironment, with a 5-72 hour inter-injection interval, as inter-injection intervals outside of this period fail to produce transgene-derived IL-10 mRNA expression, increased IL-10 protein or long-duration pain relief. [68, 72, 73, 171]

Sensitization Period

1st intrathecal injection

2nd intrathecal injection

Inter-injection interval 5-72 hours

Expression of Transgene IL-10

Initial Pain Relief

Long-duration Pain Relief

90 days post injection
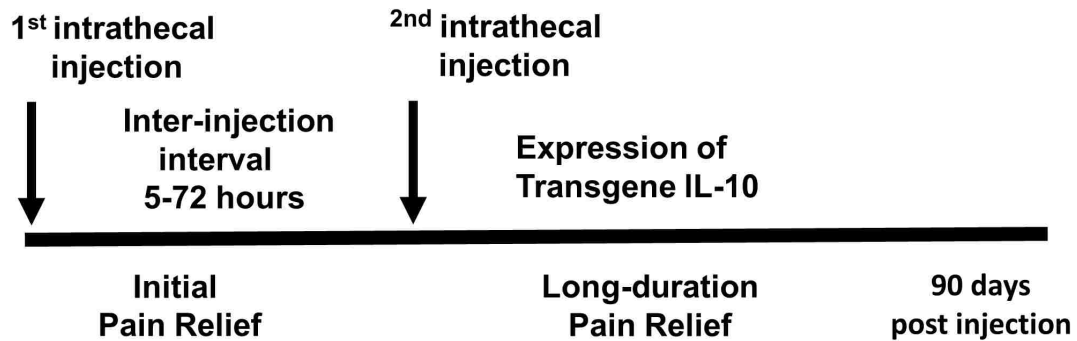
Scheme 1 Illustration depicting the "sensitization period".

This scheme describes a discrete window of time or sensitization period, from 5-72 hours following the first i.t. injection of pDNA-IL-10 (100 μg), during which the second injection of pDNA-IL-10 (25 μg) must be given to generate stable and enduring pain relief. If the second injection is given outside of this time interval, pain reversal is dramatically shortened. During the sensitization period, an accumulation of leukocytes was found surrounding the i.t. injection site, a large number identified as macrophages.[135] A possible mechanism underlying improved transgene therapeutic efficacy during this period may be a change in the macrophage cytokine profile with a switch from proinflammatory M1/classical activation to anti-inflammatory M2/alternative activation resulting in improved phagocytosis of transgene.

The goal of the present studies is to sensitize and shift peri-spinal immune phagocytes to an M2 polarized/alternative activation phenotype for enhanced pDNA-IL-10 uptake within the sensitization interval that leads to enduring pain relief. Dexamethasone and D-mannose, both previously characterized to strongly induce the expression of the M2 polarized/alternative activation phenotype, will be examined as factors capable of priming peri-spinal macrophages for improved pDNA-IL-10 transgene uptake, as assessed by the efficacy of low-dose transgene i.t. delivery (duration of therapeutic pain suppression) and increased IL-10 protein expression in discrete spinal and DRG regions critical for pain processing.

3.2 Results

3.2.1 Dexamethasone primes subsequent i.t. pDNA-IL-10 to produce transient and minimal behavioral reversal of allodynia

The synthetic glucocorticoid steroid, dexamethasone (DEX), given as an initial i.t. priming injection and followed by an i.t. pDNA-IL-10 (25 µg) injection results in a delayed and transient reversal of allodynia produced by chronic constriction injury (CCI) of one sciatic nerve. This is a well-characterized and widely used animal model of chronic peripheral neuropathic pain that results in clinically relevant neuropathic behavioral changes such as allodynia and is assessed by sensitivity to light touch using the von Frey test **(Figure 3.1)**. Following establishment of baseline (BL) responses to von Frey filaments, animals are treated with either CCI or sham surgery. Compared to sham-operated controls that reveal stable threshold responses near BL values, clear development of allodynia occurs in CCI-operated rats, as measured 3 and 10 days later. Rat hindpaw responses now occur at <1.0 grams of touch stimuli. On day 10, sham and CCI animals received 2 sequential i.t. saline injections 3 days apart. Shams remained stably non-allodynic hindpaw throughout the 27-day timecourse while neuropathic CCI-operated rats given similar injections had clear and chronic hindpaw allodynia throughout the same period. Those CCI animals given a priming i.t. injection of 62.4 ng DEX, but not 6.2 ng, followed 3 days later by an i.t. injection of pDNA-IL-10 (25 µg) experienced a delayed onset of partial but short-term reversal of allodynia, lasting only 2 weeks. Similar behavioral hindpaw responses were observed contralateral to CCI **(Figure 3.1)**.
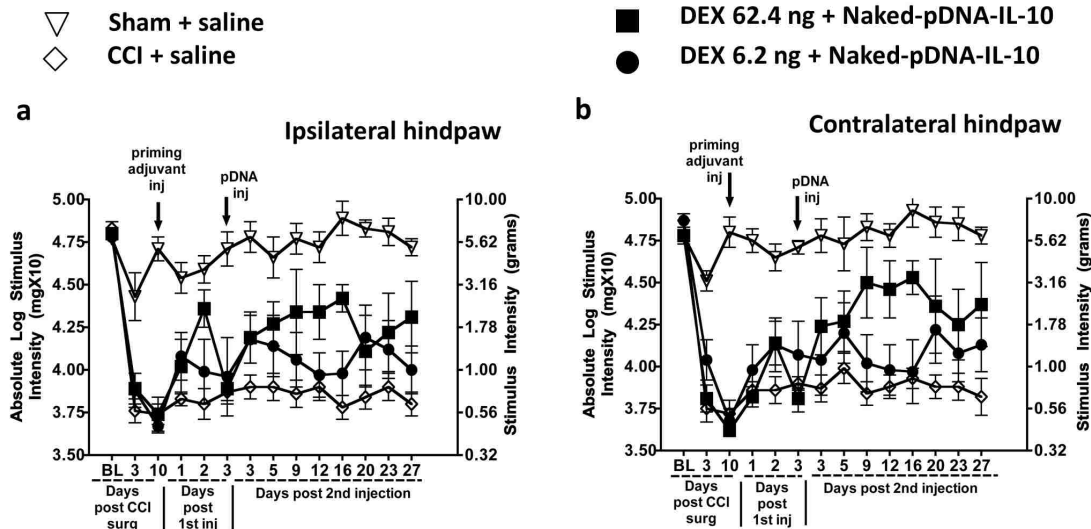
Figure 3.1 Dexamethasone for improved pDNA-IL-10 uptake does not create robust pain reversal.

(a and b) Baseline (BL) hindpaw sensory threshold responses to light mechanical touch were measured by the von Frey test with calibrated monofilaments). There were no significant differences observed between groups (Ipsilateral, $F_{(3,24)}$ =0.2154; p=0.8846; Contralateral, $F_{(3,24)}$=0.6930; p=0.5665). Following either CCI or sham surgery, behavioral testing continued at the time points indicated on the x-axis. Animals receiving CCI surgery developed stable allodynia from day 3 to day 10 compared sham-operated animals (day 10: Ipsilateral, $F_{(3, 24)}$ =53.54; p<0.0001; Contralateral, $F_{(3, 24)}$=71.70; p<0.0001). On day 10 following CCI surgery, animals received an i.t. injection of DEX (62.4 ng, n=6 or 6.2 ng, n=6), or equivolume i.t. saline (n=7) and sham-operated animals received i.t. equivolume saline (n=6). Three days later, an i.t. injection of pDNA-IL-10 (25 μg) or equivolume saline was given. Sham-control animals remained non-allodynic, while CCI animals given i.t. saline remained allodynic. I.t. pDNA-IL-10 following a priming injection of DEX (62.4 ng) revealed a delayed and partial bilateral pain reversal (Ipsilateral, $F_{(3,140)}$ =33.83; p<0.0001; Contralateral, $F_{(3,140)}$=19.7; p<0.0001). Black arrows indicate i.t. injections. (A, B- Behavioral testing by Ellen Dengler with assistance from Lauren Alberti and Brandi Bowman)

3.2.2 D-Mannose primes subsequent i.t. pDNA-IL-10 to produce long-term behavioral reversal of allodynia

An i.t. priming injection of D-mannose dose-dependently and dramatically increased the therapeutic efficacy of 25 μg i.t. pDNA-IL-10 given within a 3-day inter-injection interval **(Figure 3.2)**. Non-neuropathic sham-operated saline injected control-

84

treated rats revealed stable, bilateral non-allodynic responses, while CCI-treated rats given i.t. saline control injections revealed ongoing bilateral chronic allodynia throughout a 91-day timecourse. Strikingly, an i.t. priming injection of D-mannose (50 µg) followed three days later by i.t. pDNA-IL-10 (25 µg) produced a complete reversal of allodynia similar to BL thresholds that stably persisted for 3 months. Allodynia never returned. Also provocative was the observation that a 10-fold lower i.t. priming dose of D-mannose (5 µg) followed by i.t. pDNA-IL-10 produced a partial and enduring relief from bilateral allodynia. However, when a priming injection of D-mannose (50 µg) was followed by a 25 fold lower dose of i.t. pDNA-IL-10 (1 µg) there was complete but only transient reversal from allodynia of ~11 days **(Figure 3.2)**.
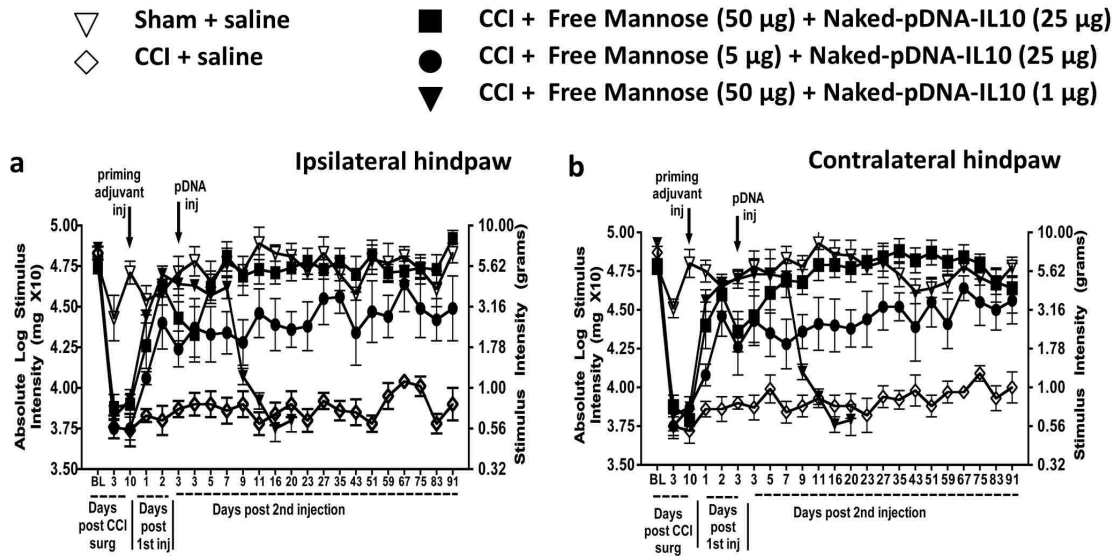
Figure 3.2 The D-Mannose used to prime M2 polarization for improved pDNA-IL-10 uptake reverses allodynia greater than 90 days.

(a and b) No significant differences in BL responses between groups prior to CCI or sham surgery were observed (Ipsilateral, $F_{(4,32)}$=1.009; p=0.4197; Contralateral, $F_{(4,32)}$=1.147; p=0.3551). Sham operated animals (open triangles; n=6) remained non-allodynic throughout the time course. CCI animals (open diamonds; n=7) revealed clear allodynia from day 3 to day 10 compared to shams (day 10: Ipsilateral,

$F_{(4,32)}$=32.87; p<0.0001; Contralateral, $F_{(4,32)}$=37.01; p<0.0001). On day 10, animals received an i.t. injection of either D-mannose (50 µg; 5 µg) , or equivolume saline followed three days later by pDNA-IL-10 (25 µg or 1 µg) or equivolume saline. Following the first priming injection of D-mannose (50 µg; closed squares; n=8), a robust reversal was observed, compared to CCI-saline injection (Ipsilateral, $F_{(3, 70)}$=15.87; p=0.0004; Contralateral, $F_{(3, 70)}$=20.40; p=0.001). Full reversal to BL levels continued for a 3 month period beyond the 2nd injection of pDNA IL-10 (25 µg) in those animals given D-mannose (Ipsilateral, $F_{(3, 384)}$ =57.46; p<0.0001; Contralateral, $F_{(3, 384)}$ =59.20; p<0.0001). A 2nd injection of a lower dose of pDNA-IL-10 (1ug: closed triangles; n=5) produced a transient 11-day reversal. Animals pretreated with the lower dose of D-Mannose (5 µg) followed by a second injection of pDNA-IL-10 (25 µg) (closed circles, n=7) showed partial bilateral reversal for the 3 month time course that was not significant (Ipsilateral, $F_{(3,17)}$= 12.71; p=0.0270; Contralateral, $F_{(3, 17)}$= 14.64; p= 0.002). (A, B- Behavioral testing by Ellen Dengler with assistance from Lauren Alberti, Brandi Bowman, Vanessa Garcia and Daniel Moezzi)

3.2.3 Characterization of D-mannose: short-term reversal of allodynia, M2-polarization, and increased IL-10 transgene expression.

Results illustrated in Figure 3.2 raise the possibility that D-mannose may exert enduring pain-suppressive effects in the absence of transgene IL-10. To examine this question, we investigated whether a single i.t. injection of D-mannose could sustain prolonged pain relief. Following BL threshold assessment, all animals underwent CCI surgery, and threshold responses revealed clear bilateral allodynia 3 and 10 days later. On day 10, a single i.t. injection of 50, 5, or 0.5 µg D-mannose or saline was delivered. Behavioral thresholds revealed robust bilateral reversal from allodynia following the highest dose of i.t. D-mannose compared to lower doses or saline **(Figure 3.3, a and b)**.

To examine whether D-mannose could directly induce an anti-inflammatory phenotype, mouse macrophage RAW264.7 cell cultures were used as a cell type comparable to macrophages that occur in high populations in high numbers in the peri-spinal subarachnoid region. A classic proinflammatory response was initiated by

Lipopolysaccharide (LPS), which is cell-wall particles from gram-negative bacteria, to mimic the local peri-spinal signaling milieu present during chronic peripheral neuropathic conditions, namely increased TNF-α, IL-1β and nitric oxide production. These data confirm that cells pre-incubated with D-mannose followed by challenge with LPS resulted in increased IL-10 protein levels **(Figure 3.3, c)** with simultaneous ablation of IL-1β protein **(Figure 3.3, d)**, and a robust reduction of protein TNF-α **(Figure 3.3, e)**, and NO production **(Figure 3.3, f)**. Interleukin-4, an anti-inflammatory cytokine strongly associated with an M2 phenotype, was also tested. However, D-mannose at the doses tested yielded no reliable IL-4 protein increases (data not shown). Thus, in cultured macrophage cells, D-mannose creates a robust reduction in pro-inflammatory markers while significantly elevating IL-10 during stimulatory conditions that activate inflammatory pathways.

A possible mechanism for increased pDNA-IL-10 efficacy on pain reversal observed in Figure 2 is that D-mannose could increase transgene uptake. To directly examine D-mannose's effects on pDNA-IL-10 uptake, cultured RAW264.7 cells (mouse cell line) were incubated with either D-mannose, pDNA-IL-10 (encoding rat IL-10 protein; 0.5 µg or 5.0 µg), or D-mannose + pDNA-IL-10 (0.5 µg or 5.0 µg). A significant increase in rat IL-10 protein levels were measured from supernatants of cells treated with D-mannose in combination with pDNA-1L-10 at either 0.5 µg or 5.0 µg **(Figure 3.3, g)**. IL-10 protein levels increased with increased dosages of the pDNA-IL-10 transgene only in the presence of D-mannose. It is important to note that the ELISA for rat IL-10 does not cross-react with mouse IL-10 protein levels, demonstrating that plasmid-derived IL-

10 protein is robustly expressed when the IL-10 transgene is delivered to RAW264.7 cells in combination with D-mannose.
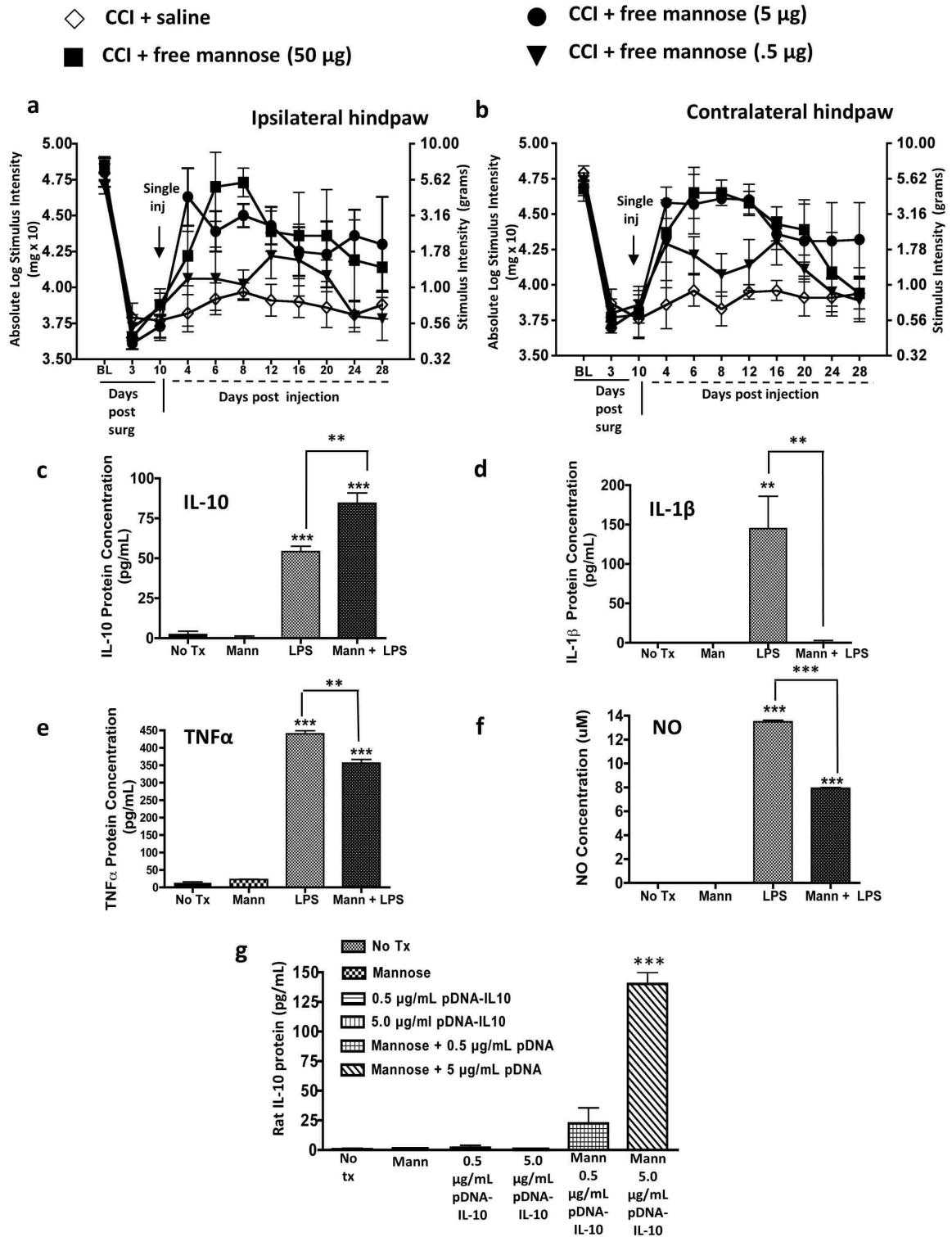
Figure 3.3 D-Mannose generates short-term reversal of allodynia without pDNA-IL-10.

89

(a and b) No significant BL response differences between groups prior to CCI was observed (Ipsilateral, $F_{(3,13)}$ =0.4995; p=0.6910; Contralateral, $F_{(3,13)}$=0.1761; p=0.9099). All animals underwent CCI surgery and revealed clear allodynia by day 10 with no significant differences between groups ($F_{(3,13)}$=0.1897; p=0.9010; Contralateral, $F_{(3,13)}$=0.2234; p=0.8780). On day 10, animals were given a single i.t. injection of D-mannose (50, 5, or .5 µg; closed squares, closed circles, or closed diamonds respectively) or an equivolume saline only (n=3-4/group). Saline-treated animals (open diamonds) remained bilaterally allodynic throughout the time course. Treatment with D-mannose (50 µg, n=3) resulted in bilateral partial reversal from allodynia that gradually returned by day 20 following injection (Ipsilateral, $F_{(3,70)}$=15.87; p<0.0005; Contralateral $F_{(3,70)}$= 20.40; p=0.0001). Black arrows indicate i.t. injection. (c-f) Cultured Raw 264.7 mouse macrophage cells were pretreated with D-Mannose (100 mM) followed by a 2 hour incubation with a combination of D-Mannose (100 mM) and LPS (10 ng). (c) Compared to control treatment (No Tx=no treatment; Mann=D-mannose), LPS-stimulated cells given D-mannose treatment resulted in significantly increased IL-10 protein production, (d) almost complete ablation of IL-1β levels (e) significantly reduced TNF-α protein levels, and (f) reduced NO production. (g) Cultured Raw 264.7 mouse macrophage cells were pretreated with D-Mannose (500 mM) for 5 hours followed by a 24 hour incubation with D-mannose with or without pDNA-IL-10, or D-Mannose and pDNA-IL-10 alone. Those cells incubated with D-mannose and pDNA-IL-10 showed robust and significantly increased exogenous rat IL-10 production over controls ($F_{(5,17)}$=69.3; p<0.001)*p<0.05; **p<0.01; ***p<0.0001 (A, B- Behavioral testing by Ellen Dengler with assistance from Lauren Alberti, Vanessa Garcia and Daniel Moezzi; C-G- Experiment run by Audra Kerwin with statistical analysis and graphics by Ellen Dengler)

3.2.4 Intrathecal D-mannose priming followed by i.t pDNA-IL-10 results in increased IL-10 and decreased IL1β expression in spinal cord and DRG

The data described above show that D-Mannose (50 µg) followed by pDNA-IL-10 (25 µg) results in enduring pain reversal. We next examined whether cytokine changes critical for neuronal pain processing occurred in regions where active glial and immune cells are found. We examined by immunohistochemical detection, IL-10 and IL1 β in lumbar and DRG tissue regions from behaviorally verified rats. Following BL assessment, behavioral thresholds were reassessed on day 3 and 10 to ensure the presence of chronic allodynia in CCI-treated rats. As before, animals received an i.t. injection of saline, or D-mannose (50 µg) followed three days later by saline or pDNA-IL-10 (25 µg).

90

Duplicating the results of our prior experiment above, i.t. D-mannose followed 3 days later by i.t. pDNA-IL-10 produced full and sustained reversal from allodynia compared to non-mannose controls receiving either i.t. saline followed by pDNA-IL-10, or 2 i.t. saline injections in CCI-treated rats **(Figure 3.4, a and b)**. Animals were deeply anesthetized on Day 29 and spinal cord and DRG tissues were collected to examine potential spinal and DRG cytokine changes corresponding to the observed behavioral profile. The anatomical regions of the spinal cord analyzed correspond to the terminals of sciatic nerve fibers entering the L4-L6 spinal cord from the corresponding DRG. Primary antibodies immunoreactive (IR) for IL-10 and IL-1β, were detected using immunoreactive Rhodamine-Red fluorophore-conjugated secondary antibodies. Immunofluorescence was quantified using computer-assisted spectral analysis software as described in the methods, below.

Analysis of ipsilateral spinal cord IL-10 **(Figure 3.4, c),** revealed significant increases in IL-10 IR in D-mannose-pDNA-IL-10 treated rats compared to non-mannose treated controls. Contralateral spinal cord IL-10 IR revealed similarly increased levels (data not shown). Representative photomicrographs of the quantified data are shown **(Figure 3.4, d-f)**, revealing IL-10 IR occurs primarily in gray matter in the deeper spinal laminae. Conversely, fluorescent quantification demonstrates that spinal IL-1β IR is significantly reduced in D-mannose primed pDNA-IL-10 injected rats compared non-mannose treated controls (**Figure 3.4, g)**. As with IL-10, representative photomicrographs are shown **(Figure 3.4, h-j)** that are part of the analyzed data of the different treatment groups, and depict a punctate pattern primarily in the white matter of the spinal cord. Contralateral IL-1β IR appears similar (data not shown) to that observed

91

in the ipsilateral spinal cord, but failed to reach significance. Unexpectedly, IL-10 IR was significantly increased in DRG following D-mannose-pDNA-IL-10 treatment compared to non-mannose treated controls **(Figure 3.4, k)**. Representative photomicrographs **(Figure 3.4, l-n)** are shown. Notably, the pattern of IL-10 IR is peri-neuronal.

Given high variance was observed only in the saline-pDNA-IL-10 group, a Grubb's Z-test[172] (as described in *Methods*) was applied to identify an outlier from the group mean, and one rat was omitted from the lumbar and DRG analyses, resulting in saline-pDNA-IL-10 data that is representative of 8, and not 12, tissue slices.
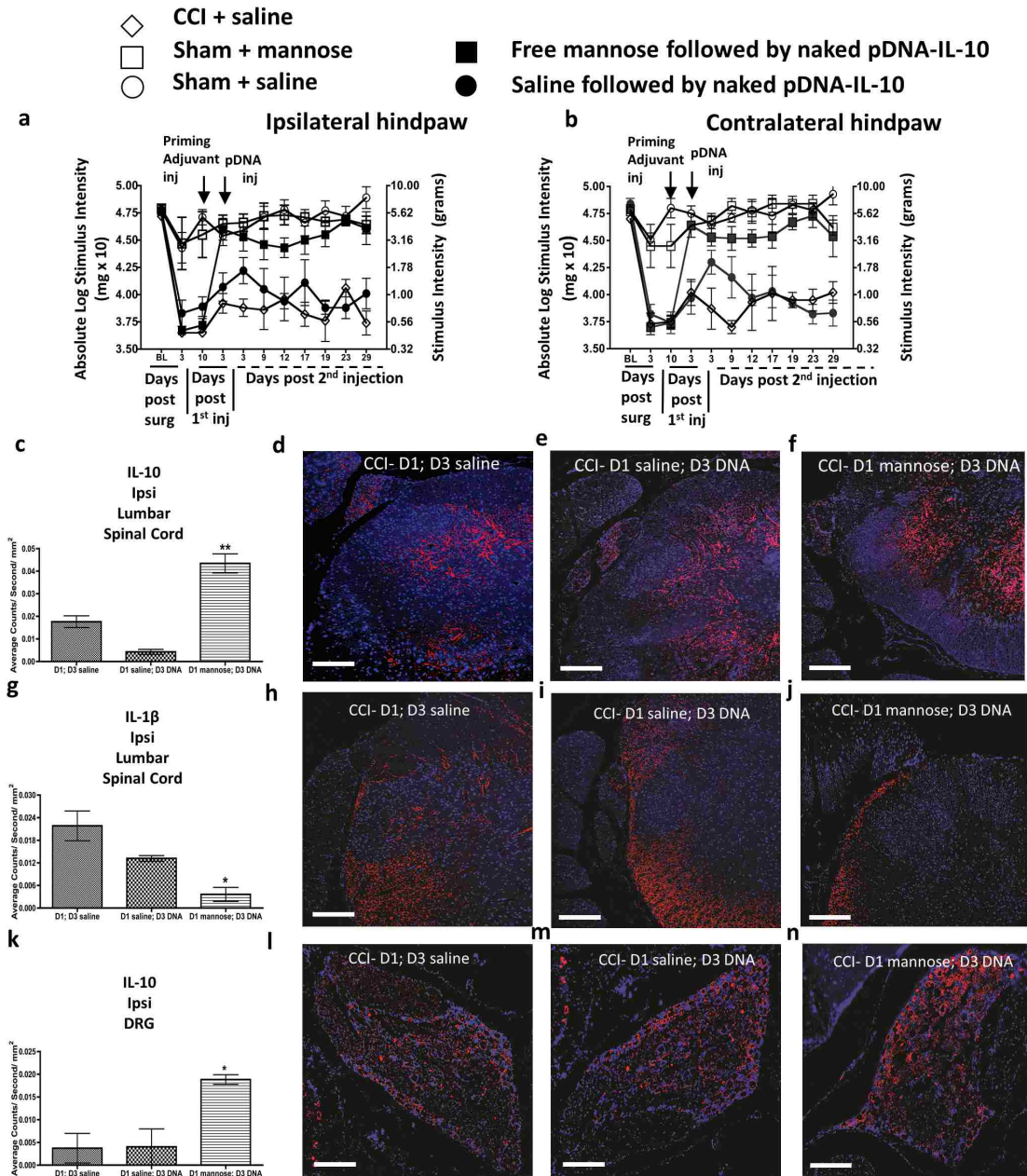
Figure 3.4 Spinal and DRG pro-and anti-inflammatory markers expression.

(a and b) Verification of animal behavior prior to tissue collection is represented. There were no differences between groups at BL prior to CCI or sham surgery (Ipsilateral, $F_{(5,18)}$ =0.2597; p=0.8999; Contralateral, $F_{(5,18)}$=0.4947; p=0.9398). As before, CCI treated animals revealed clear bilateral allodynia to day 10 compared to sham controls (Ipsilateral, $F_{(5, 18)}$ = 35.54; p<0.0001; Contralateral, $F_{(5, 18)}$=35.96; p<0.0001). On day 10 following sham or CCI surgery, animals were given an i.t. pretreatment with D-mannose (50, µg) or equivolume saline injection followed three days later by i.t. pDNA-IL-10 (25 µg; closed squares;

n=7) or equivolume saline (closed circles; n=4). Saline-CCI treated animals (open diamonds; n=3) remained bilaterally allodynic throughout the time course compared to sham-D-mannose (open squares; n=3) or sham-saline (open circles; n=6) treated animals (Ipsilateral, $F_{(3,9)}$=28.79; p=0.0001; Contralateral, $F_{(3,9)}$=19.7; p=0.0007). These data replicated our earlier results above, and reveal that i.t. pretreatment with D-Mannose (50 μg) followed by pDNA-IL-10 (25 μg) causes a full bilateral reversal of allodynia compared to CCI-control groups (Ipsilateral $F_{(4,126)}$= 30.27; p < 0.0001; Contralateral $F_{(4,126)}$= 35.75; P< 0.0001). At day 29 while rats remained fully reversed from allodynia, spinal cord and associated DRG tissues were collected and stained for the anti-inflammatory cytokine, IL-10 or the pro-inflammatory cytokine, IL-1β. (c) Animals that received D-mannose (50 μg) on day 1 and pDNA-IL-10 on day 3, revealed significantly greater IL-10 immunoreactivity (IR) in the lumbar spinal cord compared to those animals injected with saline only or saline followed by pDNA-IL-10 (Ipsilateral $F_{(3, 5)}$=34.23; p<0.01; Contralateral $F_{(3, 5)}$=2.714; p>0.05). (d,e,f). Representative images used for the data analysis are presented (red=IL-10 IR, blue=cell nuclei). (g) Adjacent tissue sections revealed significantly less IL-1β IR in the ipsilateral lumbar spinal cord compared to non-mannose treated control groups (Ipsilateral $F_{(3,5)}$=10.67; p<0.05; Contralateral $F_{(3,5)}$=3.73; p> 0.05). (h, i, j). Corresponding fluorescent images of the analyzed data are presented (red =IL-1β IR, blue=cell nuclei). (k) In addition, significantly greater IL-10 IR in the DRG is observed in the D-mannose primed treatment group compared to both non-mannose treated control groups (Ipsilateral $F_{(3, 5)}$ =10.35; p<0.05; Contralateral $F_{(3, 5)}$ =5.73; p>0.05). (l, m, n). Corresponding fluorescent images of the analyzed data are presented (red =IL-10 IR, blue=cell nuclei). Data for the contralateral DRG data are not shown. *p< 0.05; **p< 0.01; ***p<0.0001; all images were taken at 10X; scale bar =100μm (A, B- Behavioral testing by Ellen Dengler with assistance from Lauren Alberti, Vanessa Garcia and Daniel Moezzi; C-N- Tissue slicing by Ellen Dengler with assistance from Pamela Palermo; IHC and spectral microscopy by Ellen Dengler with assistance from Jenny Wilkerson; computerized analysis by Ellen Dengler with assistance from Jenny Wilkerson and Pamela Palmero)

3.2.5 A single i.t. co-injection of D-Mannose with a very low dose of pDNA-IL-10 extends reversal of allodynia

Robust and fast-acting anti-inflammatory responses of macrophage cells were observed following D-mannose exposure in culture suggesting that D-Mannose may rapidly act to shift local peri-spinal immune cells to an M2 activated phenotype. Indeed, behavioral profiles following i.t. D-mannose treatment described in Figure 2 produced reversal from allodynia within 24 hrs. To expand upon these findings, we examined

whether the efficacy of a low dose of pDNA-IL-10 (1µg) shown to induce an ~11 day pain suppression **(Figure 3.2)**, could be improved with a *single co-injection* of D-mannose. As before, von Frey BL responses were assessed, followed by sham or CCI treatment and a reassessment of allodynia through day 10. Compared to non-neuropathic sham controls, CCI produced clear bilateral allodynia by day 10, which persisted following an i.t. saline injection, while non-neuropathic sham control animals given i.t. saline remained non-allodynic through a 26 day timecourse **(Figure 3.5, a and b)**. However, animals that received a single i.t. co-injection of D-mannose (50 µg) with pDNA-IL-10 (1 µg) resulted in a clear bilateral reversal of allodynia that was sustained for 26+day**s (Figure 3.5, a and b)**, while control saline or DNA-injected rats remained fully allodynic. These data demonstrate for the first time that a single injection of D-Mannose (50 µg) co-injected with pDNA-IL-10 (1µg) reverses allodynia for ~26 days.

Figure 3.5 A single co-injection of D-mannose with low dose pDNA-IL-10 produces enduring reversal of allodynia.

95

(a and b) No significant BL response differences were observed between groups prior to CCI or sham surgery (Ipsilateral, $F_{(3, 32)}$ =0.8932; p=0.4973; Contralateral, $F_{(36, 32)}$ =1.393; p=0.231. As before, CCI treated animals revealed clear bilateral allodynia through day 10 compared to sham controls (Ipsilateral, $F_{(3,32)}$ =32.07; p<0.0001; Contralateral, $F_{(3, 32)}$=38.78; p<0.0001). On day 10 after testing, sham rats received a single i.t. saline injection (open triangles; n=8) or D-Mannose (50 µg; closed triangles; n=4), and CCI rats received a single i.t. co-injection of D-Mannose (50 µg) with pDNA-IL-10 (1 µg; closed squares; n=10), pDNA lacking the IL-10 gene (control pDNA; open circles; n=7), or equivolume saline (open diamonds; n=6). Sham-saline and CCI-saline or CCI-control pDNA resulted in no change from bilateral allodynia throughout the time course, D-mannose co-injected with a low-dose of pDNA-IL-10 (1 µg) (closed squares, n=5) resulted in a significant and full reversal of allodynia throughout the 3 week time course (Ipsilateral $F_{(3, 238)}$= 60.23; p<0.001; Contralateral =$F_{(3, 224)}$=22.18; p< 0.001). (A, B- Behavioral testing by Ellen Dengler with assistance from Lauren Alberti and Daniel Moezzi)

3.3 Discussion

The studies in the current report describe the timing and dose refinement of a non-viral peri-spinal naked plasmid DNA (pDNA) therapy by which long-term suppression of neuropathic pain is achieved. Long-term efficacy of this naked DNA therapy requires initial priming of peri-spinal intrathecal (i.t. subarachnoid) meningeal immune cells followed by i.t. injection of pDNA encoding the anti-inflammatory cytokine, interleukin-10 (IL-10), which is in line with the previous observation that i.t. stimulatory oligodeoxynucleotide (ODN) injection facilitated therapeutic pain reversal upon i.t. pDNA-IL-10 injection.[72] While i.t. ODN injection served to prime local innate immune cells for improved uptake of pDNA-IL-10, these ODN adjuvants are characterized to stimulate the immune cell receptor, Toll-like receptor 9 (TLR9) that leads to proinflammatory cytokine production,[173] suggesting that ODNs may not be the ideal adjuvant for transgene therapy. However, corticosteroids provide robust anti-inflammatory effects by suppressing the activation of multiple proinflammatory genes,[75] and thereby, may act to facilitate transgene uptake by controlling pDNA-derived

96

proinflammatory cytokine production. A recent report demonstrated that dexamethasone, a potent synthetic glucocorticoid widely used to control clinical inflammatory conditions, co-delivered with pDNA yielded greater pDNA uptake and lower proinflammatory cytokine levels.[174] Surprisingly, results in the current report demonstrate that a priming i.t. dexamethasone injection followed by i.t. pDNA-IL-10 failed to significantly improve the efficacy of pDNA-IL-10 treatment, and in fact, failed to alter behavioral sensitivity to light touch **(Figure 3.1)**, a pain-related condition referred to as allodynia. Conversely, i.t. D-mannose, characterized to exert anti-inflammatory effects,[175,176] primed subarachnoid immune cells in a dose-dependent manner, such that a subsequent i.t. pDNA-IL-10 injection produced complete and enduring suppression of allodynia induced by CCI **(Figure 3.2)**. These results suggest that D-mannose may dramatically alter the peri-spinal microenvironment in strong favor of transgene uptake. These data are the first demonstration of enduring neuropathic pain suppression by a 5-fold lower dose of i.t. naked pDNA-IL-10 (25 μg), than the 125 μg previously documented.[135] These experiments support the notion that D-mannose may alter an active and ongoing process in the subarachnoid compartment prior to transgene administration such that lower doses of i.t. pDNA-IL-10 are transformed into efficacious treatments for pain suppression.

While the combination of i.t. D-mannose followed 3 days later by i.t. pDNA-IL-10 significantly improved pDNA-IL-10 efficacy, the possibility that D-mannose could exert enduring pain reversal in the absence of IL-10 transgene treatment remained a possibility and was addressed in the current study. Intriguingly, i.t. D-mannose alone produced a dose-dependent but transient reversal of allodynia (**Figure 3.3, a and b**), demonstrating that mannose alters spinal proinflammatory cytokine actions characterized

as crucial mediators of neuropathic pain in animal models.[59] The transient reversal of allodynia additionally suggests that the enduring pain reversal is not due to the effects of mannose only, but to the effects following pDNA-IL-10 treatment.

In further of support of prior studies documenting the anti-inflammatory role of D-mannose, the current data show that D-mannose not only blunts the protein release of the proinflammatory cytokine, TNF-α, and the inflammatory signaling molecule, nitric oxide (NO) generated by calcium-independent inducible NO synthase, but also fully suppresses IL-1β protein levels with simultaneous increases in IL-10 protein levels in lipopolysaccharide (LPS) stimulated macrophage cell cultures **(Figure 3.3, c-f)**. Thus, these data suggest two important and related mechanisms could be altered by spinal application of D-mannose. First, a single injection of D-mannose creates complete but transient reversal of allodynia in an animal model of peripheral neuropathy that is mediated by spinal proinflammatory TNF-α, IL-1β and NO actions. Thus, D-mannose could exert broad spinal anti-inflammatory actions relevant to pathological pain processing. Second, the spinal anti-inflammatory effects of D-mannose may be critical for inducing a local immune cell switch to an M2 activated phenotype, thereby optimizing naked pDNA-IL-10 uptake.

Given D-mannose pretreatment profoundly improved pDNA-IL-10 efficacy as demonstrated by a >90-day pain-reversal profile at transgene doses previously shown as transiently effective,[23] we examined whether D-mannose improved transgene IL-10 uptake in cell culture. The data are striking and demonstrate that in the presence of D-mannose, transgene-derived IL-10 protein levels increase as the IL-10 transgene dose

increases. Thus, D-mannose may be acting as a transgene adjuvant in vivo, to enhance IL-10 transgene uptake that ultimately produces enduring pain reversal.

Spinal cords from rats showing enduring behavioral reversal from allodynia produced following an i.t. D-mannose injection followed 3 days later with i.t. pDNA-IL-10 (**Figure 3.4, a and b**), revealed significant increases in IL-10 protein immunoreactivity (IR). These data suggest that pretreatment with D-mannose improves transgene uptake for sustained pain suppression by priming peri-spinal immune cells to respond to transgene material by a process of enhanced phagocytosis.

Simultaneous decreases in IL-1β IR are observed **(Figure 3.4, c-n)** in spinal white matter and in corresponding DRG. While speculative, this pattern of staining observed in white matter appears similar to that observed following oligodendrocyte staining, as previously described.[177, 178] DRG is home to sensory neurons that process pain, and an i.t. injection of D-mannose followed by pDNA-IL-10 three days later, within the sensitization period, plays a role in altering DRG cellular IL-10 IR expression levels. Notably, the pattern of IL-10 IR is peri-neuronal, likely expressed by satellite glial cells and/or infiltrating macrophage that are capable of modifying sensory neuron activity and subsequent allodynia. Bilateral allodynia with bilateral spinal decreases in IL-10 IR and unilateral increases in spinal and DRG IL-1β induced by unilateral CCI observed in the present report supports recent publications.[106, 112] Bilateral IL-10 IR levels were similar to control levels in IL-10 following gene therapy treatment. IL-10 gene therapy additionally reduced ipsilateral IL-1β spinal and DRG levels. These data additionally suggests that IL-

1β in contralateral spinal cord and DRG do not play a significant role in contralateral allodynia.

The sensitization period of the peri-spinal region can be examined to understand the potential mechanism that leads to immune-mediated transgene uptake. This interval can also be exploited to achieve single-injection combination small-molecule adjuvant-pDNA co-therapy. Indeed, the data reported here show for the first time, that a previously demonstrated ineffective low dose of pDNA-IL-10 (1 μg) is now efficacious for 3+ weeks when delivered with mannose upon a single i.t. injection **(Figure 3.5)**. These observations suggest that inducing an M2 phenotypic switch to optimize transgene uptake is a viable approach for non-viral gene therapy.

Prior work demonstrates that relief from allodynia, produced chronic CCI-induced neuropathy of the rat sciatic nerve, is observed at increasingly longer intervals (reversal from allodynia) with each subsequent i.t. pDNA-IL-10 injection, but not with control pDNA. That is, allodynia is reversed 3, 7, and 26 days following an initial, second and third i.t. injection, respectively,[107] which supports that the IL-10 receptor is not desensitized following prolonged exposure, and an ongoing active cellular process is present. Adjustment of the time interval between the initial and second pDNA-IL-10 injection, such that the second injection occurs during reversal from allodynia (e.g. 3 day inter-injection interval), results in a ~2-month pain relief profile.[107] An examination of the i.t. inter-injection interval revealed the magnitude and the duration of allodynia reversal is significantly diminished and shortened if the inter-injection interval occurs outside sensitization period (5 – 72 hour),[72] suggesting time-sensitive cell-mediated

mechanism in the lumbar meninges surrounding the i.t. injection site may be important for therapeutic transgene actions.

Macrophages and dendritic cells are the predominant immune cells found in the meninges, including the pia mater which is in direct contact with underlying spinal cord pain-projection neurons.[147, 179] Increases in these cell types in meninges after chronic neuropathic pain produced by partial sciatic nerve ligation have been identified,[147] suggesting that these cell types may make up a population of sensitized cells upon initial priming and subsequent pDNA uptake within the sensitization interval. Notably, additional local macrophage cell enrichment measured in CSF from hours to days after an i.t. pDNA-IL-10 injection corresponds to the sensitization interval.[97, 135] The pro-and-anti-inflammatory phenotype of these cells in lumbar CSF shifts during the sensitization interval and beyond to 6-days, as measured by the expression the pro-inflammatory marker, ED1, and the anti-inflammatory expression of the scavenger receptor, CD163 (also known as ED2), supporting the potential importance of the M1 polarized/classical activation phenotype (pro-inflammatory state) and the M2 polarized/alternative activation phenotype[180, 54, 166-169] in mediating transgene uptake. Cells characterized as M2 polarized are strongly associated with an anti-inflammatory cytokine profile that includes interlukin-4 (IL-4) and IL-10, with low levels of TNF-α, IL-1β,[54, 55, 181] reveal enhanced phagocytic capacity.[170] Indeed, cell culture protein data from the current report demonstrate that while IL-4 protein levels remained unaltered in mannose-stimulated macrophages, significant IL-10 protein increases were measured from cell culture supernatant with simultaneous decreases in NO, TNF-α and IL-1β, supported the possibility that i.t. D-mannose induces an M2 polarized phenotype. Thus, M2 polarized

macrophages and other immune cells may be critically important for enhanced peri-spinal transgene uptake.

Interestingly, i.t. pDNA-IL10 in healthy, non-neuropathic control groups results in only small increases in IL-10 transgene expression in the meninges and DRG.[171] This observation is critical because it suggests that conditions in non-pathological spinal cord are not sufficient for substantial pDNA-based IL-10 transgene expression. Indeed, pain is only minimally alleviated when i.t. pDNA-IL-10 is injected prior to full allodynia.[171] We speculate that pre-emptive i.t pDNA-IL10 is ineffective because the local environment may not be permissive for non-viral transgene uptake and subsequent expression. Clinically, gene delivery-based therapeutics will be applicable to people who have persistent pain, and not for prophylactic pain treatment. Together, these data suggest that active and ongoing cellular processes during the sensitization period may impact continuous transgene expression and efficacy, and that anti-inflammatory signaling is necessary for enduring duration pain relief.[182]

D-Mannose is a simple hexose sugar with a molecular weight of 180.2 which decreases inflammatory processes during wound healing,[175] reduces oxidative bursts required in inflammatory processes,[183] suppresses adjuvant-induced arthritis in a rat model,[184] and inhibits LPS-induced IL-1β, TNF-α, and decreased NF-kB/p65 critical for pro-inflammatory cytokine expression, and immune cell influx following intratracheal instillation of LPS in rats, a model of sepsis-associated acute lung injury and respiratory distress syndrome.[176, 185] The macrophage mannose receptor (MR) is a glycoprotein pattern recognition receptor involved in host defense innate immunity by recognizing

mannosylated ligands (e.g. lysosomal hydrolases) and phagocytosis of a variety of bacteria, yeasts and parasites that express mannosylated molecules at their surface.[186-189] Cells identified to express the MR include brain astrocytes, microglia, in meninges and perivascular macrophages as well as some neuronal populations (hippocampus, pons cerebellum and cortex).[190, 191] Mannose-mediated MR activation leads to secretion of IL-10 and other cytokines that contribute to a down-regulation of M1 polarized immune responses including decreased IL-1β and TNF-α protein production.[192] The presently reported data are in support of these prior reports and extend these findings by demonstrating that mannose stimulates an anti-inflammatory profile both in vitro and in vivo. Indeed, macrophage cell cultures pretreated with mannose blunt or abolish NO, TNF-α and IL-1β levels while increasing IL-10 expression following LPS stimulation. Moreover, *in vivo* i.t. injection of mannose transiently reverses allodynia associated with spinal proinflammatory cytokines and significantly enhances therapeutic efficacy of IL-10 spinal gene therapy increases spinal protein IL-10 IR.

We speculate that mannose acts to 'prime' cells in the meninges to augment macrophage and dendritic cell phagocytosis of pDNA-IL-10. Importantly, the current data show the enduring effects of mannose to stimulate M2 polarized peri-spinal immune response eliminates the necessity of a second injection, as a single co-injection of mannose with pDNA-IL-10 produces enduring 3-week suppression of allodynia. Thus spinal subarachnoid mannose may be a key component for augmented transgene uptake and therapeutic expression. Studies are in progress to further define the role of the MR in enhancing spinal transgene uptake, thus further reducing required pDNA-IL-10 doses,

with the goal of producing an extended duration of neuropathic pain suppression lasting multiple months.

3.4 Materials and methods

Animals

One hundred-twelve total, adult, male Sprague-Dawley rats (Harlan Labs, Houston, TX, USA) were used in these experiments. Their weight upon arrival was 300 g +/- 5 gm; the animals were housed at 21 +/- 2°C in light controlled rooms (12:12 light: dark; lights on at 6:00 AM) and fed standard rodent chow and water available *ad libitum*. Behavioral testing was performed during the first 4 hrs of the light cycle. All procedures were approved by the Institutional Care and Use Committee (IACUC) of the University of New Mexico, following NIH Guidelines for the Care and Use of Laboratory Animals and in accordance with guidelines in the Ethical Issues of the International Association for the Study of Pain.

von Frey test for mechanical allodynia

The von Frey test was used to quantify rat hindpaw responses to tactile stimulation and conducted identically as previously described. [102, 103] Briefly, rats were habituated to the testing environment consisting of placing rats on an overhead shelf composed of open powder-coated wire grid allowing access to the entire plantar surface of the hind paw for tactile stimulation by a logarithmic series of calibrated Semmes-Weinstein monofilaments (von Frey hairs; Stoeling, Wood Dale, IL, USA). Rats were habituated for 4 consecutive days, 20-30 min/day in a quiet area with dim red lighting, at

104

26.0-27.0° C. Following habituation, baseline (BL) light touch sensitivity was assessed using monofilaments. The monofilaments were randomly applied, perpendicular to the left and right hind paws for 8 sec, to determine the threshold stiffness that would elicit paw withdrawal. Ten monofilaments were used, each with a log-stiffness value, defined as $\log_{10}$ (milligrams X 10), values in milligrams follow in parentheses: 3.61 (407), 3.84 (692), 4.08 (1202), 4.17 (1479), 4.31 (2041), 4.56 (3630), 4.74 (5495), 4.93 (8511), 5.07 (11,749) and 5.18 (15,136). Both the ipsilateral and contralateral withdrawal responses were measured and testing was conducted prior to and 3 and 10 days after surgery, and again following i.t. injections at designated time points presented in the representative figures. Three baseline measures were averaged for the right and left paws separately. The log stiffness that resulted in the 50% response threshold values (absolute threshold) was computed by fitting into a Gaussian integral psychometric function, PsychoFit, allowing parametric statistical analysis.[103, 104, 113, 193] The software for PsychoFit may be downloaded form L.O. Harvey's website (http://psych.colorado.edu/~lharvey).

Chronic constriction injury (CCI)

The surgical procedure for chronic constriction injury (CCI) was performed identically as previously described.[99, 105] Briefly, under isofluorane anesthesia (1.5-2.0% vol. in oxygen), the mid to lower back and dorsal thigh were shaved and cleaned with diluted Bactri-Stat AE (EcoLab Health Care Division, Mississauga, Ontario, Canada). Using aseptic procedures, the sciatic nerve was carefully isolated and four chromic gut sutures (Ethicon, Somerville, NJ, USA) were loosely tied around one sciatic nerve. The overlying muscle was sutured closed with two, sterile, silk sutures (Ethicon, Somerville,

NJ, USA), and the overlying skin was closed with wound clips. The sciatic nerve of sham-operated rats were identically exposed but not ligated. Animal body weight was recorded and full recovery from anesthesia was observed within 10 minutes.

Drugs

Commercially available water soluble dexamethasone (DEX; cat# D2915) and D-mannose (cat# M6020) were purchased from Sigma-Aldrich (St. Louis, MO, USA).

Intrathecal (i.t.) injections

Injections were acutely administered and conducted as described previously. [99, 107] Briefly, rats were anesthetized with isofluorane (5.0% volume in oxygen) and an 18-gauge guide cannula constructed from an 18-gauge sterile hypodermic needle (Beckton Dickinson & Co., Franklin Lakes, NJ, USA) with the plastic hub removed, was inserted percutaneously between lumbar vertebra 5 and 6 (L5-6). During this time, a small amount of CSF efflux from the 18-gauge cannula and a tail flick were observed, indicating subarachnoid catheter placement.

Injectors used for i.t. delivery were constructed as follows. A 1 ml sterilized Hamilton syringe connected to a 30 cm-length polyethylene tubing (PE-10; cat# 427401; Becton Dickinson, Sparks, MD, USA) via a 30-gauge, 0.5-inch needle inserted into a catheter. The open end of the PE-10 tubing (catheter) was then used to draw up DOTAP:Chol or DOPC protocells (1.0, 0.1 or 0.01 mg) in a total volume of 20 μl sterile, isotonic saline. The drug-filled PE-10 catheter was then inserted into the open end of the 18-gauge guide cannula and advanced 7.7 mm rostrally, placing the internal portion of

the PE-10 catheter at the lumbosacral enlargement of the spinal cord where axon terminals of sciatic afferent nerve fibers contact pain-relevant spinal cord neurons. Injections were given over a 0.5-1 minute interval. Following drug injection, the PE-10 catheter and the 18-gauge cannula was removed and were discarded. The total time required for these i.t. injections was 2-3 minutes. All animals displayed full motor activity following recovery from anesthesia.

Preparation of plasmid DNA

The plasmid vector used in these studies is described previously.[107] It consists of a 5.9 base pair circular plasmid DNA containing a transcriptional cassette consisting of a cytomegalovirus enhancer/chicken beta-actin promoter driving expression of the rat IL-10 gene including a point mutation (F129S) and a viral SV40 polyadenylation signal. The transcription cassette is flanked by a 149 base-pair inverted terminal repeat sequence. An identical plasmid lacking the IL-10 gene was used as a pDNA control. Both plasmids were amplified in SURE II competent E. coli (Stratagene, Cedar Creek, Tx., USA) and isolated using an endotoxin free Giga plasmid purification prep kit (Qiagen, Valencia, Ca., USA).

Tissue sample preparation

Procedures described for tissue processing followed those previously described.[106, 112] Briefly, following behavioral assessment at Day 29 after i.t. injection, animals were overdosed with 8-1.5 cc of sodium phenobarbital (Sleepaway, Fort Dodge Animal Health, Fort Dodge, IA, USA) and perfused transcardially with saline followed by 4% paraformaldehyde. Whole vertebral columns with intact spinal cords (cervical 2

through sacral 1 spinal column segments) were removed, and underwent overnight fixation in 4% paraformaldehyde at 4°C. This procedure ensured that all relevant anatomical components, including the spinal cord, DRG, and related meninges, were intact within the vertebral column, allowing important spatial relationships to remain intact to examine corresponding functional interactions at specific spinal cord levels. All specimens underwent ethylenediaminetetraacidic acid (EDTA; cat# EDS; Sigma Aldrich, St. Louis, MO, USA) decalcification for 30 days, and spinal cord sections were subsequently paraffin processed and embedded in Paraplast Plus Embedding Media (McCormick Scientific, St. Louis, MO, USA), as previously described. [194] Adjacent tissue sections (7 μm) were mounted on vectabond-treated slides (Vector Labs, Burlingame, CA, USA), and allowed to adhere to slides overnight at 40°C, followed by deparaffinization, and rehydration via descending alcohols to PBS (1X, pH 7.4). Sections were then processed with microwave antigen retrieval procedures (citrate buffer pH 6.0, or tris-based buffer, pH 9.0; BioCare Medical, Concord, CA, USA).

Antibody staining

Procedures conducted for antibody staining were conducted similar to that previously described.[106, 112] In brief, slides were incubated with 5% normal donkey serum (NDS), in PBS (1X, pH 7.4) for 2 hours, followed by overnight primary antibody incubation in a humidity chamber at 3° C. Slides underwent secondary antibody incubation for 2 hours in a humidity chamber at room temperature, rinsed in PBS, and then coverslipped with Vectashield containing the nuclear stain 4', 6-diamidino-2-phenylindole (DAPI) (Vector Labs, Burlingame, CA, USA). For detection of IL-10 and IL1-β expression, sections were incubated overnight with primary antibodies (IL-10; R &

D Systems, Minneapolis, MN, USA; IL1-β; Santa Cruz Biotechnology, Santa Cruz, CA, USA), incubated with biotinylated secondary antibody for 1 hour, and then treated with Vectastain ABC Elite kit (Vector Labs, Burlingame, CA, USA) and stained using TSA Plus Fluorescein System (PerkinElmer Life Sciences, Waltham, MA, USA) and finally cover slipped with Vectashield containing DAPI. Stained section orientation was kept consistent throughout for proper identification of ipsilateral and contralateral spinal cord and DRGs. For lumbar spinal cord, sections were taken from L4-L6, and the ipsilateral spinal cord analyzed. L5 DRG sections were taken with the most proximal portion of the DRG analyzed. Low magnification photomicrographs were obtained using a Nikon Optiphot fluorescent microscope equipped with a DP2-BSW (Olympus) camera.

Spectral imaging for immunofluorescent quantification

Procedures conducted for immunofluorescent quantification of stained section were conducted identically to that previously described.[106, 112] In summary, multi-spectral tissue imaging was obtained using an Axioscope microscope connected to a Nuance Camera 2.8 (FX) Multispectral Imaging System, (Perkin-Elmer, MA, USA). This camera contains a liquid crystal tunable filter (LCTF) able to filter light over a 420-720 nm interval capturing a series of images at every 10 nm increment. Every pixel of every image (series collected at specific 10 nm wavelength increment) was then analyzed by CRI software (Cambridge Research and Instrumentation Inc., (CRI) Wolburn, MA) to determine its peak spectral intensities from 400-720 nm. A different imaging protocol was established separately for spinal cord and DRG. A major aspect of the protocol requires the software to subtract background fluorescence, defined as any spectral emission falling outside that of tissue-specific autofluorescence. The image was then de-

convoluted into images containing: 1) the spectra of a true Rhodamine Red signal (Rhodamine Red emission: 600 nm+/- 5 nm), as determined from a control cover-slipped slide on which a small drop of 100 X diluted fluorophore was placed, and 2) the autofluorecence wavelength emission-spectra determined for spinal cord and DRG tissue not exposed to primary antibody. Two sets of control slides with tissue sections, one with only PBS without primary but with secondary antibody treatment, and the other, with primary but without secondary antibody treatment, were then used to objectively eliminate autofluorescence and very low-intensity fluorescence. Using these control slides, the Nuance software allows the user to set an acceptable threshold of very low-level emission fluorescent intensity (as opposed to the software's "autothreshold" option) within and outside the Rhodamine Red emission peak wavelength range between tissue samples. Stained tissue sections with Rhodamine Red are then examined under the microscope eyepiece and the very low-level emission intensity is then re-adjusted by the user to reflect the actual images observed through the eyepiece. Thus, the experimenter determines low-level emission intensity by closely replicating the composite computer image with that observed through the microscope eyepiece. The resultant image contains Rhodamine Red, but without artifactual very low-level emission intensity and without autofluorescent wavelength peaks near to the Rhodamine Red wavelength peak, while retaining all the cellular and anatomical features of the actual tissue specimen. Emission values that fall below this acceptable threshold of low-level emission or outside the Rhodamine Red wavelength peak were eliminated from our immunofluorescent quantification.

The amount of fluorescent wavelength signal was calculated by the computer software for each area of contiguous pixels defined as a region of interest (ROI). A minimum threshold intensity was set that excluded autofluorescent and artifactual low-level background. The Rhodamine Red fluorescent signal intensity for each ROI that falls above this threshold was quantified and given a numerical value. These signal "counts" were then averaged and divided by the exposure time for each image collected per ROI An image was captured for each of 4 slices (n=4 slices per rat and 3 rats per group=12 total slices analyzed per experimental group) for the spinal cord and separately for the DRG tissue region (ipsilateral or contralateral). The positive Rhodamine Red data from all 12 slices per experimental group was then averaged to represent a group average and reported as "signal counts/sec/mm^2". More detailed information regarding the Nuance spectral system can be found at URL: http://www.cri-inc.com/products/nuancew.asp.

Cell Culture

Mouse macrophage (RAW 264.7) cells were obtained from American Type Culture Collection (cat# TIB-71; ATCC Manassas, VA, USA) and cultured as adherent cells in Dulbecco's Modified Eagle's Medium (cat#D6429; Sigma-Aldrich, St Louis, MO, USA) supplemented with 10% heat-inactivated fetal bovine serum (cat# 10082-147; Gibco-Life Technologies, Grand Island, NY, USA) and 100 U/ml penicillin and 100 µg/ml streptomycin (cat# 15140122; Gibco-Life Technologies, Grand Island, NY, USA), and maintained at 37°C under humidified 5% CO_2 atmosphere. Cells were grown to 85% confluence, collected by scraping, and sub-cultured for 3 passages. For experiments, dead cells were counted by hemocytometer and trypan blue exclusion.

111

Nitric Oxide Assay

RAW 264.7 cells were seeded at a density of 3.0 x 10^5 cells/ml in 24 well plates 24 hours prior to experimentation and maintained at 37°C under humidified 5% CO_2 atmosphere. At confluence to 85%, the supernatant was removed and replaced with DMEM containing 10 mM mannose or fresh DMEM that was allowed to incubate for 1 hour. After 1 hour incubation with mannose, media from the wells was removed and replaced with fresh DMEM containing either 10 mM D-Mannose, 10 ng/ml lipopolysaccharide (LPS) from Escherichia coli (LPS; cat# L6529; Sigma-Aldrich, St Louis, MO, USA), 10 mM D-mannose and 10 ng LPS, or DMEM alone. The different treatments were allowed to incubate with the cells for 10 minutes, followed by removal of supernatant and a 2X wash with 1X Phosphate Buffered Saline (PBS, pH 7.4, cat# 10010; Gibco-Life Technologies, Grand Island, NY, USA). Supernatant was removed from each well and nitric oxide production was measured using commercially available Griess Reagent System (cat# G2930; Promega Corp., Madison, WI, USA). Briefly, 50 μl of supernatant from each well was removed and mixed with 50 μl of sulfanilamide solution and 50 μl of N-1-napthylethylenediamine dihydrochloride. The reaction was allowed to incubate protected by light and the absorbance was measured at 550 nm using a Tecan Infinite® plate reader (Tecan Systems, Inc., San Jose, CA). Limit of detection for the NO assay=1.56 μM. All experiments were run in triplicate.

Quantification of IL-1β, IL-10, TNFα protein levels

RAW 264.7 cells were treated exactly as outlined above with the exception that 100 mM D-Mannose is used and cells were allowed to incubate for 2 hours with LPS. In

a second experiment, the same number of cells were incubated with 500 mM D-mannose for 5 hours. The media from the wells was then removed and replaced with fresh DMEM containing either 500 mM D-mannose with or without pDNA-IL10 (0.5 or 5 µg), pDNA-IL10 (0.5 or 5 µg) without D-mannose, or DMEM only. After washing, the supernatant was removed from each well and assayed by mouse ELISA according to the manufacturer's instructions. (IL-1β, cat# SML800C; IL-4, cat# M4000B; IL-10, cat# M100; TNFα, cat# MTA00B, R & D Systems, Inc., Minneapolis, MN, USA) Limit of detection for the IL-10 protein assay=15.6 pg/ml; positive IL-10 kit control value= 117.68 pg/ml; limit of detection for the IL-1β assay= 12.5 pg/ml; positive IL1-β kit control value=553.75 pg/ml; limit of detection for the TNFα=10.9 pg/ml; positive kit control value=110.17 pg/ml. All experiments were run in triplicate.

Data analysis

Psychometric behavioral analysis for hindpaw threshold responses was performed as previously described[103] to compute the log stiffness that would have resulted in the 50% paw withdrawal rate. Briefly, thresholds were estimated by fitting a Gaussian integral psychometric function to the observed withdrawal rates for each of the tested von Frey hairs, using a maximum-likelihood fitting method.[113, 193] Estimated thresholds derived from a Gaussian integral function yield a mathematical continuum and thus, are appropriate for parametric statistical analyses.[103, 113, 193] The computer program PsychoFit may be downloaded from L.O. Harvey's website (http://psych.colorado.edu/~lharvey). Repeated measures two-way analysis of variance (ANOVA) procedures were applied to determine statistical significance between

experimental treatment groups, with significance determined at $p < 0.05$. All other data analyses were performed using one-way ANOVA on the computer program GraphPad Prism version 4.03 (GraphPad Software Inc., San Diego, CA). All data are expressed as mean +/- SEM. For post-hoc analysis, the Bonferroni's test was performed. Given unusually high variance was observed in immunofluorescent-quantified tissue only from the saline-pDNA-IL-10 group, a Grubb's Z-test[172] was applied to identify a potential outlier from the group.

Acknowledgements

Conflict of interest

The authors report no conflict of interest.

4. Discussion

4.1 Gene delivery to the CNS

4.1.1 Clinical uses

Over the past three decades, the development of gene based therapeutics has been rapidly growing. While advances for the treatment of genetic-based disorders such hemophilia, cystic fibrosis have been made,[195] development of gene therapeutics for neurological diseases, such as Alzheimer's, Parkinson's, Huntington's disease and chronic neuropathic pain is an important and exciting contribution to the field of neuroscience. Delivering genes to the CNS poses a particular problem in that the blood brain barrier must be crossed. Transport of genes to neurons presents some especially difficult challenges. The specialized electrical nature of the neuronal membrane, with the fluxing of membrane charge associated with the firing of action potentials, can make negatively charged DNA uptake problematic due to repulsive forces. In addition, the elongated morphology of the neuron can necessitate the transport of the therapeutic gene across long distances.[88, 196]

In general, the expression of the therapeutic gene is intended to either improve or reduce a specific cellular response. In genetic diseases, the intention is for the gene to replace the defective one. In other cases, such as in IL-10 gene therapy for neuropathic pain, the intention is to increase gene expression above endogenous levels. Conversely, protein levels can be reduced, for example by blocking transcription with small anti-sense RNA (siRNA).[88, 197] The gene of choice can be delivered in simple

116

"naked form" or loaded onto viral or synthetic vectors, such as the protocells evaluated in Chapter 2 of this dissertation. Each of these delivery platforms has its own advantages and disadvantages which will be addressed below.

Brief mention should be made of some of the methods used for gene therapy delivery in human clinical trials and animal models. Most common is standard injection of gene into the muscle, the abdomen or the vein. Another approach uses a gene gun and pressurized gas or liquid to increase permeability of cell membranes by poration. Ultrasound or electric current (electroporation) are also used for this purpose. As noted above, delivery to the CNS is difficult as the gene must pass the BBB, so gene and/or vector is usually placed into the brain by direct injection. One group injected fluorescently tagged silica particles directly into lateral ventricles.[136] Ours is the first evaluation of intrathecally injected of silica based particles.

4.2 Approaches

4.2.1 Viral vectors

Virus-based gene delivery is most often accomplished by using replication-deficient viruses containing the gene of interest, but with the disease-causing sequences deleted from the viral genome. Both RNA and DNA viruses have been utilized for this purpose.[198] Viruses are essentially composed of a protein coat or capsid that encases either DNA or RNA and are specialized to inject this nucleic acid contents into a cell and use the "host" cell transcription machinery to reproduce.[199] Consequently, viral vectors have high transfection efficiencies, as they are naturally evolved and highly specialized

for transfer of DNA across the host cell membrane.[198] Most often a virus enters a cell through receptor mediated endocytosis following binding of a protein on the capsid to a cell surface receptor.[199]

One of the most frequently used viral vector is engineered from the adeno-associated virus (AVV).[8] This vector was used in our early studies to deliver the IL-10 gene.[99] AAV vectors retain only about 300 bp of the original viral genome, so there is very little risk of recombination events with wild-type virus that might lead to infection. In fact, no viral products are actually expressed in the cell, reducing the risk of pathogenicity and immunogenicity. Other attributes are heat stability and resistance to solvents, changes in pH and temperature.[200, 201] Particularly important, AAV vectors are able to transfect not only dividing cells, but non-dividing cells which reduces the problem of "gene dilution" or loss of the therapeutic transgene in future generations of dividing cells.[201] There are 12 different serotypes of human AAV, each characterized by specific cell surface antigens, allowing a particular AAV vector to be designed for tissue specific delivery.[200, 201] An advantage for the treatment of CNS disease, one AAV serotype, AAV9, is able to cross the BBB.[202]

Lentiviral vectors (LVs), derived from human immunodeficiency virus-1 (HIV-1), have been used for gene transfer as they can transfect both non-dividing cells and dividing cells.[202] Important to gene therapy for chronic pain and neurodegenerative disease, is their ability to transduce most cell types including the cells of the CNS; neurons, astrocytes, adult neuronal stem cells, oligodendocytes and glial cells. Of special interest, some LVs can undergo retrograde transport from the neuronal axon to cell body,

118

which is critical for potential gene therapy in motor neurons. LVs are not, however, able to cross the blood brain barrier, limiting the practicality of their use for gene delivery in the CNS. An advantage of LV vectors over AVV, is that they are able to accommodate larger transgenes. It is critically important that they be replication deficient to reduce the risk of HIV infection. One of the risks of using LV, because it is a single stranded RNA, is that reverse transcriptase, the transcription enzyme that converts RNA to DNA is error-prone and may result in mutations that might possibly cause disease.[202]

One of the major drawbacks of all viral vectos is their small size, which limits the size of the therapeutic gene insertion. Gene expression is sometimes slow in onset, for example when single stranded DNA must be converted to double stranded DNA, before the transgene is transcribed.[200] Finally, it has been shown that viral vectors can preferentially integrate into transcriptionally active areas possibly leading to insertion of the therapeutic gene into the genome, "insertional mutagenesis".[201] Incorrect insertion might activate or inactivate the "wrong" gene, and can lead to tumorogenesis or leukemia.[200] In addition, mutagenesis might alter the transgene product encoded by the vector, and eliminate or pollute the expressed protein by changing its function.

One of the key problems in using viral vectors to carry a transgene, such as the gene for IL-10, are immune responses to the vector itself or the virally transduced cells. Clearly, immunogenicity and oncogenicity are the major risks of using of viral vectors for therapeutic gene delivery. In fact in human clinical trials, a gene delivered by an adenoviral vector to treat a rare disorder, ornithine transcarbamylase deficieny, caused a fatal acute inflammatory reaction in the lung. In another study a gene for treating

119

immunodeficiency disease was delivered by a LV vector and five subjects developed a leukemia-like blood disorder attributed to insertional mutagenesis and resulted in another fatality.[203] These cases heightened public concern and awareness about the potential dangers of viral vectors and hastened the development of non-viral, synthetic materials to delivery therapeutic genes. Never the less, as of May 2011, 1703 gene therapy clinical trials were being conducted across the world, the majority delivered by viral vectors.[204]

4.2.2 Non-viral vectors

Non-viral vectors are either naked DNA or synthetic vectors, composed of materials that bind to negatively charged (anionic) DNA or RNA through electrostatic interaction. Consequently, positively charged (cationic) materials are used more frequently than those with negative or neutral charge. Through these interactions, the genetic material is condensed to nano-sized complexes that are able to cross cellular and nuclear membranes more efficiently than the naked nucleic acid. The materials used for synthetic gene delivery platforms are many, but for the purposes of this discussion attention will be focused on cationic lipids, cationic polymers and mesoporous silica nanoparticles.

4.2.2.1   Naked DNA

The obvious advantage to using naked plasmid DNA are that it can be engineered to contain genes of quite a large size such as the IL-10 gene which is ~557 bp and it is easily and relatively inexpensively amplified to quantities needed for *in vivo* use by commercially available kits. It is also easily stored short term at -20°C and longer periods at -80C°.[205, 206]

120

One of the key problems in using naked DNA is transport across cell membranes.[83, 88] Being a hydrophilic negatively charged molecule, it is easily repelled by cell membranes, which contain many negatively charged proteins. As already discussed in the introduction of this manuscript, DNA must escape endosomal or phagocytic transport vesicles intracellularly and reach the nucleus to be transcribed. In addition, it can be easily degraded by nuclease enzymes, and/or the acidic environment of lysosomes. If DNA is administered directly into the blood stream or intra-muscularly, it can be degraded by serum enzymes.[14] As with virally delivered transgene, naked plasmid DNA can be diluted in subsequent generations of cells. [82] For these reasons, gene delivery by injecting naked plasmid intravenously or under the skin has been unsuccessful.[207] Intrathecal delivery, the method used to deliver the IL-10 transgene, offers an improvement in that the gene is placed directly near the dorsal spinal cord site of pain modulation, thus is poised to alter cytokine profiles of nearby glial and meningeal cells known to contribute to neuropathic pain onset.

One potential problem of naked DNA frequently cited in the literature, is that it can trigger adverse innate immune responses, as often it contains CpG base sequences that are recognized by toll-like and scavenger receptors on immune cell surfaces.[82, 195] These sequences might be actually working to our advantage in our double injection paradigm. The immune responses evoked by the 1st injections are thought to prime leukocytes, making them more capable of IL-10 transgene uptake that alters the actions of nearby spinal glia and meningeal immune cells.[72]

4.2.2.2 Cationic liposomes

Cationic liposome-mediated gene transfer, a process known as lipofection, is one of the most common method of non-viral delivery.[82, 208] Lipofectamine[TM] 2000, marketed by Life Technologies, Grand Island, New York, is one commonly used cationic lipid transfection agent. The lipids used for lipofection, share a similar structure of positively charged, water attracting (hydrophilic) head group, connected by a linker to a water repelling (hydrophobic) tail. This linkage, between the head and tail groups, is important for biodegradability. The head groups are frequently composed of amine (NH) groups containing 1, 2, 3 or 4 hydrogens (H+), known as primary (1°), secondary (2°), tertiary (3°) or quaternary amines (4°) respectively.[18] Thus, the head group binds with the negatively charged phosphate groups in nucleic acids. Also, often included in the head groups are cholesterol or steroid rings, the purpose of which will be explained later. The hydrophobic tails are usually straight or branched carbon chains.[82, 208]

Advantages and disadvantages have been noted with the use of lipoplexes. In their favor, lipoplexes are easy and cheap to produce, and are non-toxic, supporting their use in cell culture for short-duration gene expression. They can also be engineered for tissue specific delivery[208] and have been used for intrathecal gene delivery to the CNS.[260] However their use for *in vivo* gene delivery has been limited as they are prone to generate acute cellular toxicity and inflammatory responses at higher doses and durations of exposure.[82, 195]

The transfection efficiency of cationic lipids can vary dramatically depending on their composition. The nature of the linker and number of charged groups, the overall

shape and charge of the lipid can alter interaction with DNA and cellular membranes. For example, positively charged head groups improve the interaction of the lipoplex with negatively charged cell membranes.[82] The greater the positive charge the more intimate the contact with the membrane, and the logical result is that the lipoplex will have a greater chance of entry into the cell.[208] Conversely, if the charge becomes overly positive, the amount of compaction or condensation of DNA increases, reducing the probability of release and eventual transcription in the nucleus.[195]

One frequent complication in using lipoplexes for gene delivery is that they can aggregate forming a larger complex.[82, 195] When mixed with DNA, lipids immediately form compacted micellar structures due to the hydrodynamics of the lipids. The hydrophyllic heads are exposed to the surrounding extra or intra cellular fluid, while the hydrophobic tails are directed toward the interior of the micelle. While protecting DNA from degradative enzymes, the exposed positive charges of the exterior head groups can interact with negatively charged platelets, erythrocytes and serum proteins in the blood causing aggregation and the formation of small clots.[15] Moreover, a larged sized aggregate reduces interactions with the cell membrane and lowers transfection efficiency. Surface charge can be shielded by the inclusion of polyethylene glycol or (PEG), a hydrophilic, neutrally charged polymer, which can prolong the circulation half-life of lipoplexes, while at the same time reducing the charge interaction between the lipoplex and cell membrane, reducing transfection efficiency.[82, 195]

4.2.2.3   Cationic polymers

When DNA is mixed with cationic polymers, the net result is the formation of condensed nano-sized polyplexes, a complex of DNA and polymer, similar to lipoplexes. According to Kundu and Shamara,[197] ideal polymers should be non-toxic, non-immunogenic and biodegradable and package large amounts of DNA. Some of the many other polymers that are being used for gene transfer are polyethylenimine (PEI), Polyamidoamine (PAMAM), acrylate, poly(amino-ester) based polymer vectors, and the FDA approved, biodegradable formulation, poly-lactic co-glycolic (PLGA) used in our laboratory.[197] Biodegradability ensures that there is no cellular accumulation over time.

As with lipids, the interaction of the polymer with DNA and the formation of a polymer-DNA complex, is dependent on factors "intrinsic" to the polymer itself such as the number of its charge groups, the structure of charge groups (1°, 2°, 3°, 4°), and their spacing within the polymer, polymeric branching and hydrophobicity.[82] Also important to DNA loading are "extrinsic" factors, such the ionic strength of the solution in which the polyplex is formed, the charge ratios of DNA/polymer and the kinetics and thermodynamics involved with polyplex formation.[82] Polyethylenime (PEI) serves as a good example of how intrinsic and extrinsic factors effect gene delivery. Intrinsically, the structure of branched PEI has been shown to be more toxic resulting in lower DNA transfection efficiency than linear PEI.[82] The extrinsic environment surrounding the polymer-DNA complex is hypothesized to play a role in increasing transfection by improving endosomal escape. PEI contains many amine groups that are mostly unprotonated at physiological pH. In the acidic environment of the endosome, there are many protons (H+) that are readily absorbed by the amine groups on PEI. One hypothesis

124

is that this condition lowering the acidity in the endosome, leading to an influx of negative ions, resulting in a build up of H_2O and osmolytic pressure that ruptures the endosomal membrane allowing the polyplex/DNA complex to escape and travels to the nucleus. This process has been termed the proton sponge effect.[84, 209]

Several benefits of synthetic vectors are that they can be designed to release cargo in a time or pH dependent manner and their surface is easily modified.[195, 197] By attaching cell targeting molecules such as cell receptor-specific ligands, antibodies or small stimulatory molecules, they can be designed to directly target one cell type and avoid damage to others.[91, 210, 211]

Toxicity to cells is the major limitation to the use of polymeric gene delivery platforms. *In vivo,* their longevity and biodistribution remain relatively unexplored.[195] Like liposomes, some polyplexes can tend to aggregate forming larger complexes in the blood and have been found in lung and liver following intravenous administration. But, because of easy modification, inclusion of an anionic or neutrally charged polymer, such as water soluble PEG or cholesterol, can reduce aggregation and increase circulation times.[195] Like lipoplexes, polyplexes can be immunogenic, either from the polymer itself or the DNA, although one group has shown less proinflammatory cytokine induction by the use of polyplexes over lipoplexes.[212] Despite toxicity problems, their potential as therapeutic delivery agents remains high due to their flexibility of design, easy modification with targeting molecules, potential to cross the blood brain barrier.

4.2.2.4   Mesoporous silica nanoparticles

MSNs, such as those used to form the core of protocells, have many properties that make them desirable for drug and DNA delivery. Slowing et al. summarizes these factors eloquently.[96] First, their diameter and pore size are adjustable from 50-300 nm and 2-6 nm respectively. They have a rigid structure that is resistant to degradation by heat, pH, mechanical stress and hydrolysis. Their high pore volume (> 0.9 cm^3) and surface area ($>$ 900 m^2/g) allows efficient loading of drug on two functional surfaces, the internal surface of the pore and the external surface. Finally, because of the regular nature of the pores, they are easily sealed to prevent premature "leaking" of cargo.[96, 123, 129, 213] More advanced modifications for loading small molecules or drugs into MSNs involve "gating" strategies to seal cargo in the pores, such as the use of quantum dots or small nanoparticles to cap the pore.[96] In addition, they are easily customized for specific targeting. MSNs can be engineered for controlled release of cargo with changes in temperature, pH, enzymatic cleavage or exposure to light.[95, 96]

As with most nanomaterials, modulation of particle size, shape, and surface charge can greatly influence cellular uptake, cellular and bodily responses, and biodistribution.[96, 123, 129, 213] Because their ultra small size, nanoparticles do not physically behave as larger particles and the physics of their actions with each other and other molecules may be unpredictable in different tissues, cells, blood and bodily fluids. Thus it is important that their biotoxicity be evaluated with each modification.[214] Studies such as those in Chapter 2, which evaluate cell stress as a function of surface charge, are important contributions to our current understanding of these materials.

4.2.2.5   Protocells

The protocell, essentially a MSN with a lipid bilayer on its surface, offers additional advantages. According to Liu et al.,[101] the lipid bilayer on the MSN core of a protocell actually provides a "synergistic system" for simultaneously loading and sealing cargo. For example, while a negatively charged fluorescent dye was unable to load a negatively charged mesoporous core, the dye was easily loaded when a positively charged lipid was used as a bilayer. In fact, the lipid-sealed protocell was able to load a concentration of dye that was 100X that of the surrounding solution.[101] The lipid layer is easily conjugated to PEG to improve circulation time and both are easily conjugated to specific cell targeting molecules such as receptor ligands or antibodies.[95] *In vitro*, protocells have been shown to successfully deliver hydrophobic cancer therapeutics[94] and plasmid DNA.[215]

The synthesis of MSN used for the silica core of the protocell involves the hydolysis of a silica precursor such as tetraethylortosilicate (TEOS) dissolved in ethanol and water to form a homogenous solution or "gel-sol". Hydrochloric acid is used as a catalyst to begin the growth and nucleation process, while a surfactant, cetyltrimethylammonium bromide (CTAB), an alkyl ammonium salt, serves as a liquid crystalline template for the mesoporous structure. If the reactions are kept at concentrations above the critical concentration for micelle formation, regular crystalline mesoporous nanostructures are formed.[95] It has been proposed that the silica material forms "inorganic walls" between ordered surfactant micelles forming pores in a process of self assembly.[216] Further engineering lead to the development of an Evaporation Induced Self Assembly (EISA) method. This method uses a dip-coating process to form a

thin film of silica/surfactant micelles that organize into liquid-crystalline mesophases as the concentration of soluble silica increases, with the evaporation of solvent. Brinker and colleagues,[217] improved upon this procedure by forcing the silica/surfactant solution through an atomizer to form aerosol droplets. The droplets direct the process of self assembly to form spherical MSNs.[217] In the last phase of synthesis, the particles are dried in a furnace by evaporation or calcination to drive off excess solvent. There are two other approaches for forming MSNs, a growth-quench approach, which uses a dilution and pH change to "quench" or slow the silica condensation reaction and another that separates the nucleation and growth stages into two processes.[213] Important for drug or DNA delivery, regardless of which synthesis process is used, the fine tuning of the reaction temperature and relative amounts of reactants can control the orientation and diameter of pores and particle size.

Another key advantage of the MSN is that silanol groups inside the pores and on the outside surface can be altered by changing the electrostatic, hydrostatic and colloidal properties improving their biocompatibility.[95, 213] These functional groups can then be used to covalently attach other molecules for cell specific targeting or adsorb other coatings, to change the charge and hydrophobicity of the MSN. The positively charged polymer, polyethylene glycol (PEG), is one such coating, used to reduce aggregation with serum proteins and increase circulation times. On the protocell, the surface coating is the lipid bilayer. By using lipids with different charge, fluidity and melting/transition temperatures, the interaction of the protocell with biological membranes can be controlled. Such was the case in the transfection studies in Chapter 2, in which pDNA-IL-10-GFP delivered via DOTAP:Cholesterol covered protocells to HEK cells, caused

significantly more IL-10 expression than when delivered on DOPC protocells. Co-lipids or "helper" lipids such as cholesterol or dioleoylphosphatidylethanolamine (DOPE) are added to the bilayer to help increase the fluidity and favor "mixing" or fusion of the protocell with cell membranes and facilitate transfection efficiency by improving the transfer of nucleic material to the cell interior.

Intracellular endosomal vesicles are composed of a single, mostly anionic membrane on the surface exposed to the cytoplasm. Once inside the endosome, cholesterol is thought to alter membrane electrical potentials by absorbing charge via its cyclic ring structure and displace anionically charged lipids from the outside membrane to the inside, promoting transfer and escape of lipid coated particle/DNA complex from the inside to the outside, by a "flip-flop" mechanism.[85, 218] Therefore, inclusion of cholesterol with positively charged DOTAP in the protocell bilayer, might improve transfection efficiency by enhancing DNA escape from the endosome so that more was available for transcription in the nucleus.

In total, 3 different protocell cargos were used in the experiments in Chapter 1. The first was a FAM-tagged 18 bp single stranded DNA (ssDNA). FAM is a green fluorophore used as a reporter in these studies. FAM or 6-carboxyfluoroscein is a molecule composed of a number of benzene rings and other carbon ring structures (**Figure A.13 A**). It has a MW of 537.5. While the 3-dimensional structure of a molecule can vary depending upon pH and salinity and other physical characteristics of the solution surrounding it, a rough estimate of its size can be determined by its bond lengths.[258] Using this method the dimensions of FAM were determined to be ~.139 nm in width and ~0.722 nm in height. The length of the 18 bp

DNA at .34 nm/bp[253] is ~6.12 and diameter of the ssDNA is ~2 nm[253]. It nucleotide composition is 5'-CTTGAGAAAGGGCTGCCA-3' and as no self-complimentarity[254] so it will not form the hair-pin loops common to other single stranded sequences. For these reasons it is most likely that the FAM DNA would load inside the pores in the silica core.

The second cargo was a red fluorophore Dextran tetramethyl rhodamine (DexRHO) with a MW of 10,000 (**Figure A.13 B**). It is a hydrophillic polysaccharide composed of α-D-1, 6 glucose molecules to which a tetramethylrhodamine fluorophore is linked. The molecule has an overall negative charge. It has been determined that 1-2 tetramethylrhodamine groups are conjugated to each 10,000 MW of Dextran polymer.[252] Calculations of the planar bond length of the DexRHO component without the dextran polymer show the width to be ~.983 nm and the height ~.576 nm. Considering the very large size of the entire DexRHO polymer, the molecule would most likely load by adsorption to the surface of the positively charged protocell core. In fact because of these physical characteristics, DexRHO was chosen as a surrogate molecule for the large 5.9 kb plasmid DNA molecule the final protocell cargo used in these studies (**Figure A. 13 C**).

Plasmid IL-10 has previously been shown assume a supercoiled state.[79] If linearized, the length at .34 nm/basepair would be 20060 nm[253] and double stranded DNA has a diameter of ~2 nm.[253] However in actuality, the circular plasmid DNA is supercoiled with elastic qualities in "standard aqueous conditions of 0.14M univalent salt".[255] Supercoiled DNA assumes many different structures based the linking number or the number of times the two sides of circular plasmid cross. The linking number is a function of the twisting number, or the total number of turns of the duplex, and the writhing number, the total number of turns

of the duplex.[256] For size comparison, one bacterial 4361 bp plasmid, pBR322, ~1539 bp smaller than pDNA-IL-10, was examined by atomic force microscopy and was ~225 nm across.[257] Determining the actual dimensions of the supercoil is beyond the scope of this dissertation and was not a goal of the studies Chapter 1, but it can be speculated that like DexRHO, supercoiled DNA would be too large to load into the pores of the silica core but would load by charge interaction with a positively charged silica core and a positively lipid such as DOTAP:CHOL 1:1 covering the surface.

Future studies will most certainly incorporate the newest generation of protocells that have larger multi-modal pore sizes and a capacity for pDNA loading[94] and show promising potential as gene delivery vectors for spinal gene therapy. Another aim will be to reduce the size of the pDNA-IL10 to better utilize these second generation protocells.

4.3 Mesoporous silica-supported lipid bilayers (protocells) for DNA cargo delivery to the spinal cord (re-submitted to the Journal of Controlled Release)

4.3.1 Investigation of toxicity and biocompatibility of protocells

Given protocells are novel nanocarriers, their biocompatibility and potential for cell toxicity were initially examined. The testing for biocompatibility of MSNs has been complicated. Different combinations of materials and differences in synthesis result in various MSN characteristics (shapes, pore sizes, chemical composition, surface chemistry). Therefore the assessment of toxicity and cellular uptake and responses in living systems is not easily generalized to all MSNs.[95, 214, 219] As pointed out by Tarn et al.,[95] most of the toxicity studies in the past century have been related to concerns about

silicosis resulting to exposure to both crystalline and amorphous silicon dioxide. The authors emphasize that, " not all silica is created equal", but can exist in a wide variety of forms depending on synthesis and environmental exposure.[95] They explain that toxicity is mostly related to surface silanol (SiOH) groups that can hydrogen bond to membrane components or when dissociated, form SiO^-, that can interact with positively charged lipid head groups, and may lead to lysis of cell membranes such as red blood cells.[95] Silicate radicals can similarly react with H_2O to produce reactive oxygen species (ROS) known to damage proteins and upregulate cytokines and inflammatory molecules leading to cell death or carcinogenesis.[95] In support of the use of silica, these reactive silica groups can be modified to reduce or eliminate this problem. In addition, the small diameter of the MSN reduces the surface area and exposed hydroxyl groups available to react.

Depending on mode of synthesis, particle or pore diameter and *in vivo* delivery route, toxicity can vary.[93] Different cell types also can be more susceptible than others. Hudson et al.[93] evaluated biocompatibility of two different cell lines, myoblasts and macrophages to mesoporous silicates with diameters of ~150 nm, ~800 nm and ~4 μm and pore sizes of 3 nm, 7 nm and 16 nm respectively. The particles were synthesized in three different processes. All three particles showed increasing toxicity correlating with increasing their concentration in mesothelial and myoblast cells but not in macrophages, cells important to studies described in this thesis. Interestingly, differing methods of MSN delivery had differing toxicity. Mice were injected subcutaneously with 1 ml of 30 mg/ml, which was well tolerated. Histological examination showed no sign of MSN material at 2 or 3 months. Surprisingly, in contrast, mice that received an intra-peritoneal

injection of the same dose either died or became distressed after 24 hours and were euthanized. Those that received intra-peritoneal doses of 10 mg or 5 mg became ill 30-40 hours later. However, intraperitoneal injection of a lower dose, 1 mg/ml was not fatal to mice. Intravenous injection of 6 mg/ml resulted in rapid death.[93] These studies point out that careful consideration must be made of not only the dose but the method of delivery are extremely important to an assessment of toxicity of nanomaterials *in vivo*.

A biocompatibility study by Witsap et al.,[220] assessing anionic MSNs in macrophages prepared from adult human blood donors, parallels some of the results and issues in our studies with protocells that we found to co-localize with spinal macrophages. In the Witsap experiments, three different MSNs prepared by calcination only, solvent extraction only, or calcinated and covalently loaded with the green fluorophore, fluorescein isocyanate (FITC), were evaluated in primary macrophage cultures. Viability of macrophage was measured by trypan blue assay and cells remained viable at 10 and 100 ug/ml doses after a 6 or 24 hour exposure, similar to the results of our experiments with DOTAP and DOPC protocells in mouse macrophage cells (Raw 274.7) and HEK cells. Interestingly, Witsap et. al reported that the autofluorescent properties of MSNs confounded their attempt to use the colorometric 3-(4,5-dimethylthiazol-2-yl)-2,5-diphenyl-tetrazoliumbromide (MTT) assay for measuring mitochondrial metabolic activity. Protocell green autofluorescence similarly confounded our initial assays of live cells using the green fluorophore, Calcein-AM, followed by analysis using flow cytometry. We found the problem was solved instead by assessing dead cells using the red fluorophore, Ethidium homodimer-1. Protocell autofluorescence also confounded our examination of protocells in spinal cord slices by standard

133

microscopy, yet was remedied by a switch to the use of spectral analysis to determine biodistribution.

In the Hudson report,[93] uptake of MSNs was drastically reduced by an actin-inhibitor, Cytochalasin-D and a cocktail of endocytosis inhibitors, suggesting that the particles were being taken up by macrophages by the actin dependent process of endocytosis. The macrophage function was unaffected following internalization of MSNS, as the cells readily engulfed apoptosed neutrophils, Jurkat cells and Ig-opsonized sheep red blood cells as they would normally. Important to our studies, MSN containing macrophages stimulated with LPS produced their usual levels of IL-10, TNF-α and IL1-β cytokines.[220] These studies support our findings that macrophages appear viable and healthy both *in vivo* in the CNS and *in vitro* in macrophage cell cultures following exposure to mesoporous silicates such as the protocell. The fact that autofluorescence confounded their microscopic examination of cells and colorometric viability assays supports our similar observations.

While our studies have shown that 1 mg in 20 µL of both positively charged DOTAP:Chol 1:1 and DOPC protocells had no adverse effects when delivered to the CNS intrathecally, the issues of early cell stress or even programmed cell death remained a concern. The realm of nano-MSNs and their tolerance in living systems remains a largely uncharted territory, due to the many variations in synthesis, composition, size shape and immunogenicity. Toxicity could be a benefit in some cases, such as in the elimination of cancer cells. Conversely, nano-MSNs would be a risk if healthy cells are destroyed in the process.

4.3.2 Transfection capacity and efficiency of protocells

Our results show that protocells can be effectively used to deliver pDNA, thus their use in this regard will be addressed in more detail below. For an excellent study describing their use to deliver anti-cancer therapeutics please refer to the Ashley paper.[94] Due to the deprotonation of surface silanol groups on the protocell core, silica is intrinsically negatively charged.[95] To avoid repulsion of negatively charged DNA, it can be altered to become positively charged.[95] This was accomplished by adsorbing (layering) the silica with positively charged DOTAP lipid. Lui et al. found that the size of the silica core as well as the lipid charge was important for DNA loading.[215] Silica particles with an 8 nm diameter when mixed with DOTAP continued to have a negative charge (negative zeta potential) while larger particles (30, 50, 80, 130 nm diameter) assumed a positive charge (positive zeta potential). When a plasmid DNA coding for the DsRed fluorescent protein (4.8 kbp) was loaded onto these protocells it was found that pDNA loading was dependent not only on particle size, but also on the ratio of particle to DNA mass. For protocells of 30 and 80 nm diameter particle, mass of protocells needed to be 4X or 16X the DNA mass, while for larger particles of 130 nm diameter, 40X the DNA mass was needed.[215] The particles in our studies had a diameter of ~150-200 nm (data not reported). The studies by Liu et al.[215] also demonstrated that *in vitro* transfection efficiency of DOTAP: Chol 1:1 in CHO cells in studies was approximately 30 % of transfected cells and equivalent to that of Lipofectamine[TM] 2000. A casual estimate of transfection efficiency in the HEK cells used in our studies was comparable. Supporting the use of protocells for DNA delivery, Liu's group demonstrated DOTAP: Chol 1:1 protocells completely protected the pDNA-IL-10 from degradation in an assay with the

DNA specific degradative enzyme, DNAse I, and successfully transfected cells even if previously exposed to the nuclease. In a final study, the Liu team used different fluorescent labels for the lipid, silica core (50 nm diameter) and DNA and demonstrated that all the components remained intact after 2 hours, suggesting that they all entered the cell simultaneously. By 12 hours, the DNA was observed in the nucleus while most of the silica remained peri-nuclear. Larger particles of 200 nm appeared to remain in the endosome. The confocal data in our studies revealed similar peri-nuclear localization of protocells around 30 nm in diameter. While the studies of Liu et.al[215] demonstrate that protocells protect the DNA from degradation and are capable of cellular delivery of a fluorescent tagged plasmid, our HEK cell transfection studies (**Chapter 2, Figure 2.6**) are the first to demonstrate that a therapeutic gene such as IL-10, remains fully operational and generates functional protein following loading on protocells.

4.4 Adjuvants to improve pDNA therapy

4.4.1 Adjuvants defined

Classically, adjuvant compounds are used with non-pathogen based vaccinations such as protein-based vaccines to induce a safer and longer lasting immune response. Typically, they are used to enhance the immunogenicity of an antigen-based vaccination or to improve efficacy of a vaccination in immunocompromised populations.[221] Others serve as vehicles to present an immune stimulatory antigen, such as the commonly used Complete Freund's Ajuvant (CFA), which presents antigen in a water-in-oil emulsion.[222] In our studies, adjuvants are being evaluated in an attempt to reduce the dose and number of pDNA-IL10 injections required to generate enduring pain relief in the CCI model of

neuropathic pain. To be clinically successful, the candidate adjuvant must induce an innate response by stimulating antibody production or longer lasting adaptive cellular immune responses.[221]

There are two basic categories of adjuvant.[223] Conventional adjuvants can be synthetic, such as lipids, polymers or emulsions, or natural adjuvants, such as those that are pathogen-derived, using pathogen associated molecular patterns (PAMPs) from bacteria or plants. Interestingly, mannose conjugated glucoproteins are a common PAMP on bacterial pathogens. DNA based adjuvants are genetically engineered vectors that modulate expression of immune stimulatory molecules such as cytokines, B or T cell co-stimulatory molecules, complement molecules, transcription factors or heat shock proteins.[223] The route of inoculation of an adjuvant may be critical to the nature of the adaptive immune response. For example, early studies showed that intramuscular injections of adjuvant stimulate Th1 responses, while high pressure delivery by a pneumatic gene gun, elicited Th2 responses.[223]

4.4.2 Adjuvants to prime innate immunity

4.4.2.1   Stimulating cytokines and antibody immune responses

Most commonly, adjuvants stimulate innate immunity.[221] One such example are the CpGs DNA motifs that bind toll-like receptors (TLRs) with activation of patterned recognition receptors (PRRs) on antigen presenting cells (APCs), such as macrophage and dendritic cells. This binding leads to the presentation of antigen by the specialized protein complexes, MHC I and II to B and T cells, with activation of co-stimulatory

molecules and up-regulation of antibodies, cytokines and complement proteins. Complement proteins coat antigen for improved recognition by antibodies.

4.4.2.2 Adjuvants to prime adaptive cellular immunity

A second use for adjuvants is to prime the prolonged adaptive cellular responses of adaptive immunity. Presentation of adjuvant antigens by MHCII on APCs to CD4+ T cells is critical to the maturation and differentiation of CD4+ T cells. When so activated, CD4+ T cells differentiate into two distinct cell types with two different cytokine profiles, T helper type (Th1), that primarily release INF-γ and Th2 cells that produce anti-inflammatory cytokines such as IL-4 and IL-13. A third T helper cell type, Th17, thought to regulate the cytokine profiles in the other two, is also differentiated.[222] As a consequence adjuvants can be designed to polarize T cell populations with a Th1 or Th2 bias. [222]

Cytokines released by Th2 polarized CD4+ T helper cell populations have the potential to influence macrophage polarization, priming a feed forward response in the direction of the M2 phenotype, including improved ability to phagocytose a therapeutic gene. Therefore, evaluation of intrathecally delivered adjuvant compound for T cell responses might be an important future direction for our studies, given T cells and MHCII expression have been identified in the DRG and DH of the spinal cord during neuropathic conditions.

Another adaptive immune cell that can be stimulated with adjuvants is the dendritic cell.[224] Like macrophages, they are continually surveying the extracellular environment for antigens resulting from pathogens or tissue damage. They have also been

dubbed, 'Nature's adjuvant'[225] as they process and present antigens to T cells, and in doing so, regulate the Th1 or Th2 response to the antigen. For example, current therapies have been designed to target DC surface receptors with monoclonal antibody adjuvants to facilitate cytotoxic T cell responses against cancer cells or stimulation of specific antibody responses by B cells.[224, 225] DC cells in mice can be divided into CD8+ DCs, that initiate Th1, proinflammatory cytotoxic functions, and CD8- cells. The latter are better at activating CD4+ T cells and their differentiation into Th2 and a T17 regulatory (T17reg) cells, that are programmed to facilitate an anti-inflammatory cytokine profile.[224, 225] By using antibody adjuvants specific to DC surface receptors, a T cell specific population with an anti-inflammatory profile can be generated, leading to M2 polarization of nearby macrophage with improved gene uptake.[224, 225] Excitingly, the mannose receptor is highly expressed on DCs[188, 192] and its ligand, D-mannose the most successful candidate adjuvant used in our present study. Future studies using specific targeting of mannosylated protocells as an adjuvant to prime anti-inflammatory populations of DC and T cells may further enhance proliferation of M2 polarized macrophages and lead to enhanced IL-10 transgene uptake prolonging neuropathic pain reversal at lower doses and with only one injection.

4.5 Improvement of spinal non-viral IL-10 gene delivery using D-mannose as a transgene adjuvant to control chronic neuropathic pain (re-submitted to Molecular Pain)

4.5.1 Dexamethasone as an adjuvant

Dexamethasone (DEX) is a synthetic glucorticosteroid (GC) that has been found to be important in the resolution of inflammatory diseases by accelerating the apoptosis

of leukocytes, such as the eosinophil cells associated with asthma and potentiation of their phagocytosis.[226] Glucocorticoids such as Dex, act by binding the Glucocorticoid Receptor (GR). This receptor exists in its inactive form as a complex with the heat shock protein HSP90 and other chaperone proteins that bind to its cytoplasmic tail. With ligand binding, these proteins dissociate and expose a nuclear localization signal resulting in the translocation of the GC-GR complex to the nucleus.[227] In the nucleus, two GR molecules form a dimer that binds to the promoter region of corticosteroid-responsive genes, the corticosteroid-response element (GRE). The genes upregulated are mostly anti-inflammatory, and include IL-10 and the inhibitor of NFκ-B, Iκ B-α.[75] In addition, the GC-GR acts indirectly on co-activator molecules which have histone acetylation activity leading to the activation of other anti-inflammatory genes, and at the same time recruits histone deacetylases that result in the deacetylation and down regulation of proinflammatory genes.[75] *In vitro,* Dexamethasone has been shown to inhibit pro-inflammatory IL-1β gene expression by blocking the transcription factor NFκ-B and AP-1 activation.[227] Another report showed that glucocorticoids could induce the differentiation of an anti-inflammatory subtype of macrophage.[228] Because of its well-known anti-inflammatory effects and potential to induce M2 polarization in spinal macrophage cells, DEX was a logical choice as a candidate adjuvant.

Surprisingly, when used as an adjuvant to prime IL-10 transgene uptake, DEX caused only partial pain reversal in neuropathic animals, and the results were short lived. The literature regarding the pharmacokinetics of Dexamethasone, intrathecally injected into rats, is scant. One group assessed the stability, bioavailability and safety of chronically administered Dexamethasone sodium phosphate using indwelling lumbar

140

catheter in naïve Sprague-Dawley rats. Free dexamethasone, within 40 minutes and at low doses of 12.5 ng/hour, produced no side effects of neuropathy.[229] However, there were signs of inflammation observed in the lumbar sub-arachnoid space, when a higher dose of 125 ng/hour was administered in the same manner.[229] This study was used as to establish the dose of Dex used in the studies in Chapter 3. We injected 62.4 ng or 6.2 ng (62.4 mg of Dex in 1 gram of powdered compound; Sigma-Aldrich) in a 1st priming injection and attributed the observed short-term pain reversal, to inadequate IL-10 transgene uptake, possibly due to dose issues. If the dose was too high, it may have resulted in inflammatory responses of peri-spinal immune cells similar to the effect of high doses of Dexamethasone sodium phosphate described above. Alternatively, if the dose was too low or the DEX degraded early on, the switch to M2 polarization may have failed and thwarted adequate transgene uptake.

4.5.2 D-mannose as an adjuvant

4.5.2.1   The sugar

D-mannose is a 6 carbon sugar that is a C-2 epimer of glucose. In eukaryotic cells mannose is required for N-glycosylated glycophospholypid anchor synthesis and the source of mannose in eukaryotic cells is mainly derived from glucose. Glucose is broken down to fructose-6 phosphate in the Kreb's cycle and further processed by phosphomannose isomerase (PMI) to mannose-6-phosphate.[230] The literature on the pharmacokinetics of D-mannose is also scant. One study in mice showed that an intravenous injection of $[^{2-3}H]$ mannose showed a clearance half-life of 28 minutes with 98% of the label cleared after 2 hours.[231] In humans given D-mannose orally, blood

mannose levels increased in a dose dependent manner with increasing doses of mannose (0.07-0.21g mannose/kg body weight). It is possible that D-mannose in CSF would have at least a similar or even longer half-life of around 0.5 hours following our i.t. injections, long enough to bind receptors on peri-spinal macrophage and dendritic cells.

4.5.2.2 Structure of the mannose receptor

The mannose receptor (MR; also known as CD206) is a glycoprotein with one transmembrane domain and a cytosolic domain, with a single tyrosine residue that mediates receptor internalization and recycling but contains no domains involved in intracellular signaling.[76] The MR exists in both membrane bound and soluble forms.[232] It is highly expressed on dendritic and macrophage cells and in the lymph organs, liver and to some extent on smooth muscle and endothelial cells. It contains three different extracellular domains an N-terminal cytosine rich domain (CR) that can bind sulfonated sugars ending in SO4-3-GAL or SO_4-3/4-Gal NAc, a fibronectin-like domain, involved in collagen binding and eight tandemly arranged C-type lectin-like domains (CTLDs) that bind sugars terminating with D-mannose, L-fructose or N-acetyl glucosamine in a Ca^{2+} dependent manner.[76] Carbohydrate moieties containing these sugars are often found on the surfaces of pathogens and self-antigens. Thus the receptor plays an important role in the innate immune response and the internalization and processing of antigens by APCs.[76,233] Studies in transgenic knock out (k.o.) mice have shown the receptor is necessary for clearing mannosylated enzymes and proteins involved in inflammation and wound healing from the blood.[23] 70% of the receptor is localized internally in the early endosomal compartment while the other 30% is localized on the cell surface and is constantly recycling back and forth between the two via clathrin coated vesicles.[234]

Fluorescent microscopy has shown that MR is dominantly expressed in early endosomes and late endosomes which suggests that MR might be transported with its ligand to compartments involved in antigen presentation by MHC I or class II.[76] These studies support MR involvement in ligand-receptor internalization and antigen presentation by macrophage and dendritic cells with the potential to polarize both innate and adaptive immune cells in the direction of anti-inflammatory M2 polarization.

4.5.2.3 Receptor function

While the role of MR in clathrin-dependent endocytosis has been clearly demonstrated, the role of the receptor in phagocytosis remains controversial.[76, 77] Phagocytosis is an actin-mediated process involving formation of pseudopodia or extensions of cytoplasm that surround and engulf material in a large vesicle known as a phagosome. After the material is taken into the cell, the actin depolymerizes and the phagosome moves into the cell entering the endosomal pathway.[76] Non-phagocytic CHO cells, transfected with a hMR cDNA to express MR, failed to phagocytose zymosan, a yeast derived particle, mannosylated latex beads, or *Mycobacterium kansasii* but they were able to endocytose mannosylated glycoproteins in a clathrin-dependent manner. Transient expression of hMR in two human cell lines also failed to phagocytose.[235] The authors suggest that while the receptor itself is not responsible for phagocytosis, binding of ligand such as D-mannose, may cause recruitment of other cell surface receptors, which activate phagocytic processes beyond clathrin dependent endocytosis.

Notably, the MR lacks signaling domains in its cytoplasmic tail even though the receptor has been shown to contribute to down stream signaling events. Thus it appears to

require assistance form other receptors to accomplish signaling and modulation of cytokines.[76] It has been suggested that MR activation by ligands such a D-Mannose, reduces pro-inflammatory cytokine production by upregulation of IRAK-M. This inhibitor of TLR signaling acts by preventing the dissociation of the kinases, IRAK1 and 4, from the My88 adaptor molecule, preventing the downstream binding of NFκ-β to its promotor, thus preventing upregulation of pro-inflammatory molecules.[76] Tachado et al.[236] demonstrated that MR required assistance from another receptor to generate one cytokine, IL-8. The group transfected HEK-293 cells with cDNA coding for hTLR2 only, or hMR only, and found that no IL-8 was released from the cells upon challenge with *p. carinii (jirovecci)*. Suprisingly, when both receptors were co-expressed, IL-8 was detected. Their co-precipitation studies suggested that ligand binding MR might form a functional complex with toll-like receptor 2 (TLR2) on the cell surface.[236] TLR2 has been shown to stimulate phagocytosis in macrophage cells and may contribute to improved transgene uptake.[237] A second study by Chieppa et al.[192] supports the idea that MR works in concert with other receptors. They found that DCs treated with an MR specific monoclonal antibody, LAM-1, were unable to release cytokines that stimulate Th1 recruitment, suggesting the antibody was blocking the receptor. However, cells treated in the same fashion were still able to release anti-inflammatory cytokines, IL1r-a and IL-RII and recruit Th2 cells. Not all MR ligands generated these effects. Cytokine production was not significantly altered when mannan, a well characterized MR ligand was used, but changes in T cell recruitment were observed when mannose capped–LAM (man-Lam) was the ligand.[192] These results support the notion that man-Lam may have been acting

through MR in concert with other receptors such as, Dectin-2 and DC-SIGN, both with well known signaling capabilities.

An early study by Raveh et al.[238] suggests that Il-1β and IL-4 cytokines, may actually work together to enhance mannose receptor mediated phagocytosis. They showed that the Th2 cytokine, IL-4, increases both cell surface expression and endocytosis-mediated internalization of ligand bound receptor. The Th2 cytokine, IL-13, produced similar effects. The Th1 cytokine INF-γ had the opposite effects on endocytosis. Surprisingly, when applied together, the normally antagonistic cytokines, IL-4 and INF-γ, enhanced receptor mediated phagocytosis, an actin mediated process, even though they had had opposing effects on endocytosis.[238]

Recently, it has been reported that there are many other receptors in the C-Lectin family that are capable of binding mannose on macrophage and DCs, cell types common to the meningeal layer. These are macrophage inducible C-type lectin (MINCLE), which can up regulate pro-inflammatory cytokines and leukocyte migration, dendritic cell immune receptor (DCIR) expressed on DCs and many leukocytes and DECTIN-2, a Syk signaling coupled PRR on DCs, and dendritic cell-specific intercellular adhesion molecule-3 (DC-SIGN).[239] All have signaling motifs in their cytoplasmic tails that may be working cooperatively with MR to improve endocytosis and IL-10 transgene uptake leading to prolonged reversal of allodynia observed when D-mannose was used as an adjuvant to assist in IL-10 gene delivery **(Chapter 3, Figure 2)**.

4.5.3 Mannose receptor in the CNS

In the mouse CNS, the mannose receptor is most highly expressed on peri-vascular and meningeal and choroid plexus macrophages[240] which are demonstrated in the current report to uptake FAM-tagged protocells. MR are also found on dendritic cells, microglia[241,242] and to a lesser extent, on astrocytes.[190, 243] All three cell types are involved in modulating immune responses, and hence could respond to stimulation by the adjuvant D-mannnose. While expressed in some brain areas during development, the MR is not expressed on neurons in the adult brain or on oligodendrocytes, although in the periphery, they have recently been shown to be expressed on similar myelin producing Schwann cells.[244]

In summary, MR has been shown to be heavily involved in innate immunity through the recognition of mannosylated PAMP ligands. By a process that is not well understood, the ligand bound receptor is internalized and adaptive immune responses are generated. As previously discussed, the receptor may work in synergy with other receptors with active signaling motifs in their cytoplasmic domains to aide this process. Different combinations of cytokines may also be involved. The receptor/ligand complex is processed after internalization into short peptide antigen fragments that are presented on MHC I or II for the stimulation of B and T cells. The release of pro- or anti-inflammatory cytokines is capable of influencing M1 or M2 polarization of macrophage with subsequent effects on IL-10 transgene uptake.

4.6 Future directions

4.6.1 Protocells to deliver adjuvant

Protocells have excellent potential for multimodal delivery of drug or DNA to specific cells because of the high loading capacity of the porous silica core and ease with which targeting molecules can be conjugated to the lipid by layer. The *in vitro* and in *vivo studies* in Chapter 2 demonstrate that IL-10 transgene can be delivered by protocells and remain fully functional for gene expression following loading procedures. Allodynic reversal was robust and full for around two weeks in neuropathic rats intrathecally injected with 10 µg of pDNA loaded on DOTAP:CHOL protocells (**Chapter 2, Figure 2.7**). While these results are promising, there is much room to improve efficacy of intrathecal IL-10 transgene delivery using protocells. One way to advance these studies is to use cell specific targeting of pDNA-IL10 and/or adjuvant loaded protocells to DC or macrophages in the meningeal lining or to microglia or astrocytes in superficial regions of the spinal cord. In this fashion these cells could be directly stimulated to polarize to an alternatively activated M2 phenotype with improved capability for transgene uptake. As these studies point out, D-mannose is an excellent adjuvant to prime these responses. By conjugating mannosylated protein ligands to the lipid bilayer of protocells and simultaneously loading the protocell with D-mannose enduring pain relief may be achieved in a single co-injection with a very low dose of pDNA-IL10 (1 µg) that was previously shown to be ineffective when given as a single injection.

An early study Kawakami S et al.,[245] points to the feasibility of using mannose receptor targeted gene transfer. Cultured mouse peritoneal macrophage cells were

transfected with a pDNA encoding the luciferase gene complexed with the cationic liposome composed of a mannosylated cholesterol derivative, DOPE lipid or non-mannosylated cholesterol, DOPE lipsome. Mannosylated cholesterol/DOPE lipid was found to have significantly higher transfection as measured by fluorescent intensity of the luciferase by a luminometer. *In vivo,* mice were given intravenous injection of the two varieties of lipid/pDNA-luciferase and those with mannose showed 16-fold higher expression of luciferase in the liver, an organ well characterized to express high numbers of MRs. When mannosylated bovine serum was injected 5 minutes prior to the liposome injections to saturate MRs, gene expression in the liver was significantly lower, supporting the idea that the improved transfection involved the MR.[245] Improved transfection efficiency also demonstrated by another group using Mannose-C4-cholesterol containing liposomes to deliver pDNA luciferase, using the same mouse *in vitro* and *in vivo* models.[246] More recently, Jaing, H. et al.,[247] used mannosylated chitosan-grafted polyethylenimine (Man-CHI-g-PEI) to transfect Raw 264.7 mouse macrophage cells and found that the transfection efficiency of Man-CHI-g-PEI/DNA was 10948.3 than naked DNA, 9.4 higher than CHI-g-PEI/DNA , and 16.6-fold higher than, PEI/DNA complexes. Man-CHI-g-PEI/DNA complexes had a much reduced transfection efficiency in the presence of excess free mannose (50 μM) used to saturate MRs in a receptor binding competition assay, supporting that the mannosylated complexes were being taken up by a MR dependent mechanism.[247] Mannosylated cholesterol or PEI conjugated lipid bilayers on adjuvant or pDNA loaded protocells might fine-tune the use of D-mannose as an adjuvant and exploit the unique features of the protocell, namely, high loading capacity and ease of surface modification. This new generation of protocell

has great potential for generating safe and long term pain reversal with lower doses of IL-10 transgene with only one injection.

4.6.2 PLGA encapsulation

Studies using FDA approved, biodegradable, poly-lactic-co-glycolic acid (PLGA) to encapsulate pDNAIL-10 and/or adjuvant, as outlined in the original aims of this dissertation also offer great promise to improve intrathecal IL-10 gene delivery. Our studies have already demonstrated, in the CCI neuropathic rat model, that only one injection of 10 μg of PLGA encapsulated IL-10 was able to generate pain relief of ~ 3 month duration while unencapsulated pDNA at that dose had no effect.[73] Because the double emulsion synthesis process used to make the particles, loading efficiency is very poor. It took 1 mg of PLGA to encapsulate 10 μg DNA. The ideal would be to drop both the dose of pDNA and PLGA and generate the same pain reversal. One way to do this is to adjust the double emulsion synthesis process. The method involves three phases: 1) a hydrophyllic water based phase that contains the DNA 2) an intermediate organic phase composed of polymer mixed with solvent and 3) an outer water phase containing an emulsifying agent. Adjusting any of these phases has the potential to improve DNA loading efficiency in our future work and our collaborators are currently working on this issue. While plasmid DNA is difficult to load, small single stranded DNA such as ODN2006 may load without difficulty. One study planned for the future is to encapsulate this ODN or other adjuvant molecules to prime IL-10 gene uptake. Encapsulation in PLGA may protect the adjuvant from degradation as it protects DNA from nuclease digestion.[73] ODNs adsorbed on PLGA particles and co-administered with human anthrax

vaccine induced faster and greater immunoglogulin G response than when naked ODNs with the vaccine.[248]

PLGA may be ideal for delivering adjuvants such as ODNs, as it has a bimodal release profile so it would cause an initial burst of adjuvant or priming immune response during the sensitization period followed by a sustained release that might generate prolonged M2 polarization of peri-spinal macrophage. An in vitro analysis of pDNA-IL10 performed in our studies showed that 30% was released from PLGA by 3 days with a steady release continuing greater than 72 days.[73]

The terminal carboxyl groups on PLGA can be conjugated with other molecules for cell targeting but the efficiency is low as there are few of these groups available per particle.[249] One strategy is to coat the microparticle with another polymer that contains higher densities of functional groups of polyamines. Another strategy is to coat the particle with avidin to which biotinylated ligands are attached.[249] Either strategy might allow mannosylation of PLGA and targeted delivery for IL-10.

4.7 Concluding remarks

The research and development of therapeutic gene based methods of treating chronic neuropathic pain such as those presented here have been progressing for greater than a decade. While lumbar delivery of transgene has been shown to successfully to treat this problem in a number of animal models,[68,73,79,99,131,250] there is much room for improvement to achieve greater efficiency. Using synthetic particles is an excellent approach to advance the effectiveness of such therapy.

The use of synthetic particles for biomedical purposes such as drug delivery, cell-specific targeting, medical imaging and gene delivery has rapidly expanded in recent years. As discussed herein, these particles are advantageous in that they can be engineered to be highly stable in physiological conditions, and tuned for release of cargo at a certain time or pH. They are readily functionalized with ligands, molecules or antibodies for specific cell targeting, loaded with therapeutic drugs and administered to the CNS safely.[214, 251]

Cell specific targeting is being increasingly used in approaches to treat neurodegenerative diseases and cancer, where the BBB and neuronal anatomy have limited other gene therapy approaches.[91] Specific targeting of adjuvant or pDNA-IL-10 to peri-spinal macrophage or DCs, may offer key improvements in delivery of Il-10 transgene as a therapeutic treatment to relieve chronic neuropathic pain states. Modifying biodegradable polymers such as PLGA or non-toxic nanomaterials such as protocell with cell specific ligand holds exciting promise to advance the work presented here. It is of upmost importance that while improving the efficiency of the gene therapy approach, that biocompatibility and safety are maintained and continually monitored.

5. References

1. Kandel ER, Schwartz JH, Jessell TM. Principles of Neural Science. In, 4 ed. McGraw-Hill: New York, 2000, pp 22-24.

2. Young PA, Young, Paul H., Tolbert, Daniel L. Basic Clinical Neuroscience. In, 2nd ed. Wolters Kluwer/ Lippincott Williams and Wilkins: Philadelphia, 2008, pp 9-10.

3. Kandel ER, Schwartz JH, Jessell TM. Principles of Neural Science. In. McGraw-Hill: New York, 2000, pp 29-32.

4. Kandel ER, Schwartz JH, Jessell TM. Principles of Neural Science. In. McGraw-Hill: New York, 2000, pp 222-226.

5. Young PA, Young, Paul H., Tolbert, Daniel L. Basic Clinical Neuroscience. In, 2nd ed. Wolters Kluwer/ Lippincott Williams and Wilkins: Philadelphia, 2008, pp 11-12.

6. Young PA, Young, Paul H., Tolbert, Daniel L. Basic Clinical Neuroscience. In, 2nd ed. Wolters Kluwer/ Lippincott Williams and Wilkins: Philadelphia, 2008, pp 15-19.

7. Siegel A, Sapru, Hereday. Essential Neuroscience. In. Lippincott Williams and Wilkins: Philadelphia, 2006, pp 136-140.

8. Siegel A, Sapru, Hereday. Essential Neuroscience. In. Lippincott Williams and Wilkins: Philadelphia, 2006, pp 257-259.

9. Kandel ER, Schwartz JH, Jessell TM. Principles of Neural Science. In. McGraw-Hill: New York, 2000, pp 431-441.

10. Kandel ER, Schwartz JH, Jessell TM. Principles of Neural Science. In, 4 ed. McGraw-Hill: New York, 2000, pp 473-475.

11. Basbaum AI, Bautista DM, Scherrer G, Julius D. Cellular and molecular mechanisms of pain. Cell 2009; 139(2): 267-84.

12. Kandel ER, Schwartz JH, Jessell TM. Principles of Neural Science. In, 4 ed. McGraw-Hill: New York, 2000, pp 129-132.

13. Young PA, Young, Paul H., Tolbert, Daniel L. Basic Clinical Neuroscience. In, 2nd ed. Wolters Kluwer/ Lippincott Williams and Wilkins: Philadelphia, 2008, pp 129-132.

14. Siegel A, Sapru, Hereday. Essential Neuroscience. In. Lippincott Williams and Wilkins: Philadelphia, 2006, pp 263-264.

15. Light AR, Perl ER. Spinal termination of functionally identified primary afferent neurons with slowly conducting myelinated fibers. J Comp Neurol 1979; 186(2): 133-50.

16. Kandel ER, Schwartz JH, Jessell TM. Principles of Neural Science. In, 4 ed. McGraw-Hill: New York, 2000, pp 474-477.

17. Siegel A, Sapru, Hereday. Essential Neuroscience. In. Lippincott Williams and Wilkins: Philadelphia, 2006, pp 263-264.

18. Melzak R., Wall, P. Melzak and Wall's Textbook of Pain. McMahon S., Kotzenburg, M. (ed). Elsevier, Churchill Livingtone: Philadelphia, Pa., 2006, pp 35-36.

19. Young PA, Young, Paul H., Tolbert, Daniel L. Basic Clinical Neuroscience. In, 2nd ed. Wolters Kluwer/ Lippincott Williams and Wilkins: Philadelphia, 2008, pp 133-135.

20. Siegel A, Sapru, Hereday. Essential Neuroscience. In. Lippincott Williams and Wilkins: Philadelphia, 2006, pp 142-145; 262

21. D'Mello R, Dickenson AH. Spinal cord mechanisms of pain. Br J Anaesth 2008; 101(1): 8-16.

22. Kandel ER, Schwartz JH, Jessell TM. Principles of Neural Science 4 edn: New York, 2000, p 489.

23. Leith JL, Wilson AW, Donaldson LF, Lumb BM. Cyclooxygenase-1-derived prostaglandins in the periaqueductal gray differentially control C- versus A-fiber-evoked spinal nociception. J Neurosci 2007; 27(42): 11296-305.

24. Heinricher MM, Tavares I, Leith JL, Lumb BM. Descending control of nociception: Specificity, recruitment and plasticity. Brain Res Rev 2009; 60(1): 214-25.

25. Hohmann AG, Suplita RL, Bolton NM, Neely MH, Fegley D, Mangieri R et al. An endocannabinoid mechanism for stress-induced analgesia. Nature 2005; 435(7045): 1108-12.

26. Melzak R., Wall, P. Melzak and Wall's Textbook of Pain. McMahon S, Koltzenburg M. (ed). Elsevier, Churchill Livingtone: Philadelphia, Pa., 2006, pp 125-128.

27. Melzak R., Wall, P. Melzak and Wall's Textbook of Pain. McMahon S., Koltzenburg, M. (ed). Elsevier, Churchill Livingtone: Philadelphia, Pa., 2006, p 135.

28. Fields HL, Malick A, Burstein R. Dorsal horn projection targets of ON and OFF cells in the rostral ventromedial medulla. J Neurophysiol 1995; 74(4): 1742-59.

29. Haws CM, Williamson AM, Fields HL. Putative nociceptive modulatory neurons in the dorsolateral pontomesencephalic reticular formation. Brain Res 1989; 483(2): 272-82.

30. Watkins LR, Milligan ED, Maier SF. Glial activation: a driving force for pathological pain. Trends in Neuroscience 2001; 24: 450-455.

31. National Institutes of Health Ngndipr, B, MD: National Institutes of Health. 1998 Sept. 4. Available from: http://grants.nih.gov/grants/guide/pa-files/PA-98-102.html. . In.

32. Melzak R.,Wall, P. Melzak and Wall's Textbook of Pain. McMahon S., Koltzenburg, M. (ed). Elsevier, Churchill Livingtone: Philadelphia, Pa., 2006, p 23.

33. Melzak R., Wall, P. Melzak and Wall's Textbook of Pain. McMahon S., Koltzenburg, M. (ed). Elsevier, Churchill Livingtone: Philadelphia, Pa., 2006, pp 15-16; 23.

34. http://www.painfoundation.org/newsroom/reporter-resources/voices-survey-report.pdf VoCPSAf. In.

35. Melzak R.,Wall, P. Melzak and Wall's Textbook of Pain. McMahon S., Koltzenburg, M. (ed). Elsevier, Churchill Livingtone: Philadelphia, Pa., 2006, pp 95-96.

36. Mendell LM. Modifiability of spinal synapses. Physiological Reviews 1984; 64: 260-324.

37. Costigan M, Scholz J, Woolf CJ. Neuropathic pain: a maladaptive response of the nervous system to damage. Annu Rev Neurosci 2009; 32: 1-32.

38. Herrero JF, Laird JM, Lopez-Garcia JA. Wind-up of spinal cord neurones and pain sensation: much ado about something? Prog Neurobiol 2000; 61(2): 169-203.

39. Latremoliere A, Woolf CJ. Central sensitization: a generator of pain hypersensitivity by central neural plasticity. The journal of pain : official journal of the American Pain Society 2009; 10(9): 895-926.

40. Marchand F, Perretti M, McMahon SB. Role of the immune system in chronic pain. Nat Rev 2005; 6: 521-530.

41. Xu Q, Yaksh TL. A brief comparison of the pathophysiology of inflammatory versus neuropathic pain. Curr Opin Anaesthesiol 2011; 24(4): 400-7.

42. Ji RR, Kohno T, Moore KA, Woolf CJ. Central sensitization and LTP: do pain and memory share similar mechanisms? Trends Neurosci 2003; 26(12): 696-705.

43. Song I, Huganir RL. Regulation of AMPA receptors during synaptic plasticity. Trends Neurosci 2002; 25(11): 578-88.

44. Coull JA, Beggs S, Boudreau D, Boivin D, Tsuda M, Inoue K et al. BDNF from microglia causes the shift in neuronal anion gradient underlying neuropathic pain. Nature 2005; 438: 923-925.

45. Moore KA, Kohno T, Karchewski LA, Scholz J, Baba H, Woolf CJ. Partial peripheral nerve injury promotes a selective loss of GABAergic inhibition in the superficial dorsal horn of the spinal cord. J Neurosci 2002; 22(15): 6724-31.

46. Pinto M, Lima D, Tavares I. Neuronal activation at the spinal cord and medullary pain control centers after joint stimulation: a c-fos study in acute and chronic articular inflammation. Neuroscience 2007; 147(4): 1076-89.

47. Milligan ED, Watkins LR. Pathological and protective roles of glia in chronic pain. Nat Rev Neurosci 2009; 10(1): 23-36.

48. Scholz J, Woolf CJ. The neuropathic pain triad: neurons, immune cells, and glia. Nat Neuroscience 2007; 10(11): 1361-68.

49. Guo W, Wang H, Watanabe M, Shimizu K, Zou S, LaGraize SC et al. Glial-cytokine-neuronal interactions underlying the mechanisms of persistent pain. J Neurosci 2007; 27(22): 6006-18.

50. Watkins LR, Maier SF. Targeting glia to control clinical pain: An idea whose time has come. Drug Discovery Today: Therapeutic Strategies 2004.

51. Pham LD, Hayakawa K, Seo JH, Nguyen MN, Som AT, Lee BJ et al. Crosstalk between oligodendrocytes and cerebral endothelium contributes to vascular remodeling after white matter injury. Glia 2012; 60(6): 875-81.

52. Favrais G, van de Looij Y, Fleiss B, Ramanantsoa N, Bonnin P, Stoltenburg-Didinger G et al. Systemic inflammation disrupts the developmental program of white matter. Annals of neurology 2011; 70(4): 550-65.

53. Iwasaki A, Medzhitov R. Regulation of adaptive immunity by the innate immune system. Science 2010; 327(5963): 291-5.

54. Gordon S. Alternative activation of macrophages. Nat Rev Immunol 2003; 3(1): 23-35.

55. Martinez FO, Helming L, Gordon S. Alternative activation of macrophages: an immunologic functional perspective. Annu Rev Immunol 2009; 27: 451-83.

56. Porcheray F, Viaud S, Rimaniol AC, Leone C, Samah B, Dereuddre-Bosquet N et al. Macrophage activation switching: an asset for the resolution of inflammation. Clin Exp Immunol 2005; 142(3): 481-9.

155

57. Engelhardt B, Coisne C. Fluids and barriers of the CNS establish immune privilege by confining immune surveillance to a two-walled castle moat surrounding the CNS castle. Fluids Barriers CNS 2011; 8(1): 4.

58. Abbott NJ, Ronnback L, Hansson E. Astrocyte-endothelial interactions at the blood-brain barrier. Nat Rev Neurosci 2006; 7(1): 41-53.

59. Watkins LR, Maier SF. Glia: A novel drug discovery target for clinical pain. Nat Rev Drug Discov 2003; 2: 973-985.

60. Bazzoni F, Tamassia N, Rossato M, Cassatella MA. Understanding the molecular mechanisms of the multifaceted IL-10-mediated anti-inflammatory response: lessons from neutrophils. Eur J Immunol 2010; 40(9): 2360-8.

61. Ledeboer A. Interleukin-10 and Interleukin-10 receptor in Neuroinflammation. Ph.D., Research Institute Neurosciences, VU University Medical Center, Amsterdam, the Netherlands, 2002.

62. Moore KW, de Waal Malefyt R, Coffman RL, O'Garra A. Interleukin-10 and the interleukin-10 receptor. Annu Rev Immunol 2001; 19: 683-765.

63. Heyen JR, Ye S, Finck BN, Johnson RW. Interleukin (IL)-10 inhibits IL-6 production in microglia by preventing activation of NF-kappaB. Brain research. Molecular brain research 2000; 77(1): 138-47.

64. Kremlev SG, Palmer C. Interleukin-10 inhibits endotoxin-induced pro-inflammatory cytokines in microglial cell cultures. J Neuroimmunol 2005; 162(1-2): 71-80.

65. Ledeboer A, Breve JJ, Wierinckx A, van der Jagt S, Bristow AF, Leysen JE et al. Expression and regulation of interleukin-10 and interleukin-10 receptor in rat astroglial and microglial cells. Eur J Neurosci 2002; 16(7): 1175-85.

66. Bogdan C, Vodovotz Y, Nathan C. Macrophage deactivation by interleukin 10. The Journal of experimental medicine 1991; 174(6): 1549-55.

67. Fiorentino DF, Zlotnik A, Mosmann TR, Howard M, O'Garra A. IL-10 inhibits cytokine production by activated macrophages. J Immunol 1991; 147(11): 3815-22.

68. Milligan ED, Sloane EM, Langer SJ, Hughes TR, Jekich BM, Frank MG et al. Repeated intrathecal injections of plasmid DNA encoding interleukin-10 produce prolonged reversal of neuropathic pain. Pain 2006; 126: 294-308.

69. Sloane E, Langer S, Jekich B, Mahoney J, Hughes T, Frank M et al. Immunological priming potentiates non-viral anti-inflammatory gene therapy treatment of neuropathic pain. Gene Ther 2009; 16(10): 1210-22.

70. Elward K, Gasque P. "Eat me" and "don't eat me" signals govern the innate immune response and tissue repair in the CNS: emphasis on the critical role of the complement system. Mol Immunol 2003; 40(2-4): 85-94.

71. Krieg AM. CpG motifs in bacterial DNA and their immune effects. Annu Rev Immunol 2002; 20: 709-60.

72. Sloane EM, Langer SJ, Jekich BM, Mahoney JH, Hughes TS, Seibert W et al. Immunological priming potentiates non-viral anti-inflammatory gene therapy treatment of neuropathic pain. Gene therapy 2009; (1): 1-13.

73. Soderquist RG, Sloane EM, Loram LC, Harrison JA, Dengler EC, Johnson SM et al. Release of Plasmid DNA-Encoding IL-10 from PLGA Microparticles Facilitates Long-Term Reversal of Neuropathic Pain Following a Single Intrathecal Administration. Pharm Res 2010.

74. Qiao B, Li B, Yang X, Zhang H, Chu Y, Wang Y et al. Specific siRNA downregulated TLR9 and altered cytokine expression pattern in macrophage after CpG DNA stimulation. Cell Mol Immunol 2005; 2(2): 130-5.

75. Barnes PJ. How corticosteroids control inflammation: Quintiles Prize Lecture 2005. Br J Pharmacol 2006; 148(3): 245-54.

76. Gazi U, Martinez-Pomares L. Influence of the mannose receptor in host immune responses. Immunobiology 2009; 214(7): 554-61.

77. Kerrigan AM, Brown GD. C-type lectins and phagocytosis. Immunobiology 2009; 214(7): 562-75.

78. McMenamin PG, Wealthall RJ, Deverall M, Cooper SJ, Griffin B. Macrophages and dendritic cells in the rat meninges and choroid plexus: three-dimensional localisation by environmental scanning electron microscopy and confocal microscopy. Cell Tissue Res 2003; 313(3): 259-69.

79. Milligan ED, Soderquist RG, Malone SM, Mahoney JH, Hughes TS, Langer SJ et al. Intrathecal polymer-based interleukin-10 gene delivery for neuropathic pain. Neuron Glia Biol 2006; 2(4): 293-308.

80. Khalil IA, Kogure K, Akita H, Harashima H. Uptake pathways and subsequent intracellular trafficking in nonviral gene delivery. Pharmacol Rev 2006; 58(1): 32-45.

81. Lam AP, Dean DA. Progress and prospects: nuclear import of nonviral vectors. Gene Ther 2010; 17(4): 439-47.

82. Al-Dosari MS, Gao X. Nonviral gene delivery: principle, limitations, and recent progress. AAPS J 2009; 11(4): 671-81.

83. Kaneda Y. Biological barriers to gene transfer. In: Amiji MM (ed) Polymeric Gene Delivery: Principles and Apllications. CRC Press LLC: Boca Raton, 2005, pp 29-41.

84. Akinc A, Thomas M, Klibanov AM, Langer R. Exploring polyethylenimine-mediated DNA transfection and the proton sponge hypothesis. J Gene Med 2005; 7(5): 657-63.

85. Kol MA, van Laak AN, Rijkers DT, Killian JA, de Kroon AI, de Kruijff B. Phospholipid flop induced by transmembrane peptides in model membranes is modulated by lipid composition. Biochemistry 2003; 42(1): 231-7.

86. Edelstein ML, Abedi MR, Wixon J. Gene therapy clinical trials worldwide to 2007--an update. J Gene Med 2007; 9(10): 833-42.

87. Kaiser J. Gene therapists celebrate a decade of progress. Science 2011; 334: 29-30.

88. Perez-Martinez FC, Guerra J, Posadas I, Cena V. Barriers to non-viral vector-mediated gene delivery in the nervous system. Pharm Res 2011; 28(8): 1843-58.

89. Morille M, Passirani C, Vonarbourg A, Clavreul A, Benoit JP. Progress in developing cationic vectors for non-viral systemic gene therapy against cancer. Biomaterials 2008; 29(24-25): 3477-96.

90. Trewyn BG, Giri S, Slowing, II, Lin VS. Mesoporous silica nanoparticle based controlled release, drug delivery, and biosensor systems. Chem Commun (Camb) 2007; (31): 3236-45.

91. Rogers ML, Rush RA. Non-viral gene therapy for neurological diseases, with an emphasis on targeted gene delivery. J Control Release 2012; 157(2): 183-9.

92. Park EJ, Park K. Oxidative stress and pro-inflammatory responses induced by silica nanoparticles in vivo and in vitro. Toxicol Lett 2009; 184(1): 18-25.

93. Hudson SP, Padera RF, Langer R, Kohane DS. The biocompatibility of mesoporous silicates. Biomaterials 2008; 29(30): 4045-55.

94. Ashley CE, Carnes EC, Phillips GK, Padilla D, Durfee PN, Brown PA et al. The targeted delivery of multicomponent cargos to cancer cells by nanoporous particle-supported lipid bilayers. Nat Mater 2011; 10(5): 389-97.

95. Tarn D, Ashley, C., Xue, M., Carnes, E., Zink, J., Brinker, J. Mesoporous Silica Nanoparticle Nanocarries- Biofunctionality and Biocompatiblity. Accounts of Chemical Research 2012.

96. Slowing, II, Vivero-Escoto JL, Wu CW, Lin VS. Mesoporous silica nanoparticles as controlled release drug delivery and gene transfection carriers. Adv Drug Deliv Rev 2008; 60(11): 1278-88.

158

97. Sloane EM, Soderquist RG, Maier SF, Mahoney MJ, Watkins LR, Milligan ED. Long-term control of neuropathic pain in a non-viral gene therapy paradigm. Gene Ther 2009; 16(4): 470-5.

98. Milligan ED, Langer SJ, Sloane EM, He L, Wieseler-Frank J, O'Connor K et al. Controlling pathological pain by adenovirally driven spinal production of the anti-inflammatory cytokine, interleukin-10. Eur J Neurosci 2005; 21(8): 2136-48.

99. Milligan ED, Sloane EM, Langer SJ, Cruz PE, Chacur M, Spataro L et al. Controlling neuropathic pain by adeno-associated virus driven production of the anti-inflammatory cytokine, interleukin-10. Mol Pain 2005; 1: 9.

100. Liu J, Jiang X, Ashley C, Brinker CJ. Electrostatically mediated liposome fusion and lipid exchange with a nanoparticle-supported bilayer for control of surface charge, drug containment, and delivery. J Am Chem Soc 2009; 131(22): 7567-9.

101. Liu J, Stace-Naughton A, Jiang A, Brinker CJ. Porous nanoparticle supported lipid bilayers (protocells) as delivery vehicles. J. Am. Chem. Soc. 2009; http://pubs.acs.org.

102. Chaplan SR, Bach FW, Pogrel JW, Chung JM, Yaksh TL. Quantitative assessment of tactile allodynia in the rat paw. J Neurosci Methods 1994; 53(1): 55-63.

103. Milligan ED, Mehmert KK, Hinde JL, Harvey LO, Martin D, Tracey KJ et al. Thermal hyperalgesia and mechanical allodynia produced by intrathecal administration of the human immunodeficiency virus-1 (HIV-1) envelope glycoprotein, gp120. Brain Res 2000; 861(1): 105-16.

104. Milligan ED, O'Connor KA, Nguyen KT, Armstrong CB, Twining C, Gaykema RP et al. Intrathecal HIV-1 envelope glycoprotein gp120 induces enhanced pain states mediated by spinal cord proinflammatory cytokines. J Neurosci 2001; 21(8): 2808-19.

105. Bennett GJ, Xie YK. A peripheral mononeuropathy in rat that produces disorders of pain sensation like those seen in man. Pain 1988; 33(1): 87-107.

106. Wilkerson JL, Gentry KR, Dengler EC, Wallace JA, Kerwin AA, Armijo LM et al. Intrathecal cannabilactone CB(2)R agonist, AM1710, controls pathological pain and restores basal cytokine levels. Pain 2012; 153(5): 1091-106.

107. Milligan ED, Sloane EM, Langer SJ, Hughes TS, Jekich BM, Frank MG et al. Repeated intrathecal injections of plasmid DNA encoding interleukin-10 produce prolonged reversal of neuropathic pain. Pain 2006; 126(1-3): 294-308.

108. Langer R. Drug delivery and targeting. Nature 1998; 392(6679 Suppl): 5-10.

109. Crook K, Stevenson BJ, Dubouchet M, Porteous DJ. Inclusion of cholesterol in DOTAP transfection complexes increases the delivery of DNA to cells in vitro in the presence of serum. Gene Ther 1998; 5(1): 137-43.

110. Barrett E, Joyner, L., Halenda,P. The Determination of Pore volume and Area distributions in Porous Substances. I. Computations from Nitrogen isotherms. J. Am. Chem. Soc. 1951; 73(1): pp.373-380.

111. Brunauer S, Emmett, P., Teller, E. . Adsorption of Gases in Multimolecular Layers. J. Am. Chem. Soc. 1938; 60(2): pp 309-319.

112. Wilkerson JL GK, Dengler E, Wallace J, Kerwin A, Kuhn M, Zvonok A, Thakur G, Makriyannis A, Milligan E, . Immunofluorescent spetral analysis reveals the intrathecal cannabinoid agonist AM1241, produces spinal anti-inflammatory cytokine responses in neuropathic rats exhibiting relief form allodynia. Brain and Behavior 2012; Open Acess.

113. Harvey LO, Jr. Efficient estimation of sensory thresholds. Behav Research Methods Instruments and Computers 1986; 18: 623-632.

114. Liu J, Stace-Naughton A, Jiang X, Brinker CJ. Porous nanoparticle supported lipid bilayers (protocells) as delivery vehicles. J Am Chem Soc 2009; 131(4): 1354-5.

115. Khan S, Shin EM, Choi RJ, Jung YH, Kim J, Tosun A et al. Suppression of LPS-induced inflammatory and NF-kappaB responses by anomalin in RAW 264.7 macrophages. J Cell Biochem 2011; 112(8): 2179-88.

116. Lee JK. Anti-inflammatory effects of eriodictyol in lipopolysaccharide-stimulated raw 264.7 murine macrophages. Arch Pharm Res 2011; 34(4): 671-9.

117. Qureshi AA, Tan X, Reis JC, Badr MZ, Papasian CJ, Morrison DC et al. Suppression of nitric oxide induction and pro-inflammatory cytokines by novel proteasome inhibitors in various experimental models. Lipids Health Dis 2011; 10: 177.

118. Zha LY, Mao LM, Lu XC, Deng H, Ye JF, Chu XW et al. Anti-inflammatory effect of soyasaponins through suppressing nitric oxide production in LPS-stimulated RAW 264.7 cells by attenuation of NF-kappaB-mediated nitric oxide synthase expression. Bioorg Med Chem Lett 2011; 21(8): 2415-8.

119. Bimbo LM, Peltonen L, Hirvonen J, Santos HA. Toxicological Profile of Therapeutic Nanodelivery Systems. Curr Drug Metab 2012.

120. Sackmann E. Supported membranes: scientific and practical applications. Science 1996; 271(5245): 43-8.

121. Troutier AL, Ladaviere C. An overview of lipid membrane supported by colloidal particles. Adv Colloid Interface Sci 2007; 133(1): 1-21.

122. Davis RW, Flores A, Barrick TA, Cox JM, Brozik SM, Lopez GP et al. Nanoporous microbead supported bilayers: stability, physical characterization, and incorporation of functional transmembrane proteins. Langmuir 2007; 23(7): 3864-72.

123. Singh KP, Panwar P, Kohli P, Sanjesh. Liposome-mesoporous silica nanoparticles fused cores: a safer mode of drug carrier. J Biomed Nanotechnol 2011; 7(1): 60-2.

124. Yang TH, Yee CK, Amweg ML, Singh S, Kendall EL, Dattelbaum AM et al. Optical detection of ion-channel-induced proton transport in supported phospholipid bilayers. Nano Lett 2007; 7(8): 2446-51.

125. Son Y, Cheong YK, Kim NH, Chung HT, Kang DG, Pae HO. Mitogen-Activated Protein Kinases and Reactive Oxygen Species: How Can ROS Activate MAPK Pathways? J Signal Transduct 2011; 2011: 792639.

126. Murphy SaG, D. Glial NO: Normal and Pathological Roles. The Neuroscientist 1996; 2(2): 90-99.

127. Wang J, Lenardo MJ. Roles of caspases in apoptosis, development, and cytokine maturation revealed by homozygous gene deficiencies. J Cell Sci 2000; 113 (Pt 5): 753-7.

128. Bernardos A, Mondragon L, Aznar E, Marcos MD, Martinez-Manez R, Sancenon F et al. Enzyme-responsive intracellular controlled release using nanometric silica mesoporous supports capped with "saccharides". ACS Nano 2010; 4(11): 6353-68.

129. Rosenholm JM, Sahlgren C, Linden M. Towards multifunctional, targeted drug delivery systems using mesoporous silica nanoparticles--opportunities & challenges. Nanoscale 2010; 2(10): 1870-83.

130. Edelstien M. Gene Therapy Clinical Trials Worldwide (http://www.wiley.com/legacy/wileychi/genmed/clinical/). In: The Journal of Gene Medicine: John Wiley and Sons, Ltd., 2012.

131. Goss JR, Goins WF, Glorioso JC. Gene therapy applications for the treatment of neuropathic pain. Expert Rev Neurother 2007; 7(5): 487-506.

132. Campbell JN, Meyer RA. Mechanisms of neuropathic pain. Neuron 2006; 52(1): 77-92.

133. Milligan ED, Riddle Penzkover, K., Soderquist, R., Mahoney, M. Spinal Interleukin-10 Therapy to Treat Peripheral Neuroopathic Pain. Neuromodulation: Technology at the Neural Interface 1012; in press.

134. Miraucourt LS, Dallel R, Voisin DL. Glycine inhibitory dysfunction turns touch into pain through PKCgamma interneurons. PLoS One 2007; 2(11): e1116.

135. Sloane E, Langer S, Jekich B, Mahoney J, Hughes T, Frank M et al. Immunological priming potentiates non-viral anti-inflammatory gene therapy treatment of neuropathic pain. Gene therapy 2009; 16(10): 1210-22.

136. Roy I, Ohulchanskyy TY, Bharali DJ, Pudavar HE, Mistretta RA, Kaur N et al. Optical tracking of organically modified silica nanoparticles as DNA carriers: a nonviral, nanomedicine approach for gene delivery. Proc Natl Acad Sci U S A 2005; 102(2): 279-84.

137. Bharali DJ, Klejbor I, Stachowiak EK, Dutta P, Roy I, Kaur N et al. Organically modified silica nanoparticles: a nonviral vector for in vivo gene delivery and expression in the brain. Proc Natl Acad Sci U S A 2005; 102(32): 11539-44.

138. Milligan ED, Sloane EM, Langer SJ, Cruz PE, Chacur M, Spataro L et al. Controlling neuropathic pain by adeno-associated virus driven production of the anti-inflammatory cytokine, interleukin-10. Molecular Pain 2005; 1: 9-22.

139. Bouhassira D, Lanteri-Minet M, Attal N, Laurent B, Touboul C. Prevalence of chronic pain with neuropathic characteristics in the general population. Pain 2008; 136(3): 380-7.

140. Torrance N, Smith BH, Bennett MI, Lee AJ. The epidemiology of chronic pain of predominantly neuropathic origin. Results from a general population survey. The journal of pain : official journal of the American Pain Society 2006; 7(4): 281-9.

141. Chiang CY, Dostrovsky JO, Iwata K, Sessle BJ. Role of glia in orofacial pain. Neuroscientist 2011; 17(3): 303-20.

142. Milligan ED, Soderquist RG, Mahoney MJ. Microglia, cytokines and pain. In: Malcangio M (ed) Synaptic Plasticity and Pain. Springer: New York, 2009, pp 367-86.

143. Hu P, Bembrick AL, Keay KA, McLachlan EM. Immune cell involvement in dorsal root ganglia and spinal cord after chronic constriction or transection of the rat sciatic nerve. Brain Behav Immun 2007; 21(5): 599-616.

144. Takeda M, Takahashi M, Matsumoto S. Contribution of the activation of satellite glia in sensory ganglia to pathological pain. Neurosci Biobehav Rev 2009; 33(6): 784-92.

145. White FA, Jung H, Miller RJ. Chemokines and the pathophysiology of neuropathic pain. Proc Natl Acad Sci U S A 2007; 104(51): 20151-8.

146. Zhang J, De Koninck Y. Spatial and temporal relationship between monocyte chemoattractant protein-1 expression and spinal glial activation following peripheral nerve injury. J Neurochem 2006; 97(3): 772-83.

162

147. Zhang J, Shi XQ, Echeverry S, Mogil JS, De Koninck Y, Rivest S. Expression of CCR2 in both resident and bone marrow-derived microglia plays a critical role in neuropathic pain. J Neurosci 2007; 27(45): 12396-406.

148. Romero-Sandoval A, Nutile-McMenemy N, DeLeo JA. Spinal microglial and perivascular cell cannabinoid receptor type 2 activation reduces behavioral hypersensitivity without tolerance after peripheral nerve injury. Anesthesiology 2008; 108(4): 722-34.

149. Cao L, DeLeo JA. CNS-infiltrating CD4+ T lymphocytes contribute to murine spinal nerve transection-induced neuropathic pain. Eur J Immunol 2008; 38: 448-458.

150. Echeverry S, Shi XQ, Rivest S, Zhang J. Peripheral Nerve Injury Alters Blood-Spinal Cord Barrier Functional and Molecular Integrity through a Selective Inflammatory Pathway. J Neurosci 2011; 31(30): 10819-28.

151. Ma W, Lim W, Gee K, Aucoin S, Nandan D, Kozlowski M et al. The p38 mitogen-activated kinase pathway regulates the human interleukin-10 promoter via the activation of Sp1 transcription factor in lipopolysaccharide-stimulated human macrophages. J Biol Chem 2001; 276(17): 13664-74.

152. Foey AD, Parry SL, Williams LM, Feldmann M, Foxwell BM, Brennan FM. Regulation of monocyte IL-10 synthesis by endogenous IL-1 and TNF-alpha: role of the p38 and p42/44 mitogen-activated protein kinases. J Immunol 1998; 160(2): 920-8.

153. Mizuno T, Sawada M, Marunouchi T, Suzumara A. Production of interleukin-10 by mouse glial cells in culture. Biochem Biophys Res Commun 1994; 205(3): 1907-15.

154. Gonzalez P, Burgaya F, Acarin L, Peluffo H, Castellano B, Gonzalez B. Interleukin-10 and interleukin-10 receptor-I are upregulated in glial cells after an excitotoxic injury to the postnatal rat brain. Journal of neuropathology and experimental neurology 2009; 68(4): 391-403.

155. Ledeboer A, Wierinckx A, Bol JGJM, Floris S, Renardel de Lavaletter C, DeVries HE et al. Regional and temporal expression patterns of interleukin-10, interleukin-10 receptor and adhesion molecules in the rat spinal cord during chronic relapsing EAE. J. Neuroimmunol. 2003; 136: 94-103.

156. Abraham KE, McMillen D, Brewer KL. The effects of endogenous interleukin-10 on gray matter damage and pain behaviors following excitotoxic spinal cord injury in the mouse. Neurosci. 2004; 124: 945-922.

157. Plunkett JA, Yu C-G, Easton Jm, Bethea JR, Yezierski RP. Effects of interleukin-10 (IL-10) on pain behavior and gene expression following excitotoxic spinal cord injury in the rat. Exper. Neurol. 2001; 168: 144-154.

158. Soderquist RG, Milligan ED, Harrison JA, Chavez R, Johnson K, Watkins LR et al. PEGylation of interleukin-10 for the mitigation of enhanced pain states. Experimental Neurology 2009; submitted.

159. Goss JR. The therapeutic potential of gene transfer for the treatment of peripheral neuropathies. Expert Rev Mol Med 2007; 9(8): 1-20.

160. Goss JR, Mata M, Goins WF, Wu HH, Glorioso JC, Fink DJ. Antinociceptive effect of a genomic herpes simplex virus-based vector expressing human proenkephalin in rat dorsal root ganglion. Gene Ther 2001; 8(7): 551-6.

161. Huang L, Hung M-C, Wagner E. Nonviral vectors for gene therapy, Academic Press: San Diego, 1999.

162. Braun JS, Kaissling B, Hir LH, Zenker W. Cellular components of the immune barrier in the spinal meninges and dorsal root ganglia of the normal rat: immunohistochemical (MHC class II) and electron-microscopic observations. Cell Tissue Res 1993; 273: 209-217.

163. Kreutzberg GW. Microglia: a sensor for pathological events in the CNS. Trends Neurosci 1996; 19(8): 312-8.

164. Wang Y, Abel K, Lantz K, Krieg AM, McChesney MB, Miller CJ. The Toll-like receptor 7 (TLR7) agonist, imiquimod, and the TLR9 agonist, CpG ODN, induce antiviral cytokines and chemokines but do not prevent vaginal transmission of simian immunodeficiency virus when applied intravaginally to rhesus macaques. J Virol 2005; 79(22): 14355-70.

165. Yew NS, Cheng SH. Reducing the immunostimulatory activity of CpG-containing plasmid DNA vectors for non-viral gene therapy. Expert Opin Drug Deliv 2004; 1(1): 115-25.

166. Gratchev A, Schledzewski K, Guillot P, Goerdt S. Alternatively activated antigen-presenting cells: molecular repertoire, immune regulation, and healing. Skin Pharmacol Appl Skin Physiol 2001; 14(5): 272-9.

167. Komohara Y, Ohnishi K, Kuratsu J, Takeya M. Possible involvement of the M2 anti-inflammatory macrophage phenotype in growth of human gliomas. J Pathol 2008; 216(1): 15-24.

168. Lan YY, Wang Z, Raimondi G, Wu W, Colvin BL, de Creus A et al. "Alternatively activated" dendritic cells preferentially secrete IL-10, expand Foxp3+CD4+ T cells, and induce long-term organ allograft survival in combination with CTLA4-Ig. J Immunol 2006; 177(9): 5868-77.

169. Ponomarev ED, Maresz K, Tan Y, Dittel BN. CNS-derived interleukin-4 is essential for the regulation of autoimmune inflammation and induces a state of alternative activation in microglial cells. J Neurosci 2007; 27(40): 10714-21.

170. Lingnau M, Hoflich C, Volk HD, Sabat R, Docke WD. Interleukin-10 enhances the CD14-dependent phagocytosis of bacteria and apoptotic cells by human monocytes. Hum Immunol 2007; 68(9): 730-8.

171. Ledeboer AM, Jekich BM, Sloane EM, Mahoney JH, Langer SJ, Milligan ED et al. Intrathecal interleukin-10 gene therapy attenuates paclitaxel-induced mechanical allodynia and proinflammatory cytokine expression in dorsal root ganglia in rats. Brain Behavior and Immunity 2007; 21(5): 686-698.

172. NIST/SEMATECH e-Handbook of Statistical Methods, http://www.itl.nist.gov/div898/handbook/, April, 2012. In.

173. Ghosh TK, Mickelson DJ, Fink J, Solberg JC, Inglefield JR, Hook D et al. Toll-like receptor (TLR) 2-9 agonists-induced cytokines and chemokines: I. Comparison with T cell receptor-induced responses. Cell Immunol 2006; 243(1): 48-57.

174. Kim HA, Park JH, Lee S, Choi JS, Rhim T, Lee M. Combined delivery of dexamethasone and plasmid DNA in an animal model of LPS-induced acute lung injury. J Control Release 2011; 156(1): 60-9.

175. Kossi J, Peltonen J, Ekfors T, Niinikoski J, Laato M. Effects of hexose sugars: glucose, fructose, galactose and mannose on wound healing in the rat. Eur Surg Res 1999; 31(1): 74-82.

176. Xu XL, Xie QM, Shen YH, Jiang JJ, Chen YY, Yao HY et al. Mannose prevents lipopolysaccharide-induced acute lung injury in rats. Inflamm Res 2008; 57(3): 104-10.

177. Terayama R, Bando Y, Murakami K, Kato K, Kishibe M, Yoshida S. Neuropsin promotes oligodendrocyte death, demyelination and axonal degeneration after spinal cord injury. Neuroscience 2007; 148(1): 175-87.

178. Yang H, Lu P, McKay HM, Bernot T, Keirstead H, Steward O et al. Endogenous neurogenesis replaces oligodendrocytes and astrocytes after primate spinal cord injury. J Neurosci 2006; 26(8): 2157-66.

179. DeLeo JA, Sorkin LS, Watkins LR (eds). Immune and Glial Regulation of Pain. IASP Press: Seattle, 2007.

180. Medzhitov R, Janeway CA, Jr. Decoding the patterns of self and nonself by the innate immune system. Science 2002; 296(5566): 298-300.

181. Mantovani A, Sozzani S, Locati M, Allavena P, Sica A. Macrophage polarization: tumor-associated macrophages as a paradigm for polarized M2 mononuclear phagocytes. Trends Immunol 2002; 23(11): 549-55.

182. Sloane E, Ledeboer A, Seibert W, Coats B, van Strien M, Maier SF et al. Anti-inflammatory cytokine gene therapy decreases sensory and motor dysfunction in

experimental Multiple Sclerosis: MOG-EAE behavioral and anatomical symptom treatment with cytokine gene therapy. Brain Behav Immun 2009; 23(1): 92-100.

183. Rest RF, Farrell CF, Naids FL. Mannose inhibits the human neutrophil oxidative burst. J Leukoc Biol 1988; 43(2): 158-64.

184. Willenborg DO, Parish CR, Cowden WB. Inhibition of adjuvant arthritis in the rat by phosphosugars and the alpha-glucosidase inhibitor castanospermine. Immunol Cell Biol 1992; 70 (Pt 6): 369-77.

185. Xu X, Xie Q, Shen Y, Lu G, Yao H, Chen Y et al. Involvement of mannose receptor in the preventive effects of mannose in lipopolysaccharide-induced acute lung injury. Eur J Pharmacol 2010; 641(2-3): 229-37.

186. Stahl PD, Ezekowitz RA. The mannose receptor is a pattern recognition receptor involved in host defense. Curr Opin Immunol 1998; 10(1): 50-5.

187. Linehan SA, Martinez-Pomares L, Gordon S. Mannose receptor and scavenger receptor: two macrophage pattern recognition receptors with diverse functions in tissue homeostasis and host defense. Adv Exp Med Biol 2000; 479: 1-14.

188. Engering AJ, Cella M, Fluitsma D, Brockhaus M, Hoefsmit EC, Lanzavecchia A et al. The mannose receptor functions as a high capacity and broad specificity antigen receptor in human dendritic cells. Eur J Immunol 1997; 27(9): 2417-25.

189. Tan MC, Mommaas AM, Drijfhout JW, Jordens R, Onderwater JJ, Verwoerd D et al. Mannose receptor-mediated uptake of antigens strongly enhances HLA class II-restricted antigen presentation by cultured dendritic cells. Eur J Immunol 1997; 27(9): 2426-35.

190. Burudi EM, Riese S, Stahl PD, Regnier-Vigouroux A. Identification and functional characterization of the mannose receptor in astrocytes. Glia 1999; 25(1): 44-55.

191. Burudi EM, Regnier-Vigouroux A. Regional and cellular expression of the mannose receptor in the post-natal developing mouse brain. Cell Tissue Res 2001; 303(3): 307-17.

192. Chieppa M, Bianchi G, Doni A, Del Prete A, Sironi M, Laskarin G et al. Cross-linking of the mannose receptor on monocyte-derived dendritic cells activates an anti-inflammatory immunosuppressive program. J Immunol 2003; 171(9): 4552-60.

193. Treutwein B, Strasburger H. Fitting the psychometric function. Percept Psychophys 1999; 61(1): 87-106.

194. Wallace JA, Romero AA, Gabaldon AM, Roe VA, Saavedra SL, Lobner J. Tyrosine hydroxylase-containing neurons in the spinal cord of the chicken. I. Development

and analysis of catecholamine synthesis capabilities. Cell Mol Neurobiol 1996; 16(6): 625-48.

195. Xu L, Anchordoquy T. Drug delivery trends in clinical trials and translational medicine: challenges and opportunities in the delivery of nucleic acid-based therapeutics. J Pharm Sci 2011; 100(1): 38-52.

196. Bergen JM, Park IK, Horner PJ, Pun SH. Nonviral approaches for neuronal delivery of nucleic acids. Pharm Res 2008; 25(5): 983-98.

197. Kundu P, Vinay,S. synthetic polymeric vectors in gene therapy. Current Opinion in Solid State Materials Science 2008; 12: 89-102.

198. Kamimura K, Suda T, Zhang G, Liu D. Advances in Gene Delivery Systems. Pharmaceut Med 2011; 25(5): 293-306.

199. Chazal N, Gerlier D. Virus entry, assembly, budding, and membrane rafts. Microbiol Mol Biol Rev 2003; 67(2): 226-37, table of contents.

200. Daya S, Berns KI. Gene therapy using adeno-associated virus vectors. Clin Microbiol Rev 2008; 21(4): 583-93.

201. Coura Rdos S, Nardi NB. The state of the art of adeno-associated virus-based vectors in gene therapy. Virol J 2007; 4: 99.

202. Matrai J, Chuah MK, VandenDriessche T. Recent advances in lentiviral vector development and applications. Molecular therapy : the journal of the American Society of Gene Therapy 2010; 18(3): 477-90.

203. Raper SE, Chirmule N, Lee FS, Wivel NA, Bagg A, Gao GP et al. Fatal systemic inflammatory response syndrome in a ornithine transcarbamylase deficient patient following adenoviral gene transfer. Mol Genet Metab 2003; 80(1-2): 148-58.

204. http://www.wiley.co.uk/genetherapy/clinical/. In: The Jouranl of Gene Medicine Clinical Trial Site.

205. Gill DR, Pringle IA, Hyde SC. Progress and prospects: the design and production of plasmid vectors. Gene therapy 2009; 16(2): 165-71.

206. Gorecki D. "Dressed-up" naked plasmids: Emerging vectors for non-viral gene therapy. Discovery Medicine 2009; (July 28).

207. Wattiaux R. L, N., Coninck,S., Jadot, M.,. Endosomes, lysosomes: their implication in gene transfer. Advanced Drug Delivery Reviews 2000; 41: 201-208.

208. Wasungu L, Hoekstra D. Cationic lipids, lipoplexes and intracellular delivery of genes. J Control Release 2006; 116(2): 255-64.

209. Yamashiro DJ, Fluss SR, Maxfield FR. Acidification of endocytic vesicles by an ATP-dependent proton pump. J Cell Biol 1983; 97(3): 929-34.

210. Rezaei N. Therapeutic targeting of pattern-recognition receptors. International immunopharmacology 2006; 6(6): 863-9.

211. Rosenholm JM, Peuhu E, Eriksson JE, Sahlgren C, Linden M. Targeted intracellular delivery of hydrophobic agents using mesoporous hybrid silica nanoparticles as carrier systems. Nano Lett 2009; 9(9): 3308-11.

212. Hwang SJ, Davis ME. Cationic polymers for gene delivery: designs for overcoming barriers to systemic administration. Curr Opin Mol Ther 2001; 3(2): 183-91.

213. Wu S, Hung,Y., Mou, C. Mesoporous silica nanoparticles as nanocariiers. Chemical Communications 2011; 47: 9972-9985.

214. Fadeel B, Garcia-Bennett AE. Better safe than sorry: Understanding the toxicological properties of inorganic nanoparticles manufactured for biomedical applications. Adv Drug Deliv Rev 2010; 62(3): 362-74.

215. Liu J, Stace-Naughton A, Brinker CJ. Silica nanoparticle supported lipid bilayers for gene delivery. Chem Commun (Camb) 2009; (34): 5100-2.

216. Kresge CT, Leonowicz, M.E., Roth, W.J., Vartuli, J.C., Deck, J.S. Ordered mesoporous molecular sieves synthesized by a liqid-crystal template mechanism. Nature 1992; 359(Oct 22): 710-712.

217. Lu Y, Fan, H., Stump, A., Ward, T., Reiker, T., Brinker, C.J. Aerosol-assisted self-assembly of mesostructured spherical nanoparticles. Nature 1999; 398(March 18): 223-226.

218. Xu Y, Szoka FC, Jr. Mechanism of DNA release from cationic liposome/DNA complexes used in cell transfection. Biochemistry 1996; 35(18): 5616-23.

219. Kunzmann A, Andersson B, Thurnherr T, Krug H, Scheynius A, Fadeel B. Toxicology of engineered nanomaterials: focus on biocompatibility, biodistribution and biodegradation. Biochim Biophys Acta 2011; 1810(3): 361-73.

220. Witasp E, Kupferschmidt N, Bengtsson L, Hultenby K, Smedman C, Paulie S et al. Efficient internalization of mesoporous silica particles of different sizes by primary human macrophages without impairment of macrophage clearance of apoptotic or antibody-opsonized target cells. Toxicol Appl Pharmacol 2009; 239(3): 306-19.

221. Aguilar JC, Rodriguez EG. Vaccine adjuvants revisited. Vaccine 2007; 25(19): 3752-62.

222. Baumgartner CK, Malherbe LP. Regulation of CD4 T-cell receptor diversity by vaccine adjuvants. Immunology 2010; 130(1): 16-22.

223. Sasaki S, Takeshita F, Xin KQ, Ishii N, Okuda K. Adjuvant formulations and delivery systems for DNA vaccines. Methods 2003; 31(3): 243-54.

224. Caminschi I, Shortman K. Boosting antibody responses by targeting antigens to dendritic cells. Trends Immunol 2012; 33(2): 71-7.

225. Shortman K, Lahoud MH, Caminschi I. Improving vaccines by targeting antigens to dendritic cells. Exp Mol Med 2009; 41(2): 61-6.

226. McColl A, Michlewska S, Dransfield I, Rossi AG. Effects of glucocorticoids on apoptosis and clearance of apoptotic cells. ScientificWorldJournal 2007; 7: 1165-81.

227. Jeon YJ, Han SH, Lee YW, Lee M, Yang KH, Kim HM. Dexamethasone inhibits IL-1 beta gene expression in LPS-stimulated RAW 264.7 cells by blocking NF-kappa B/Rel and AP-1 activation. Immunopharmacology 2000; 48(2): 173-83.

228. Ehrchen J, Steinmuller L, Barczyk K, Tenbrock K, Nacken W, Eisenacher M et al. Glucocorticoids induce differentiation of a specifically activated, anti-inflammatory subtype of human monocytes. Blood 2007; 109(3): 1265-74.

229. Kroin JS, Schaefer RB, Penn RD. Chronic intrathecal administration of dexamethasone sodium phosphate: pharmacokinetics and neurotoxicity in an animal model. Neurosurgery 2000; 46(1): 178-82; discussion 182-3.

230. R. H. Mannose metabolism I. The American Journal of Clinical Metabolism 1971; 24(April): 488-498.

231. Davis J. Studies of mannose metabolism and effects of long-term mannose injection in rats. Biochim Biophys Acta 2001; 1528(Oct 3): 116-26.

232. Martinez-Pomares L, Mahoney JA, Kaposzta R, Linehan SA, Stahl PD, Gordon S. A functional soluble form of the murine mannose receptor is produced by macrophages in vitro and is present in mouse serum. J Biol Chem 1998; 273(36): 23376-80.

233. Kawai T, Akira S. Toll-like receptors and their crosstalk with other innate receptors in infection and immunity. Immunity 2011; 34(5): 637-50.

234. Lee SJ, Evers S, Roeder D, Parlow AF, Risteli J, Risteli L et al. Mannose receptor-mediated regulation of serum glycoprotein homeostasis. Science 2002; 295(5561): 1898-901.

235. Le Cabec V, Emorine LJ, Toesca I, Cougoule C, Maridonneau-Parini I. The human macrophage mannose receptor is not a professional phagocytic receptor. J Leukoc Biol 2005; 77(6): 934-43.

236.   Tachado SD, Zhang J, Zhu J, Patel N, Cushion M, Koziel H. Pneumocystis-mediated IL-8 release by macrophages requires coexpression of mannose receptors and TLR2. J Leukoc Biol 2007; 81(1): 205-11.

237. Underhill DM, Ozinsky A, Hajjar AM, Stevens A, Wilson CB, Bassetti M et al. The Toll-like receptor 2 is recruited to macrophage phagosomes and discriminates between pathogens. Nature 1999; 401(6755): 811-5.

238. Raveh D, Kruskal BA, Farland J, Ezekowitz RA. Th1 and Th2 cytokines cooperate to stimulate mannose-receptor-mediated phagocytosis. J Leukoc Biol 1998; 64(1): 108-13.

239. Lee RT, Hsu TL, Huang SK, Hsieh SL, Wong CH, Lee YC. Survey of immune-related, mannose/fucose-binding C-type lectin receptors reveals widely divergent sugar-binding specificities. Glycobiology 2011; 21(4): 512-20.

240. Galea I, Palin K, Newman TA, Van Rooijen N, Perry VH, Boche D. Mannose receptor expression specifically reveals perivascular macrophages in normal, injured, and diseased mouse brain. Glia 2005; 49(3): 375-84.

241. Zimmer H, Riese S, Regnier-Vigouroux A. Functional characterization of mannose receptor expressed by immunocompetent mouse microglia. Glia 2003; 42(1): 89-100.

242. Marzolo MP, von Bernhardi R, Inestrosa NC. Mannose receptor is present in a functional state in rat microglial cells. J Neurosci Res 1999; 58(3): 387-95.

243. Regnier-Vigouroux A. The mannose receptor in the brain. Int Rev Cytol 2003; 226: 321-42.

244. Baetas-da-Cruz W, Alves L, Pessolani MC, Barbosa HS, Regnier-Vigouroux A, Corte-Real S et al. Schwann cells express the macrophage mannose receptor and MHC class II. Do they have a role in antigen presentation? J Peripher Nerv Syst 2009; 14(2): 84-92.

245. Kawakami S, Sato A, Nishikawa M, Yamashita F, Hashida M. Mannose receptor-mediated gene transfer into macrophages using novel mannosylated cationic liposomes. Gene Ther 2000; 7(4): 292-9.

246. White KL, Rades T, Furneaux RH, Tyler PC, Hook S. Mannosylated liposomes as antigen delivery vehicles for targeting to dendritic cells. J Pharm Pharmacol 2006; 58(6): 729-37.

247. Jiang HL, Kim YK, Arote R, Jere D, Quan JS, Yu JH et al. Mannosylated chitosan-graft-polyethylenimine as a gene carrier for Raw 264.7 cell targeting. Int J Pharm 2009; 375(1-2): 133-9.

248. Xie H, Gursel I, Ivins BE, Singh M, O'Hagan DT, Ulmer JB et al. CpG oligodeoxynucleotides adsorbed onto polylactide-co-glycolide microparticles improve the immunogenicity and protective activity of the licensed anthrax vaccine. Infect Immun 2005; 73(2): 828-33.

249. Mohamed F, van der Walle CF. Engineering biodegradable polyester particles with specific drug targeting and drug release properties. J Pharm Sci 2008; 97(1): 71-87.

250. Mata M, Hao S, Fink DJ. Gene therapy directed at the neuroimmune component of chronic pain with particular attention to the role of TNF alpha. Neurosci Lett 2008; 437(3): 209-13.

251. Silva GA. Nanotechnology approaches to crossing the blood-brain barrier and drug delivery to the CNS. BMC Neurosci 2008; 9 Suppl 3: S4.

252. Mulherkar, P. Flex test: a fluorescent dextran test for UF membrane characterization. Journal of Membrane Science, 2004; Vol. 236 (1-4).

253. Lewin, B. Genes; 1997; Chapter 5; Oxford University Press, N.Y., p. 107.

254. http://www.basic.northwestern.edu/biotools/oligocalc.html

255. Marko, J. and Siggia, E., Statistical mechanics of supercoiled DNA. Physical Review E 1995, 52 (3): 51.

256. Witz, G. and Stasiak, A. DNA supercoiling and its role in DNA decatenation and unknotting. Nucleic Acids Research, 2010; 38 (7): 2119-2133.

257. Lyubchenko, Y. and Shlyakhtenko, L. Visualization of supercoiled DNA with atomic force microscopy in situ. PNAS 1997; 94 (2): 496-501.

259. Lee, C. Density functional study of the structure of small cycloalkanes, J. of the Korean Physical Society 1999; 35 (5): 451.

260. Meuli-Simmen C, Liu Y, Yeo, T, Liggitt, D, Tu, G, Yang, T, Meuli, M, Knauer, S, Heath, T, Longo, F, Debs, Gene expression along the cerebral-spinal axis after regional gene delivery, Human Gene Therapy 2004, 10 (16): 2689-2700.
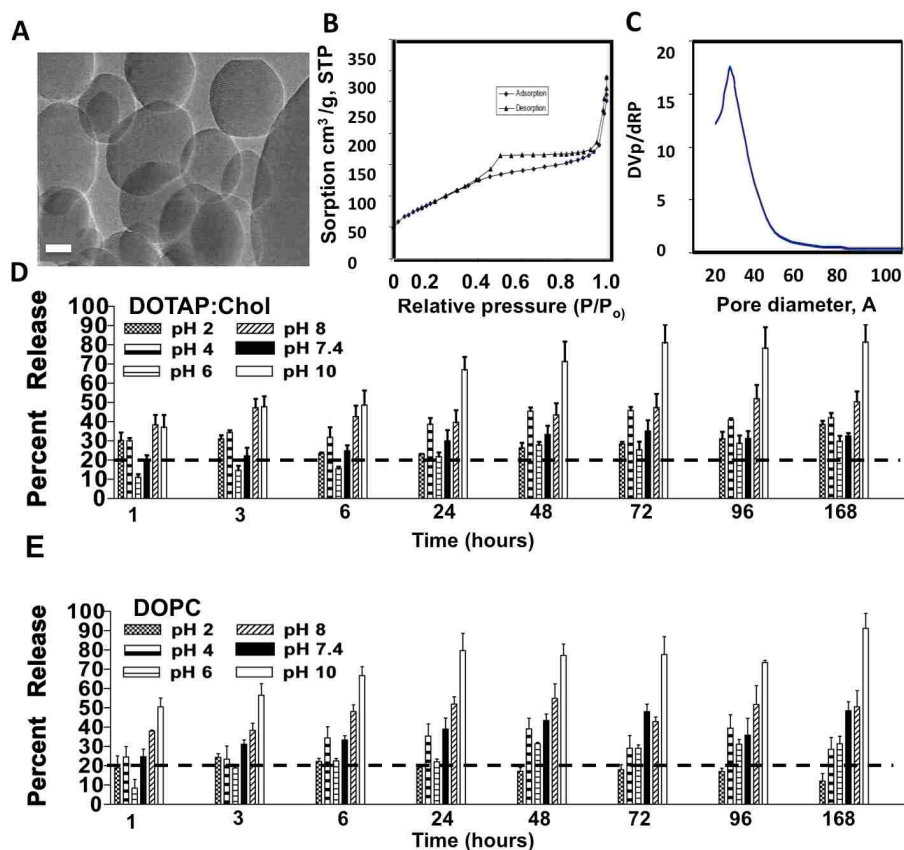
Appendix A: Figures

Figure A.1 Characterizations of protocells.

(A) TEM image of mesoporous silica nanoparticles; scale bar = 50 nm. (B) Nitrogen sorption isotherm of 10% aminated silica nanoparticles. (C) Determination of pore size of 10% aminated silica nanoparticles by the Barrett-Joyner–Halenda (BJH) method [27]. (D) DOTAP:Chol protocells and (E) DOPC protocells examined from 1 – 168 hours in specific pH solutions. The negatively charged fluorophore, dextran tetramethylrhodamine (DexRho) loaded into the protocells served as cargo. Dashed line indicates 20% release for ease of comparison between groups and conditions. For both DOTAP:Chol and DOPC protocells cargo release increased as time and pH increased. A significant interaction between time and pH was revealed (DOTAP:Chol: $F_{(35,84)}$= 2.16, p = 0021; DOPC: $F_{(35,84)}$ = 2.35; p = 0.0008. A trend for increased cargo release at pH 4 compared to pH 7.4 from DOTAP:Chol protocells was observed. DOTAP:Chol protocells at pH 6 revealed the greatest degree of cargo retention at 3 and 72 hours (p < 0.05). The pattern of greater cargo retention (~15%) at pH 7.4 and 6.0 in DOTAP:Chol protocells suggests that cargo will remain associated with protocells until taken up within the cell and released within the late lysosome for optimal cargo delivery.
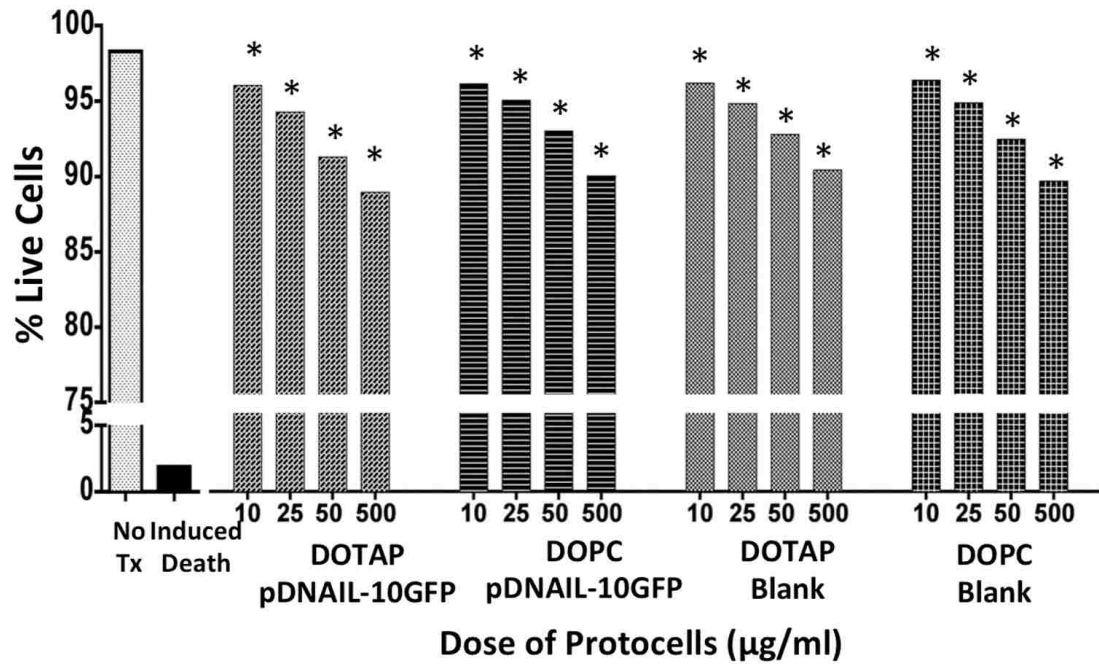
172

Figure A.2 Cells remain highly viable following application of DOTAP:Chol and DOPC protocells containing pDNA-IL-10-GFP.

Cells were incubated for 24 hours with DOTAP:Chol or DOPC protocells loaded with pDNA-IL-10-GFP or blank control protocells (no pDNA) at varying concentrations across a 50-fold dose range, 500, 50, 25 and 10 ug/ml. Dead cells were identified by flow cytometry after staining with ethidium-homodimer-1. Results are representative of the percentage of gated cells (average of 4 experiments) compared to untreated control cells, **p < 0.01; ***p < 0.0001.
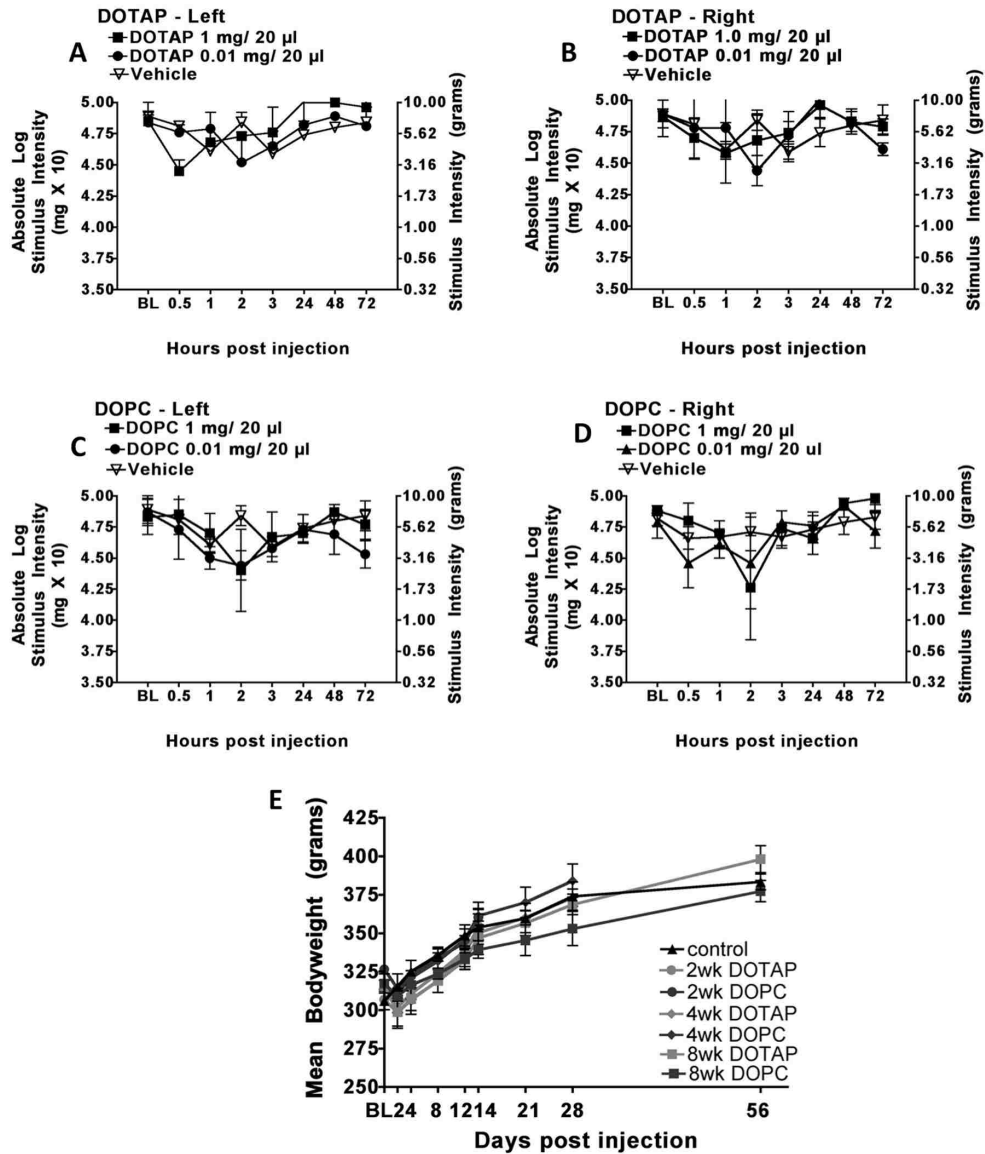
Figure A.3 In vivo subtle differences in biocompatibility are revealed between DOTAP:Chol and DOPC protocells.

Baseline threshold responses of both hindpaws (left and right) between animal groups were similar; at 10 g (right y-axis) $F_{(4,14)}= 0.3721$; $p > 0.05$). (A, B) Following i.t. injection with either 1 or 0.01 mg of DOTAP:Chol or (C, D) DOPC protocells, threshold responses remained unchanged throughout the timecourse (0.5, 1, 2, 3, 24, 48 and 72 hrs) suggesting no spinal inflammation. (C, D) For DOPC - treated animals, while a decrease in thresholds was not observed across the majority of the timecourse (left- $F_{(24,60)}$ = 1.88, $p > 0.05$; right- $F_{(24, 60)}$ = 1.01 $p > 0.05$), there was a small but significant decrease at 2 hours in both hindpaws ($p < 0.05$ left and right), indicating a subtle and transient spinal cord inflammation resulting in decreased sensory thresholds [35]. All animals exhibited normal feeding, grooming and exploratory

behavior throughout the 8-week observation. (E) Body weight gain remains normal following i.t. injection with DOTAP:Chol or DOPC protocells. At BL, there was no significant difference in body weight between untreated (open triangles) and treated animals that received i.t. DOTAP:Chol (2 wks, solid circles; 4 wks, solid diamonds; 8 wks, solid squares) or DOPC protocells (2 wks, open circles; 4 wks, open diamonds; 8 wks, open squares)($F_{(6, 14)}$ = 2.837, p = 0.0506), followed by a normal gain in body weight. This normal gain in body weight between control animals and those receiving protocells by i.t. injection remained consistent over time in all groups of animals (n = 3 per group).
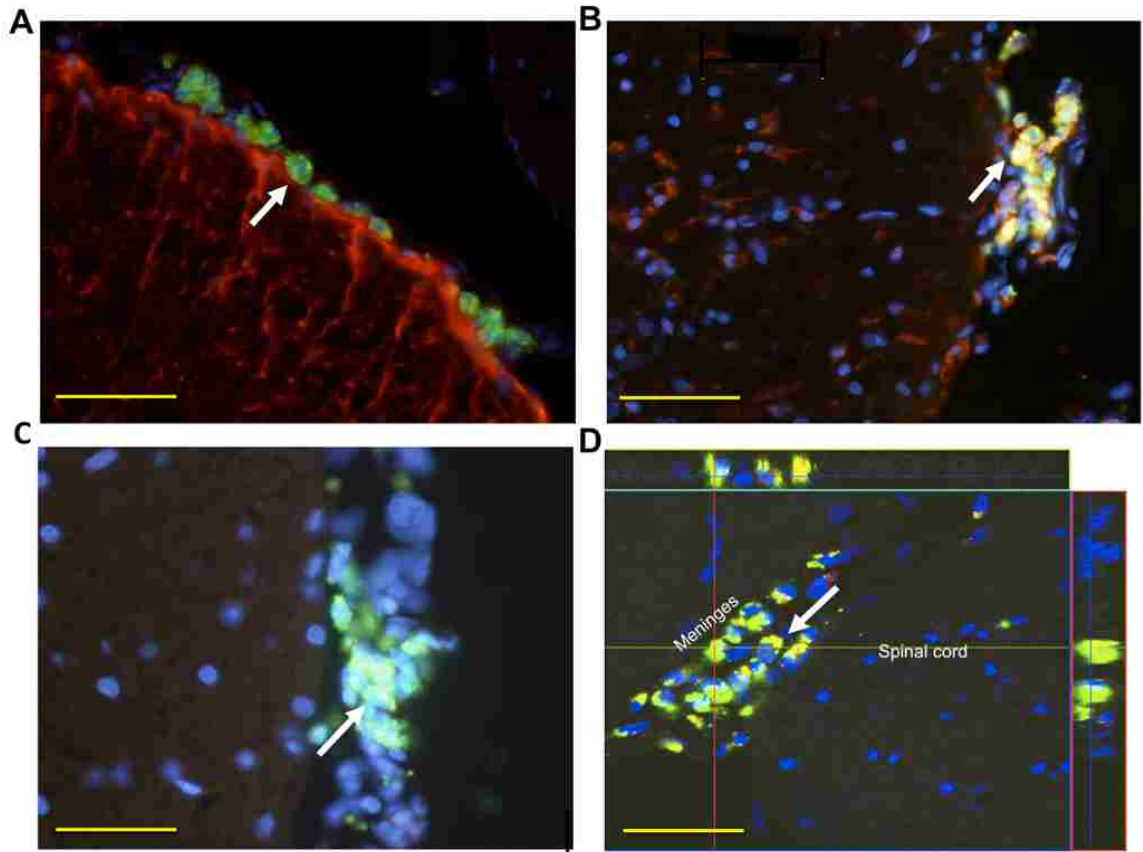
ll

Figure A.4 Histological examination of DOTAP:Chol protocells with DNA cargo.

Fluorescent histological examination of spinal cord sections near the lumbar spinal cord injection site (segments L3-4) 8 weeks after i.t. injection of DOTAP:Chol protocells loaded with FAM-tagged 18 base pair (18bp) DNA oligomer. (A) Protocells containing DNA cargo (green; white arrow) are not colocalized with astroglia stained for glial fibrillary acidic protein, GFAP (red). (B) However, protocells are colocalized in the pial meninges with activated microglia/macrophage stained for OX2 (red). Colocalization of microglia with DNA cargo (green) results is indicated (white arrow). (C) There is no evidence of cellular death in the meninges or spinal cord, as indicated by the absence of positive staining for the apoptotic marker, activated Caspase 3 (red) while protocell-containing DNA cargo (green; white arrow) is clearly present. (D) Confocal image identifying DOTAP:Chol protocell cargo of FAM-tagged 18 bp DNA (green) in the peri-nuclear area (cell nuclei stained with DAPI; blue) of meningeal macrophage cells stained for the classic activation marker, EDI (red; white arrow) in the dorsal spinal cord. Overlap reveals yellow cytoplasmic and peri-nuclear staining. All images are at 20X; scale bar = 40 μm.
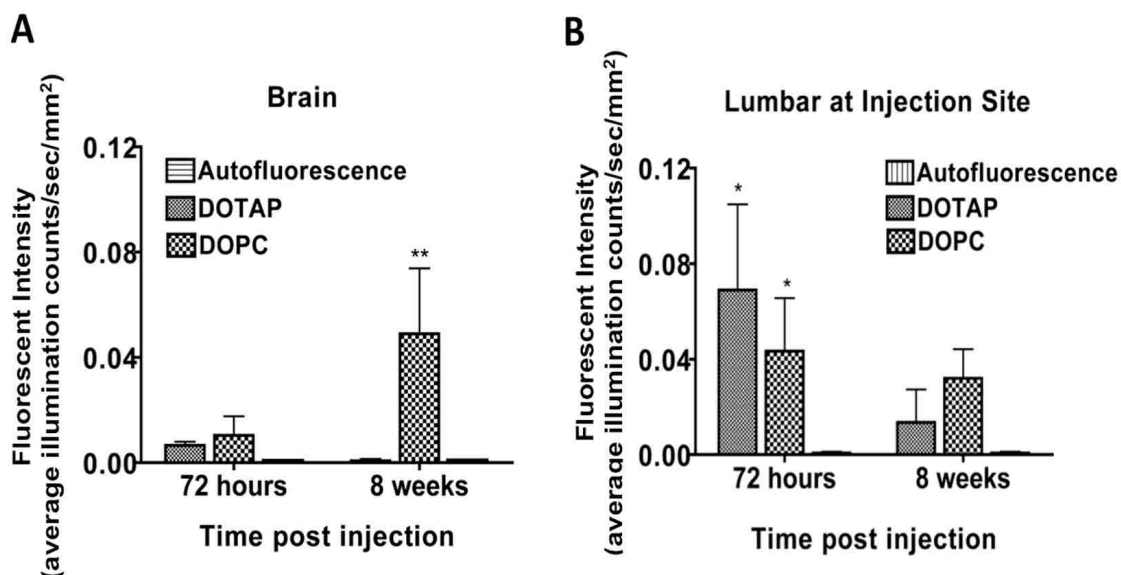
A

Brain

Fluorescent Intensity (average illumination counts/sec/mm²)

- Autofluorescence
- DOTAP
- DOPC

0.12 / 0.08 / 0.04 / 0.00

** (8 weeks DOPC)

72 hours | 8 weeks

Time post injection

B

Lumbar at Injection Site

Fluorescent Intensity (average illumination counts/sec/mm²)

- Autofluorescence
- DOTAP
- DOPC

0.12 / 0.08 / 0.04 / 0.00

* (72 hours DOTAP), * (72 hours DOPC)

72 hours | 8 weeks

Time post injection

Table 1 — Biodistribution of Fluorescent Tagged 18mer Signal: Quantification by Spectral Analysis (All numbers 1 X E-04)

	Auto fluorescence Naïve tissue		72 hours				8 weeks			
			DOTAP		DOPC		DOTAP		DOPC	
	Mean	SEM	Mean	SEM	Mean	SEM	Mean	SEM	Mean	SEM
Inside CNS										
[1] Brain	1.53	0.136	65.3	14.6	104	72.3	7.2	7.2	**491	0.248
Cervical spine	2.62	0.158	15.6	11.4	119	110	2.68	1.5	**580	359
10 mm rostral	22	16.2	624	232	682	262	26.7	5.7	286	16.4
[2] Lumbar protocell delivery site	6.6	5.9	*689	359	*434	222	*134.8	0.013	*320.2	121.9
5 mm caudal	17.7	10.5	325	147	230	175	17.1	9.69	***2419	259.9
1.5 mm caudal	10.5	5.8	194	76.7	158	169	24.5	1.23	***2111	274.1
2.5 mm caudal	7.14	3.45	*203	68.7	*250	55	3.16	0.625	2737	519
Outside CNS										
nodes	0.11	1.5	19.2	11.7	12.3	1.34	8.01	4.61	4.2	2.6
Thymus	13.3	6.8	*1044	471	648	97.4	9.4	0.657	16.4	4.66
Spleen	10.5	0.422	*45.2	10.07	10.4	12.69	12.2	12.7	6.2	1.8
Liver	25.2	3.7	24.1	4.87	36.6	6.45	14.6	0.395	18.7	2.65
Kidney	96.2	2.93	1.13	1.5	10.5	0.244	8.92	0.587	11.7	1.21

*** $p < 0.001$ ** $p < 0.01$ * $p < 0.05$ [1] See figure 5A   [2] See figure 5B

Figure A.5 The spread to brain following i.t. protocell injection is determined by the lipid bilayer formulation.

Graphs are representative of the key data in the corresponding Table I. Fluorescent spectral signal from FAM-tagged 18bp DNA cargo in cryo-sliced tissue sections (n = 4) of DOTAP:Chol or DOPC protocell i.t. treated animals is compared to the spectra of background autofluorescence from naïve animals. (A) In the brain, after 72 hours, there was no significant signal from FAM-tagged DNA delivered by either DOTAP:Chol or DOPC protocells. By 8 weeks, background signal in DOTAP:Chol protocell treated tissue

was comparable to that of auto-fluorecence (p > 0.05), while the signal from FAM-tagged DNA delivered by DOPC protocells had significantly increased compared to autofluorescence (F_2, 6 = 8.60; p = 0.0173. (B) At the lumbar spinal cord protocell delivery site, FAM-tagged DNA delivered by both DOPC and DOTAP:Chol prototocells was clearly present at both 72 hours and 8 weeks when levels of FAM signal analysis was compared to levels from autofluorescence ($F_{(2, 6)}$ = 6.18; p = 0.0348), with the signal at 72 hours significantly higher than that at 8 weeks ($F_{(2, 6)}$ = 10.71; p = 0.0170). (Table 1) Values (1 X E-04) of each anatomical region are an average of computer-generated spectral analyses taken from 4 separate images of four 10 μm sliced tissue sections. Yellow boxes indicate those areas in which the signal from FAM-tagged DNA cargo reached levels that were significantly higher than control autofluorescence for that tissue. Asterisks indicate the amount of significance. Very low levels of DOTAP:Chol protocells were detected in the lymph organs, such as thymus and spleen, while DOPC remained in the CNS. *p < 0.05; **p < 0.01; ***p < 0.0001.
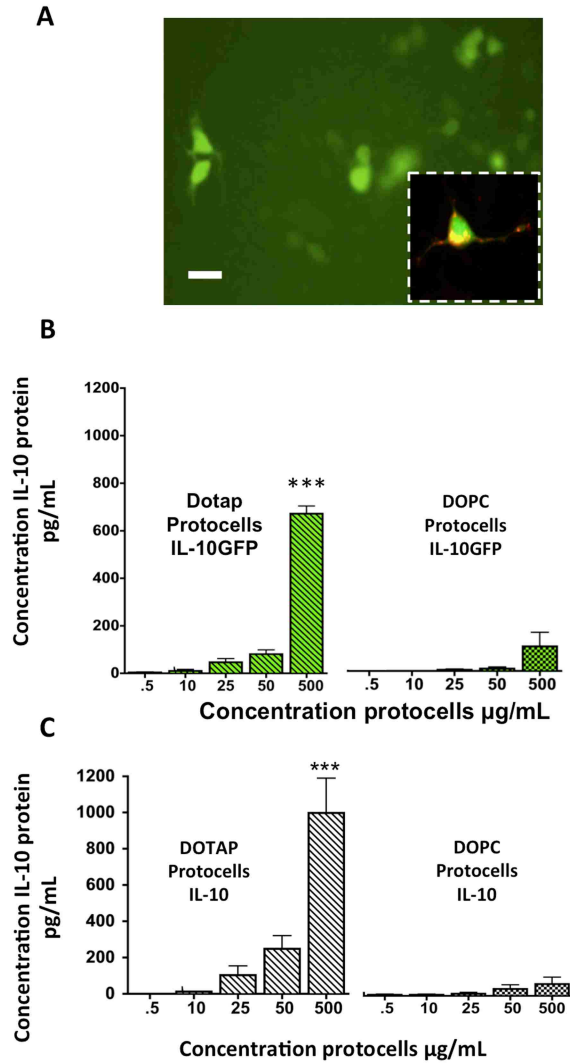
Figure A.6 DOTAP:Chol protocells improve cellular transfection of pDNA-IL10 transgene.

In vitro transfection of HEK cells with a bicistronic plasmid containing the genes for both IL-10 and GFP employing an internal ribosomal entry site results in expression of GFP (A; green). Staining with antibody for IL-10 (red) shows colocalization (yellow) in a GFP-positive HEK cell (green), indicating functional bicistronic transgene expression (A; insert). pDNA IL-10-GFP (B) or pDNA-IL-10 (C) delivered by DOTAP:Chol protocells results in functional transgene expression as measured by IL-10 protein release in culture supernatants following a 24 hour incubation. Results are the average of 4 representative experiments ($F_{(1, 4)}$ = 24.85; ***p < 0.0001, **p < 0.01). Scale bar = 10 μm in both Figure 6A and insert.

179

Figure A.7 Intrathecal delivery of protocells loaded with pDNA-IL-10 causes therapeutic reversal of allodynia.

(A and B) At pre-treatment baseline (BL) values, no significant differences were observed (ipsilateral and contralateral; $p > 0.05$). Following BL assessment, animals underwent CCI of the left sciatic nerve, and threshold values were reassessed 3 and 10 days later. Robust allodynia was observed compared to sham-treated controls (ipsilateral- $F_{(8, 36)} = 4.94$; $p < 0.0004$; contralateral- $F_{(8, 36)} = 19.89$; $p < 0.0001$). On day 10 after CCI, rats then received an i.t. injection with DOTAP:Chol/ pDNA-IL-10 protocells or control DOTAP:Chol protocells without DNA. A significant bilateral reversal of allodynia beginning on day 12 after CCI (day 2 after i.t. injection), and continuing through day 22 was observed (overall treatment effect, ipsilateral- $F_{(4, 108)} = 44.91$; $p < 0.0001$; contralateral- $F_{(4, 108)} = 85.09$; $p < 0.0001$). Each CCI operated group (closed symbols) received an i.t injection of DOTAP:Chol protocells loaded with pDNA-IL-10 (squares; n = 7) or a non-coding DNA (triangles; n = 5) (10 µg pDNA in 1mg protocells in 20 µl PBS) or PBS vehicle (circles; n = 3) (20 µl). Each sham-operated group (open symbols) received an i.t. injection of non- coding DNA (triangles; n = 5) (10 µg pDNA in 1 mg protocells in 20 µl PBS) or PBS vehicle (circles; n = 3) (20ul). Black arrow indicates i.t. injection; *p < 0.05; **p < 0.01; ***p < 0.0001. Nitric oxide concentration was measured in cultured Raw 264.7 cells (C) in LPS (black bar) and non LPS-stimulated cells (white bar) and those treated with whole protocells or constituents of protocells; silica core (500 µg) or Dotap:Chol lipid (20 µl)(hatched bars); All three treatments resulted in significantly less NO production than the LPS stimulated positive control ($F_{(4,14)} = 321.8$; $p < 0.0001$).
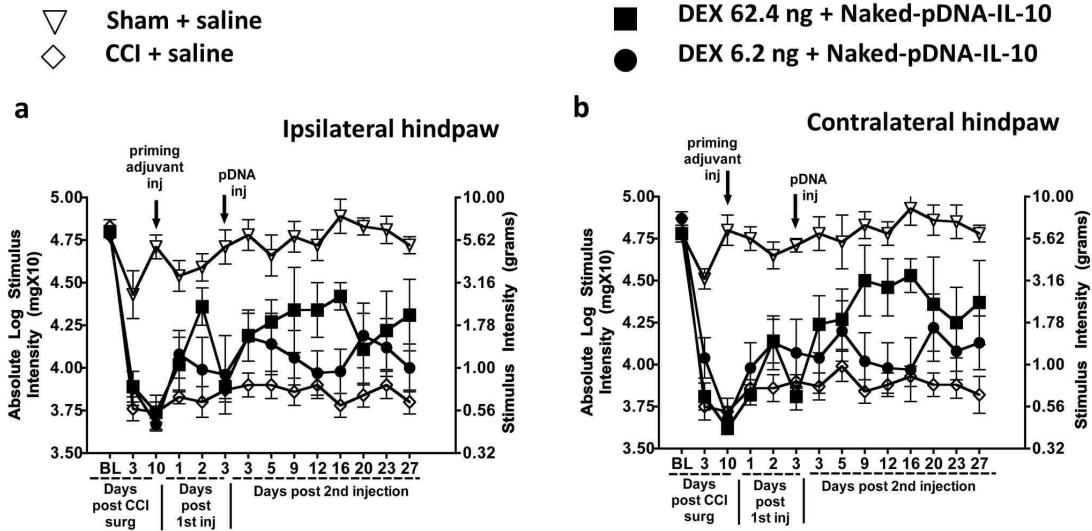
Figure A.8 Dexamethasone for improved pDNA-IL-10 uptake does not create robust pain reversal.

(a and b) Baseline (BL) hindpaw sensory threshold responses to light mechanical touch were measured by the von Frey test with calibrated monofilaments). There were no significant differences observed between groups (Ipsilateral, $F_{(3,24)}$ =0.2154; p=0.8846; Contralateral, $F_{(3,24)}$=0.6930; p=0.5665). Following either CCI or sham surgery, behavioral testing continued at the time points indicated on the x-axis. Animals receiving CCI surgery developed stable allodynia from day 3 to day 10 compared sham-operated animals (day 10: Ipsilateral, $F_{(3, 24)}$=53.54; p<0.0001; Contralateral, $F_{(3, 24)}$=71.70; p<0.0001). On day 10 following CCI surgery, animals received an i.t. injection of DEX (62.4 ng, n=6 or 6.2 ng, n=6), or equivolume i.t. saline (n=7) and sham-operated animals received i.t. equivolume saline (n=6). Three days later, an i.t. injection of pDNA-IL-10 (25 µg) or equivolume saline was given. Sham-control animals remained non-allodynic, while CCI animals given i.t. saline remained allodynic. I.t. pDNA-IL-10 following a priming injection of DEX (62.4 ng) revealed a delayed and partial bilateral pain reversal (Ipsilateral, $F_{(3,140)}$ =33.83; p<0.0001; Contralateral, $F_{(3,140)}$=19.7; p<0.0001). Black arrows indicate i.t. injections.
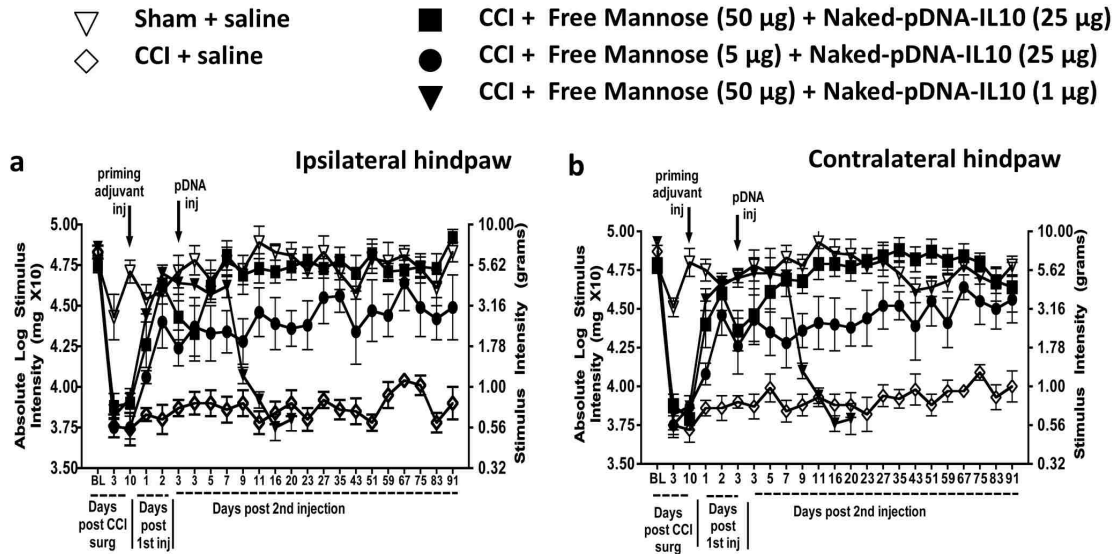
Figure A.9 The D-Mannose used to prime M2 polarization for improved pDNA-IL-10 uptake reverses allodynia greater than 90 days.

(a and b) No significant differences in BL responses between groups prior to CCI or sham surgery were observed (Ipsilateral, $F_{(4,32)}$=1.009; p=0.4197; Contralateral, $F_{(4,32)}$=1.147; p=0.3551). Sham operated animals (open triangles; n=6) remained non-allodynic throughout the time course. CCI animals (open diamonds; n=7) revealed clear allodynia from day 3 to day 10 compared to shams (day 10: Ipsilateral, $F_{(4,32)}$=32.87; p<0.0001; Contralateral, $F_{(4,32)}$=37.01; p<0.0001). On day 10, animals received an i.t. injection of either D-mannose (50 µg; 5 µg) , or equivolume saline followed three days later by pDNA-IL-10 (25 µg or 1 µg) or equivolume saline. Following the first priming injection of D-mannose (50 µg; closed squares; n=8), a robust reversal was observed, compared to CCI-saline injection (Ipsilateral, $F_{(3, 70)}$=15.87; p=0.0004; Contralateral, $F_{(3, 70)}$=20.40; p=0.001). Full reversal to BL levels continued for a 3 month period beyond the 2nd injection of pDNA IL-10 (25 µg) in those animals given D-mannose (Ipsilateral, $F_{(3, 384)}$ =57.46; p<0.0001; Contralateral, $F_{(3, 384)}$ =59.20; p<0.0001). A 2nd injection of a lower dose of pDNA-IL-10 (1ug: closed triangles; n=5) produced a transient 11-day reversal. Animals pretreated with the lower dose of D-Mannose (5 µg) followed by a second injection of pDNA-IL-10 (25 µg) (closed circles, n=7) showed partial bilateral reversal for the 3 month time course that was not significant (Ipsilateral, $F_{(3.17)}$= 12.71; p=0.0270; Contralateral, $F_{(3, 17)}$= 14.64; p= 0.002).
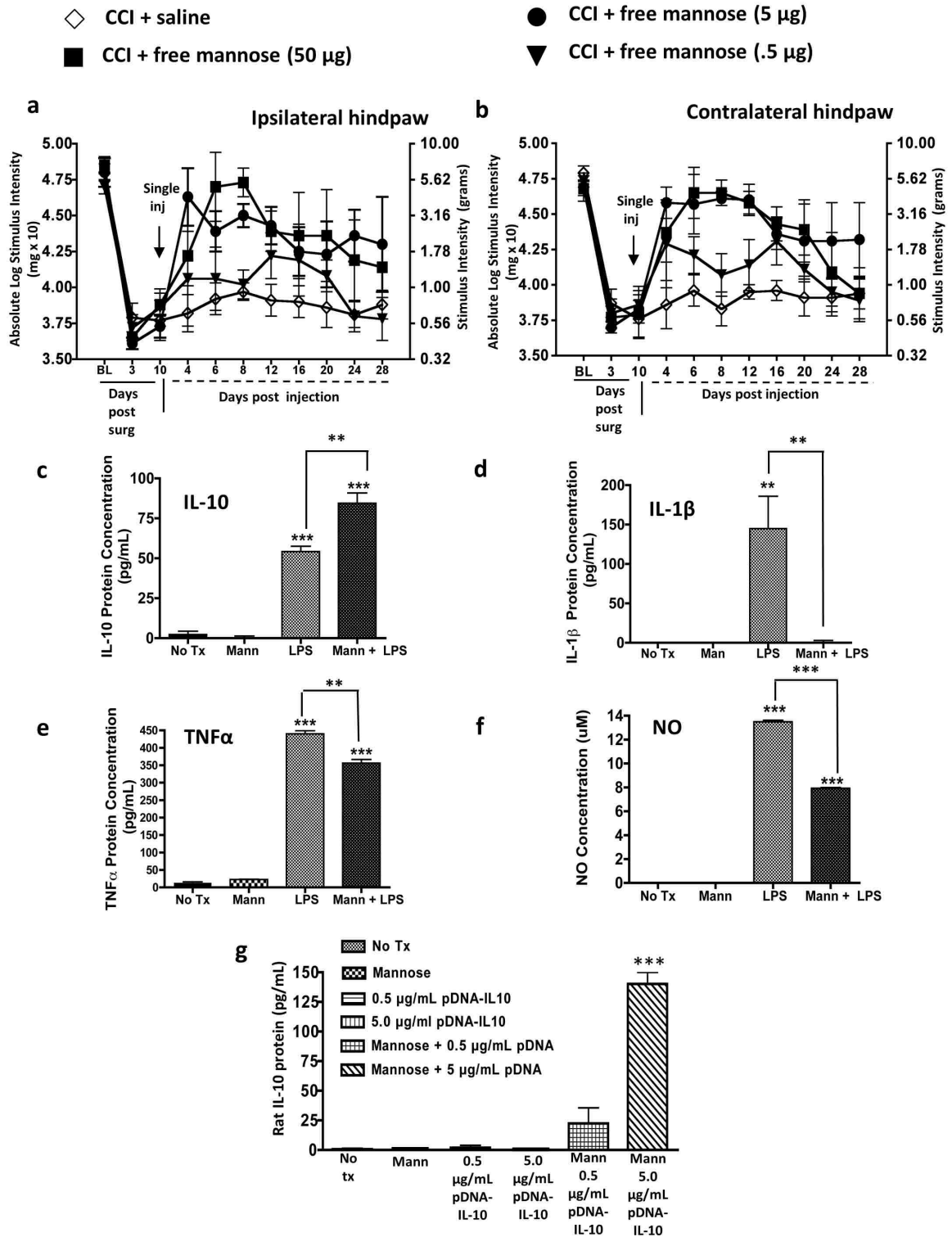
Figure A.10 D-Mannose generates short-term reversal of allodynia without pDNA-IL-10.

(a and b) No significant BL response differences between groups prior to CCI was observed (Ipsilateral, $F_{(3,13)}$ =0.4995; p=0.6910; Contralateral, $F_{(3,13)}$=0.1761; p=0.9099). All animals underwent CCI surgery and revealed clear allodynia by day 10 with no significant differences between groups ($F_{(3,13)}$ =0.1897; p=0.9010; Contralateral, $F_{(3,13)}$=0.2234; p=0.8780). On day 10, animals were given a single i.t. injection of D-mannose (50, 5, or .5 µg; closed squares, closed circles, or closed diamonds respectively) or an equivolume saline only (n=3-4/group). Saline-treated animals (open diamonds) remained bilaterally allodynic throughout the time course. Treatment with D-mannose (50 µg, n=3) resulted in bilateral partial reversal from allodynia that gradually returned by day 20 following injection (Ipsilateral, $F_{(3,70)}$=15.87; p<0.0005; Contralateral $F_{(3,70)}$= 20.40; p=0.0001). Black arrows indicate i.t. injection. (c-f) Cultured Raw 264.7 mouse macrophage cells were pretreated with D-Mannose (100 mM) followed by a 2 hour incubation with a combination of D-Mannose (100 mM) and LPS (10 ng). (c) Compared to control treatment (No Tx=no treatment; Mann=D-mannose), LPS-stimulated cells given D-mannose treatment resulted in significantly increased IL-10 protein production, (d) almost complete ablation of IL-1β levels (e) significantly reduced TNF-α protein levels, and (f) reduced NO production. (g) Cultured Raw 264.7 mouse macrophage cells were pretreated with D-Mannose (500 mM) for 5 hours followed by a 24 hour incubation with D-mannose with or without pDNA-IL-10, or D-Mannose and pDNA-IL-10 alone. Those cells incubated with D-mannose and pDNA-IL-10 showed robust and significantly increased exogenous rat IL-10 production over controls ($F_{(5,17)}$=69.3; p<0.001)*p<0.05; **p<0.01; ***p<0.0001
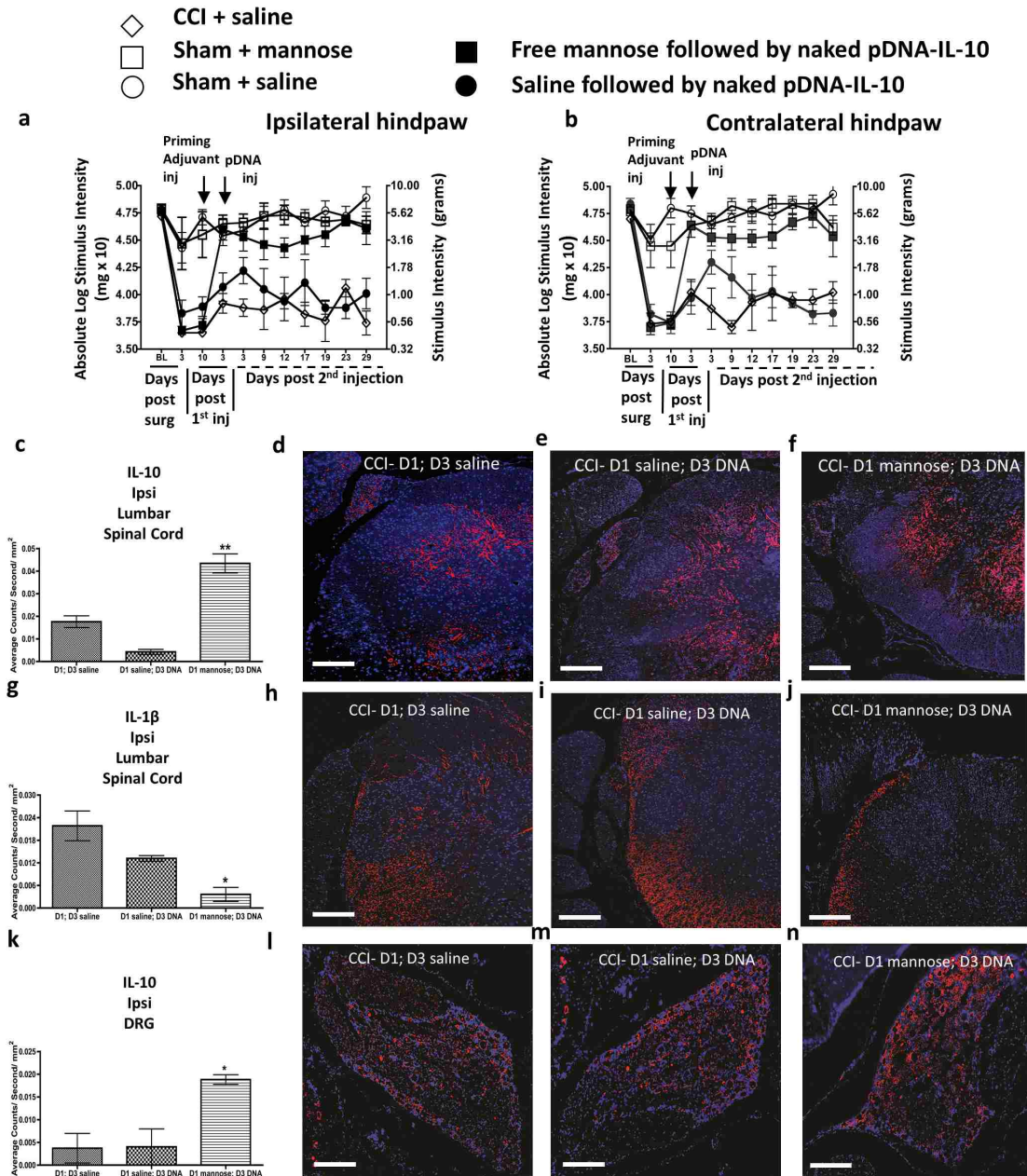
Figure A.11 Spinal and DRG pro-and anti-inflammatory markers expression.

(a and b) Verification of animal behavior prior to tissue collection is represented. There were no differences between groups at BL prior to CCI or sham surgery (Ipsilateral, $F_{(5,18)}$ =0.2597; p=0.8999; Contralateral, $F_{(5,18)}$=0.4947; p=0.9398). As before, CCI treated animals revealed clear bilateral allodynia to day 10 compared to sham controls (Ipsilateral, $F_{(5, 18)}$ = 35.54; p<0.0001; Contralateral, $F_{(5, 18)}$=35.96; p<0.0001). On day 10 following sham or CCI surgery, animals were given an i.t. pretreatment with D-mannose (50, μg) or equivolume saline injection followed three days later by i.t. pDNA-IL-10 (25 μg; closed squares;

n=7) or equivolume saline (closed circles; n=4). Saline-CCI treated animals (open diamonds; n=3) remained bilaterally allodynic throughout the time course compared to sham-D-mannose (open squares; n=3) or sham-saline (open circles; n=6) treated animals (Ipsilateral, $F_{(3,9)}$=28.79; p=0.0001; Contralateral, $F_{(3,9)}$=19.7; p=0.0007). These data replicated our earlier results above, and reveal that i.t. pretreatment with D-Mannose (50 µg) followed by pDNA-IL-10 (25 µg) causes a full bilateral reversal of allodynia compared to CCI-control groups (Ipsilateral $F_{(4,126)}$= 30.27; p < 0.0001; Contralateral $F_{(4,126)}$= 35.75; P< 0.0001). At day 29 while rats remained fully reversed from allodynia, spinal cord and associated DRG tissues were collected and stained for the anti-inflammatory cytokine, IL-10 or the pro-inflammatory cytokine, IL-1β. (c) Animals that received D-mannose (50 µg) on day 1 and pDNA-IL-10 on day 3, revealed significantly greater IL-10 immunoreactivity (IR) in the lumbar spinal cord compared to those animals injected with saline only or saline followed by pDNA-IL-10 (Ipsilateral $F_{(3, 5)}$ =34.23; p<0.01; Contralateral $F_{(3, 5)}$ =2.714; p>0.05). (d,e,f). Representative images used for the data analysis are presented (red=IL-10 IR, blue=cell nuclei). (g) Adjacent tissue sections revealed significantly less IL-1β IR in the ipsilateral lumbar spinal cord compared to non-mannose treated control groups (Ipsilateral $F_{(3,5)}$=10.67; p<0.05; Contralateral $F_{(3,5)}$=3.73; p> 0.05). (h, i, j). Corresponding fluorescent images of the analyzed data are presented (red =IL-1β IR, blue=cell nuclei). (k) In addition, significantly greater IL-10 IR in the DRG is observed in the D-mannose primed treatment group compared to both non-mannose treated control groups (Ipsilateral $F_{(3, 5)}$ =10.35; p<0.05; Contralateral $F_{(3, 5)}$ =5.73; p>0.05). (l, m, n). Corresponding fluorescent images of the analyzed data are presented (red =IL-10 IR, blue=cell nuclei). Data for the contralateral DRG data are not shown. *p< 0.05; **p< 0.01; ***p<0.0001; all images were taken at 10X; scale bar =100µm
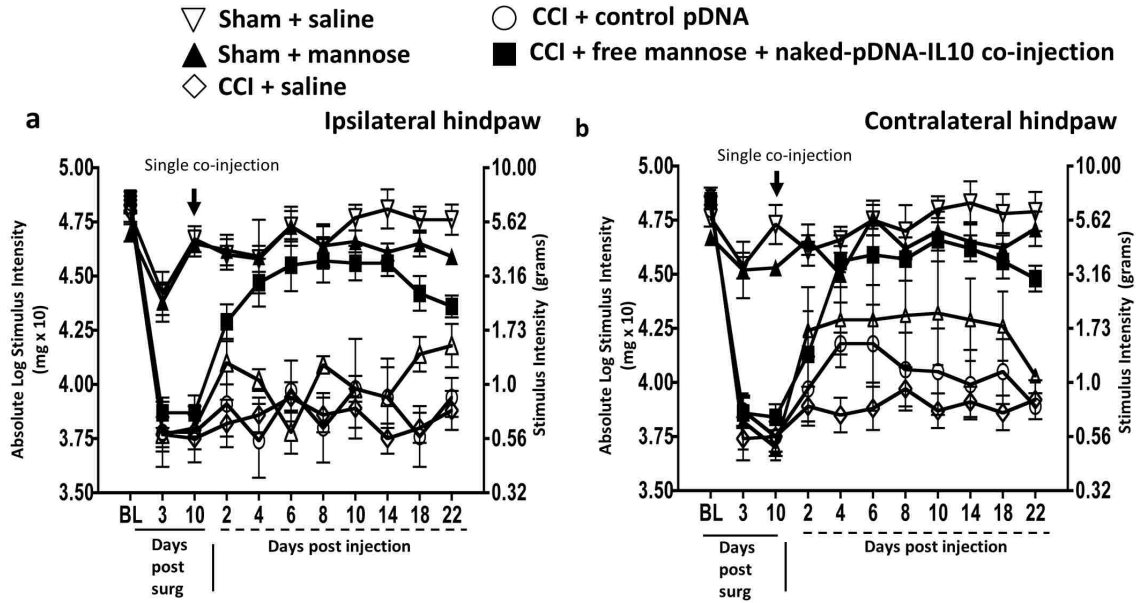
Figure A.12 A single co-injection of D-mannose with low dose pDNA-IL-10 produces enduring reversal of allodynia.

(a and b) No significant BL response differences were observed between groups prior to CCI or sham surgery (Ipsilateral, $F_{(3, 32)}$=0.8932; p=0.4973; Contralateral, $F_{(36, 32)}$=1.393; p=0.231). As before, CCI treated animals revealed clear bilateral allodynia through day 10 compared to sham controls (Ipsilateral, $F_{(3,32)}$ =32.07; p<0.0001; Contralateral, $F_{(3, 32)}$=38.78; p<0.0001). On day 10 after testing, sham rats received a single i.t. saline injection (open triangles; n=8) or D-Mannose (50 µg; closed triangles; n=4), and CCI rats received a single i.t. co-injection of D-Mannose (50 µg) with pDNA-IL-10 (1 µg; closed squares; n=10), pDNA lacking the IL-10 gene (control pDNA; open circles; n=7), or equivolume saline (open diamonds; n=6). Sham-saline and CCI-saline or CCI-control pDNA resulted in no change from bilateral allodynia throughout the time course, D-mannose co-injected with a low-dose of pDNA-IL-10 (1 µg) (closed squares, n=5) resulted in a significant and full reversal of allodynia throughout the 3 week time course (Ipsilateral $F_{(3, 238)}$= 60.23; p<0.001; Contralateral =$F_{(3, 224)}$=22.18; p< 0.001).
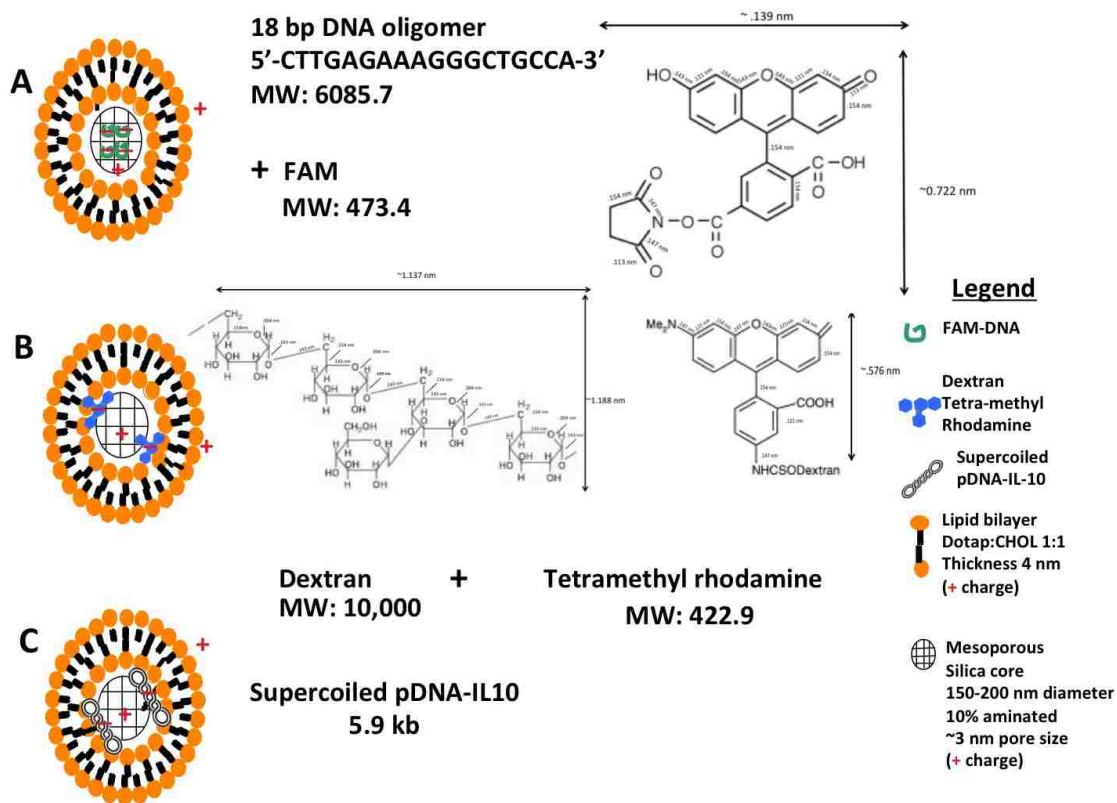
Figure A.13 Schematic showing theoretical loading of 3 protocell cargos

A) This cargo is a negatively charged, 18 bp DNA oligomer with an approximate length of 6.12 nm and a diameter of ~2. It is tagged with a negatively charged fluorophore, FAM which has a MW of 473.4 and an approximate planar length of .139 nm and height of .722 nm, as calculated by bond lengths. FAM-tagged DNA may load directly into the silica pores (~3 nm diameter). B) Negatively charged dextran tetramethyl-rhodamine (DEXRHO) is composed of a dextran polymer with a MW of 10,000 conjugated with tetra-methyl rhodamine groups. The tetramethyl-rhodamine group has an approximate planar length of .983 nm and height of .576 nm as calculated by bond lengths. This very large molecule is thought to load onto the protocell by adsorption with the positively charged DOTAP:CHOL 1:1 lipid bilayer and positively charged 10% aminated mesoporous silica core. C) Negatively charged plasmid encoding the gene for IL-10 most likely assumes a supercoiled structure and is thought to load by adsorption in a manner similar to DEXRHO. During the synthesis process each cargo was mixed with the silica and rinsed 3xs with PBS before the liposomes were added.